

LUNAR SOIL MECHANICS:  
DISTRIBUTION OF CONTACT STRESS  
BENEATH A RIGID PLATE RESTING ON SAND

by  
WILLIAM DAVID CARRIER, III  
SB, MIT  
(1965)  
SM, MIT  
(1966)

Submitted in partial fulfillment  
of the requirements for the degree of  
Doctor of Science

at the  
Massachusetts Institute of Technology  
(1968) i.e. Feb 1969

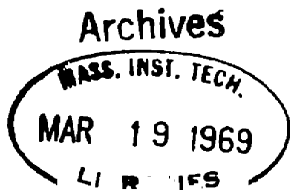
Signature of Author  
Department of Civil Engineering, October 4, 1968

Certified by . . . Thesis Supervisor

Certified by . . . Thesis Supervisor

Certified by . . . Thesis Supervisor

Accepted by . . .  
Chairman, Departmental Committee on Graduate Students



# ABSTRACT

## LUNAR SOIL MECHANICS: DISTRIBUTION OF CONTACT STRESS BENEATH A RIGID PLATE RESTING ON SAND

by

WILLIAM DAVID CARRIER, III

Submitted to the Department of Civil Engineering on October 4, 1968, in partial fulfillment of the requirements for the degree of Doctor of Science.

The present work is a new application of bearing capacity theory. It has two purposes: to contribute to knowledge in this field; and to explore the possibility of developing a new in situ testing device for measuring the strength properties of the lunar surface. Theoretical and experimental investigations were made of the contact stress distribution beneath a rigid strip resting on soil.

In the theoretical investigation, an analysis was made for a non-homogeneous elastic soil in which Young's Modulus ( $e$ ) increased linearly with depth and Poisson's Ratio ( $\nu$ ) was constant. It was found that the contact stress is uniform for all values of  $\nu$ , but that the settlement for a given load is extremely dependent on  $\nu$ . The value of  $\nu$  also greatly affects the distribution of vertical and horizontal stresses in the soil mass; for  $\nu = 1/2$ , these stresses are the same as that given by a uniform strip load on a homogeneous halfspace. It was found that roughness did not affect the distribution of vertical and horizontal stresses, nor did it alter the magnitude of settlement. It was also found that the shear stresses imposed by a rough plate are of such small magnitude that any real plate would necessarily be rough.

In the experimental investigation, a rectangular plate was instrumented with force and pressure transducers for measuring the distribution of contact stress along the short axis of the plate. The plate was pushed into a prepared sand bed in stages and the stresses recorded and plotted by computer. The results were compared with the Schultze Model and good

agreement was obtained. In particular, it was found that the friction angle of the sand could be back-calculated from the distribution of stress remarkably well.

A better design for the instrumented plate has been proposed and it is recommended that further experiments be run. More theoretical work is also needed: different elastic-plastic models must be explored.

The concept of an instrumented plate has been identified as the most desirable in situ testing device for the lunar surface. However, its full potential will not be realized until it can be attached to a roving vehicle, which will not be sent to the moon for several years. Until then, the plate can only be used by jacking against the LEM. A hand-operated cone penetrometer is also recommended for statistical studies of the non-homogeneity of the surface and for comparison with terrestrial soils. The LEM footpads should be instrumented to measure the force during and after landing to aid in a bearing capacity analysis.

Thesis Supervisors: T. W. Lambe, Professor of Civil Engineering  
L. G. Bromwell, Assistant Professor of  
Civil Engineering  
J. T. Christian, Assistant Professor of  
Civil Engineering

## ACKNOWLEDGEMENTS

The author owes a debt of gratitude to:

NASA, for providing a fellowship during the third graduate year.

NSF, for providing a traineeship during the first graduate year.

Prof. L.G. Bromwell, for helping in all the work.

Prof. E.H. Davis, for helping in the theoretical aspects.

Prof. J.T. Christian, for helping with the finite element computer work.

Prof. T.W. Lambe, for providing guidance and advice.

Prof. A.E.Z. Wissa, for making numerous suggestions for the improvement of the experimental work.

Prof. C.C. Ladd, for providing moral support.

J. Rixner, S. Lucks, K. Rocker, and R. Monti, for running related soil tests.

Macy Lawrence, for taking superb photographs of the work.

Carl Stahle, for much of the machining for the experimental work.

Gail Stevens, for typing the thesis.

In addition, the author will forever be grateful to David D'Appolonia for performing yeoman duty on his computer program in the author's behalf.

Finally, I wish to say thank you to Lillian who shares all of my failures and all of my successes.

## TABLE OF CONTENTS

	<u>PAGE</u>
TITLE PAGE	
ABSTRACT	i
ACKNOWLEDGEMENTS	iii
TABLE OF CONTENTS	iv
LIST OF TABLES	vi
LIST OF FIGURES	vii
1.0 INTRODUCTION	1
2.0 REVIEW OF PREVIOUS THEORETICAL WORK	6
2.1 Elastic Theory	6
2.2 Plasticity Theory	10
2.3 Elastic-Plastic Theory	15
3.0 NON-HOMOGENEOUS ELASTIC HALFSPACE	17
3.1 Finite Element Grid	18
3.2 Non-Homogeneity	18
3.3 Effect of $\nu$ - Smooth Plate	18
3.4 Smooth vs. Rough Plate	19
3.5 Stresses and Strains	21
4.0 EXPERIMENTAL INVESTIGATION	25
4.1 Previous Experimental Investigations	28
4.2 Selection of Model to Compare with Data	30
4.3 Value of $m$ Back-Calculated for Whole Plate	31
4.4 Modification of Schultze Model	32
4.5 Selection of $\phi$ and $N_\gamma$	33
4.6 Evaluation of Results	35
5.0 <u>IN SITU</u> TESTING DEVICES FOR THE LUNAR SURFACE	38
5.1 Instrumented Plate	38
5.2 Cone Penetrometer	40
5.3 LEM Footpads	41
5.4 Astronaut Footprint	41

	<u>PAGE</u>
6.0 CONCLUSIONS AND RECOMMENDATIONS	43
REFERENCES	45
BIOGRAPHY	48
NOTATION	49
PHOTOGRAPHS OF EXPERIMENTAL APPARATUS	51
TABLES	53
FIGURES	62
APPENDIX A: Standard Soil Mechanics Tests	115
APPENDIX B: Experimental Apparatus and Procedures	119
APPENDIX C: Computer Plotting Program	127
APPENDIX D: Finite Element Computer Program	130
APPENDIX E: Earlier Experimental Runs	132
APPENDIX F: Davis Plasticity Parameters	145

## LIST OF TABLES

<u>NO.</u>	<u>TITLE</u>	<u>PAGE</u>
2.1	Solutions for a Rigid Plate Resting on an Elastic Soil	53
2.2	Solutions for a Rigid Plate at Ultimate Load	54
3.1	Summary of Finite Element Computer Runs	55
4.1	Summary of Plate Load Tests	56
4.2	Experimental Parameters Selected to Compare with Plate Load Test Data	58
5.1	<u>In Situ</u> Testing Devices for the Lunar Surface	59
A.1	Summary of Direct Shear Tests	60
A.2	Summary of CID Triaxial Tests	61

## LIST OF FIGURES

<u>NO.</u>	<u>TITLE</u>	<u>PAGE</u>
2.1	Terzaghi Method for Determining $N_{\gamma}$	62
2.2	Terzaghi Bearing Capacity Factor - $N_{\gamma}$	63
3.1	Finite Element Grid	64
3.2	Effect of Poisson's Ratio	66
3.3	Rough vs. Smooth Plate	67
3.4	Numerical Stability of Rough Plate Solution	68
3.5	Settlement of a Rigid Plate	69
3.6	Centerline Settlement of a Rigid Plate	70
3.7	Distribution of Stress at Centerline	71
3.8	Vertical Stress Distribution Beneath a Rigid Plate	72
3.9	Horizontal Stress Distribution Beneath a Rigid Plate	73
3.10	Contact Shear Stress Distribution Beneath a Rough Rigid Plate	74
3.11	Lateral Displacement Distribution Beneath a Smooth Rigid Strip	75
3.12	Distribution of Vertical Strain at Centerline	76
4.1 to 4.10	Predicted vs. Measured Contact Stress Beneath Experimental Rigid Plate	77
4.11	Value of $m$ Back-Calculated for Whole Plate	87
4.12	Schultze Model Modification	88
4.13	Davis Plasticity Parameters from Triaxial CID Tests	89
4.14	Triaxial Friction Angle	90
4.15	Comparison of $\phi_{tri}$ and $\phi_{ps}$ From $N_{\phi f}$ and $\mu$	91
4.16	Friction Angle: Triaxial vs. Plane Strain	92
4.17	Experimental Parameters Selected to Compare with Plate Load Test Data	93
4.18	Load-Settlement Curves for Plate Load Tests	94
4.19	Predicted vs. Measured Failure Load for Whole Plate	95
4.20	Normalized Load-Settlement Curves for Plate Load Tests	96



	<u>PAGE</u>	
4.21	Error Analysis of Stresses in Elastic Zone	97
4.22	Error Analysis of Stresses in Plastic Zone	98
4.23	Comparison of Predicted and Measured $N_{\gamma}$	99
4.24	Comparison of Predicted and Measured $\phi_{ps}$	100
5.1	Improved Design for Instrumented Plate	101
5.2	Alternate Design for Instrumented Plate	102
A.1	Grain Size Distribution of Experimental Sand	103
A.2	Relative Density of Experimental Sand	104
A.3 to		
A.5	Direct Shear Tests	105
A.6 to		
A.8	Triaxial Test Data: CID Dry	108
B.1	Instrumented Loading Plate	111
B.2	Force Transducer Housing	112
B.3	Load-Settlement Curve: Soil 19, Stage 4	113
B.4	Change of Contact Stress With Time	114

## CHAPTER 1

### INTRODUCTION

The idea for this investigation developed while the author was engaged in research for a report to NASA, entitled, "Lunar Soil Mechanics" (April, 1968). The report concluded that to measure the strength properties of the lunar soil (i.e., friction angle  $\phi$  and cohesion  $c$ ), an in situ testing device would be required that is based on a rational approach. Those terrestrial devices which are based on empirical experience to find  $\phi$  and  $c$  just could not be used on the moon. The only tool presently used in soil mechanics to determine  $\phi$  and  $c$  which is based on theory is the standard bearing capacity test; and so the author decided to investigate this area further.

A survey of previous theoretical work for a rigid plate resting on soil (Chapter 2) revealed that only one investigator, Schultze (1961), had considered the effect of local plastic zones in the soil. As the plate is forced into the soil, a failure zone develops at the edge and spreads inward until the ultimate condition is reached or the plate moves into the soil an intolerable amount. (The magnitude of settlement that is considered intolerable depends on the situation.) Schultze's work suggested to the author that by measuring the distribution of contact stress near the edge of a rigid plate on a soil of known unit weight it would be possible to calculate  $N_\gamma$  and  $N_c$ , and from them  $\phi$  and  $c$ .

The author decided that three things were necessary: the theory for the contact stress beneath a rigid plate must be extended; the distribution of stress beneath a real plate on soil must be measured; and the strength properties must be back-calculated from the stresses.

In the theoretical work, it was intended that an elastic-plastic soil model would be used in conjunction with the finite element computational technique (similar to work performed by Christian, 1966). It was hoped that a better theoretical prediction of the distribution than that of Schultze could be developed. In the early stages of the theoretical work, a computer program was used which was a bi-linear elastic program based on a secant modulus approach. This program was modified to consider a Mohr-Coulomb failure criterion, but it became apparent that it was also necessary to consider the strains after yield (Appendix F), and thus a secant Poisson's Ratio was introduced. It was found that this approach was numerically unstable; the solution would not converge. At this point, a new computer program became available (Appendix C) based on a bi-linear elastic incremental analysis that included a different Poisson's Ratio after yield. This program was also modified to consider a Mohr-Coulomb yield criterion. It was hoped that the Davis parameters (Appendix F) could be used with this program to analyze a rigid plate resting on sand. This approach did not work; the stress paths did not remain on the yield surface after failure. It now appears that it is necessary to consider the incremental plastic behavior of the soil. However, the analyses did show that the elastic properties have a pronounced effect on the solutions, and so the author decided to investigate a purely elastic soil model (Chapter 3). A non-homogeneous halfspace was selected in which Young's Modulus ( $E$ ) is equal to zero at the soil surface and increases linearly with depth and Poisson's Ratio ( $\nu$ ) is constant. Although other soil models are possible (such as  $E$  increasing with the square root of the depth), this model was chosen because limited solutions from other investigators (Zaretsky and Tsytoovich, 1965, and Gibson, 1967) were available for comparison.

Since the failure of the soil at the edge of the plate is ignored in this analysis, the detailed results can only be used at high factors of safety where the edge failure can safely be

neglected. However, several discoveries were made which are especially important to this investigation. It was found that for this soil model, the shear stresses imposed by a rough plate are of such small magnitude that any real plate would necessarily be rough; and that roughness does not affect the distribution of vertical and horizontal stresses in the soil mass, nor does it alter the magnitude of settlement of the plate. The solution also indicates that the distribution of contact stress away from the edge of a real plate would be uniform. It was further found that the value of  $\nu$  had a very strong effect on the settlement of the plate, as well as the distribution of horizontal stress in the soil mass.

This analysis together with the experimental investigation has also served to show the following. (1) Schultze was correct in assuming a homogeneous soil for the elastic portion of his solution. Even though Young's Modulus increases with depth in a real soil, as a plate is pushed into the soil, the modulus under the plate is increased. (2) In the present theoretical analysis,  $E$  was assumed to be a material property, independent of loading geometry. In future theoretical analyses, it will be necessary to consider the effect of imposed stresses on the value of  $E$ .

For the experimental investigation (Chapter 4), it was first necessary to select a soil. No attempt was made to model the lunar surface for two reasons: (1) There is still considerable controversy concerning the origin and nature of the lunar surface; even after the highly successful Orbiter and Surveyor programs, the dispute between the proponents of the volcanic and meteoric theories has remained unsettled. In fact, the disagreement will probably continue even after the first samples are returned during the Apollo program. The author did not wish to tie the present work to any specific model. (2) Assuming the surface is particulate in nature (which the Surveyor photographs have clearly shown), it is believed that the lunar soil will behave in a manner that is similar to terrestrial soils. Thus the general results of the experimental study will not depend on the soil used.

As a further simplification, it was decided to use a cohesionless sand (Appendix A) and to concentrate only on the frictional aspects of the strength of soil. As this is a preliminary investigation of the concept of back-calculating  $\phi$  from the distribution of contact stress, only one soil was employed at different densities. This resulted in a range of friction angle of only about  $5^{\circ}$ . Clearly, other soils with different friction angles must also be tested, but provided the elastic-plastic behavior is similar to that of the soil used in this investigation, the general conclusions should still hold.

Studies must also be made for cohesive soils, as well as for soils with both friction and cohesion. Schultze's work included these cases, and thus a theory already exists. Problem soils in which the friction angle and cohesion are strongly dependent on strain (such as collapsing soils) will be extremely difficult to interpret, particularly since the theoretical analysis of such soils is not well developed.

A rectangular plate was instrumented with transducers (Appendix B) and pushed by stages into a prepared bed of sand at known densities and strengths. The transducers measured the plane strain distribution of stress along the short axis of the plate; these were plotted by means of computer and compared with the predicted stress for the Schultze Model. It was found that in the interior of the plate, where the stresses are still "elastic", the agreement is quite good. In the "plastic" zone at the edge, the agreement is poorer. But an algorithm was devised to interpret the data and the values of  $N_y$  and  $\phi$  which were back-calculated agreed remarkably well with the known values. However, more experience is needed to establish the validity of this algorithm.

Having established the concept of back-calculating the strength properties of soil by measuring the distribution of contact stress beneath a rigid plate, the author has reflected on its possible use on the lunar surface during the Apollo

program (Chapter 5). The author concluded that this type of device offers the best possibility for analyzing the lunar surface. An improved design, involving individually instrumented parallel strips, is recommended. However, in the early stages of the Apollo program, before roving vehicles are sent to the moon, it will be necessary to use the Lunar Excursion Module as a resisting force for the plate. This limits the area of investigation to the vicinity of the LEM (which will be disturbed during landing). To obtain qualitative information about the lunar surface at a distance from the LEM, a hand-held cone penetrometer is recommended.

It has been concluded that further experiments with an improved instrumented plate are justified and that elastic-plastic soil models are required to aid in the analysis of the experimental data.

The units used in this thesis should be mentioned. Usually, stresses in soil mechanics are reported in psi or  $\text{kg/cm}^2$ ; as this work is related to the space program, it was decided to use metric force units. Thus, stress is in  $\text{newton/m}^2$  (1 newton = 1  $\text{kg-m/sec}^2$ ; 1 psi = 6900  $\text{newton/m}^2$ ; 1  $\text{kg/cm}^2$  = 98000  $\text{newton/m}^2$  on earth). Positive stresses and strains are in compression.

All of the experimental data were analyzed with the aid of the Civil Engineering Systems Laboratory 1130 IBM Computer. All of the finite element computer runs were made at the MIT Information Processing Services Center.

A NASA grant provided the funds for the purchase of the equipment.

## CHAPTER 2

### REVIEW OF PREVIOUS THEORETICAL WORK

The theoretical analysis of a rigid plate on soil has received considerable attention by many other writers. As explained in the introduction, the author's purpose has been to define better the stresses and displacements associated with a rough rigid strip resting on the surface of cohesionless soil, with particular emphasis on the contact stresses between the soil and plate. This section is a brief review of work performed by other investigators. Many mathematical models have been used to describe real soil; these models have been grouped into three main areas for discussion: Elastic, Plastic, and Elastic-Plastic. The Elastic solutions are summarized in Table 2.1; and the Plastic solutions in Table 2.2.

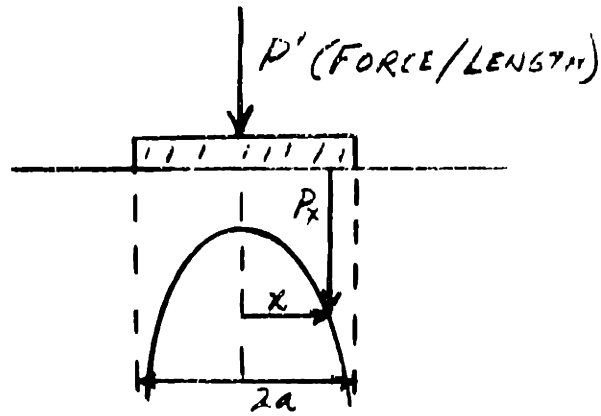
#### 2.1 ELASTIC THEORY

Elastic theory is used in soil mechanics to analyze situations in which the soil is far from failure. In the case of a rigid footing, it would be used to predict the stresses and displacements when the footing has a factor of safety against failure on the order of 5 or more.

#### BOUSSINESQ

Sadowsky (1930), using the work of Boussinesq (1885), considered a smooth rigid strip on an elastic halfspace (homogeneous and isotropic) and arrived at the following equation for the normal contact stress between the plate and the soil:

$$p_x = \frac{P'}{\pi a \left(1 - \frac{x^2}{a^2}\right)^{\frac{1}{2}}} \quad \text{Eqn. 2.1}$$

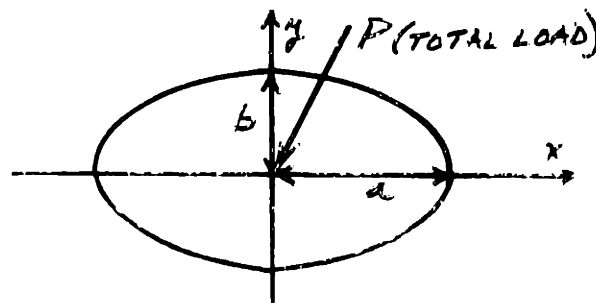


This solution is remarkable in several ways. It is independent of the elastic parameters of the soil ( $E$  and  $\nu$ ); and the stress goes to infinity at the edge of the strip, a physical impossibility for real soil. Furthermore, the displacement of the footing into the halfspace is infinite.

SCHIFFMAN AND AGGARWALA

The most complete analysis of a rigid plate on a homogeneous halfspace is that of Schiffman and Aggarwala (1961). They considered a smooth elliptical footing and found the contact stress to be:

$$P_{xy} = \frac{P}{2\pi ab \left(1 - \frac{x^2}{a^2} - \frac{y^2}{b^2}\right)^{1/2}} \quad \text{Eqn 2.2}$$



The Boussinesq solution, of course, is a special case of the Schiffman-Aggarwala solution for  $b \rightarrow \infty$ . Schiffman and Aggarwala also developed general formulae for the stresses and displacements throughout the halfspace and presented figures for the vertical and lateral stresses along the centroidal axis of



the ellipse for a range of Poisson's Ratio.

ZARETSKY AND TSYTOVICH

Zaretsky and Tsytovich (1965) and Gibson (1967) have investigated the case of a non-homogeneous elastic halfspace.

Zaretsky and Tsytovich considered a smooth rigid strip resting on an incompressible ( $\nu = .5$ ), non-linear, non-homogeneous elastic halfspace, described by:

$$\begin{aligned} \gamma_{ij} &= \tau_{ij}^{\delta} / A \quad (\delta \geq 1) \\ A &= A_0 z^{\eta} \end{aligned} \qquad \text{Eqn. 2.3}$$

where:

- $\gamma_{ij}$  = shear strain on the i-j plane
- $\tau_{ij}$  = shear stress on the i-j plane
- $\delta$  = non-linearity factor
- $z$  = depth below soil surface
- $\eta$  = non-homogeneity factor
- $A$  =  $E/3$  for  $\delta = 1$  and  $\eta = 0$  (linear and homogeneous)

For a line load applied to a rigid strip =  $P'$ , the normal contact stress is given by:

$$P_x = \frac{\Gamma[(1-\alpha)/2] \Gamma(1+\alpha/2) \cos(\pi\alpha/2)}{\dots} \times \frac{P'}{\pi a [1-x^2/a^2]^{[(1-\alpha)/2]}}$$

Eqn. 2.4

$\Gamma(x)$  is the GAMMA FUNCTION

$$\alpha = 1 - \left(\frac{1-\eta}{\delta}\right)$$

For  $\eta = 0$  and  $\delta = 1$  ( $\alpha = 0$ ), the halfspace is linear and homogeneous and the stress reduces to that given by Boussinesq (Eqn. 2.1).

For  $\eta = 1$  and  $\delta = 1$  ( $\alpha = 1$ ), the halfspace is linear and non-homogeneous (the same case considered by Gibson below; see Eqn. 2.5) and the stress is found to be constant beneath the plate ( $=P'/2a$ ), except at the edge, where the stress is not defined ( $=P'/2a0^0$ ).

Thus, as  $\alpha$  increases from 0 to 1, the distribution becomes increasingly more uniform. Also, it is interesting to note that for  $\eta = 1$ ,  $\alpha = 1$  for any value of  $\delta \leq 1$ ; that is, the contact stress is uniform for this specific non-homogeneous case and is independent of whether or not the halfspace is linearly elastic.

Zaretsky and Tsytovich did not solve for displacements.

#### GIBSON

Gibson (1967) considered a uniform strip load of magnitude  $q$  acting on a non-homogeneous halfspace with linearly increasing Young's modulus:

$$E(z) = m\gamma z \quad \text{Eqn. 2.5}$$

where  $m$  is a constant. He further assumed the soil to be incompressible; i.e., Poisson's Ratio equal to .5. His results were quite surprising, as the surface displacement was found to be:

$$\begin{aligned} \rho &= \frac{3q}{2m\gamma} && \text{within the loaded area} \\ &= 0 && \text{outside the loaded area} \end{aligned} \quad \text{Eqn. 2.6}$$

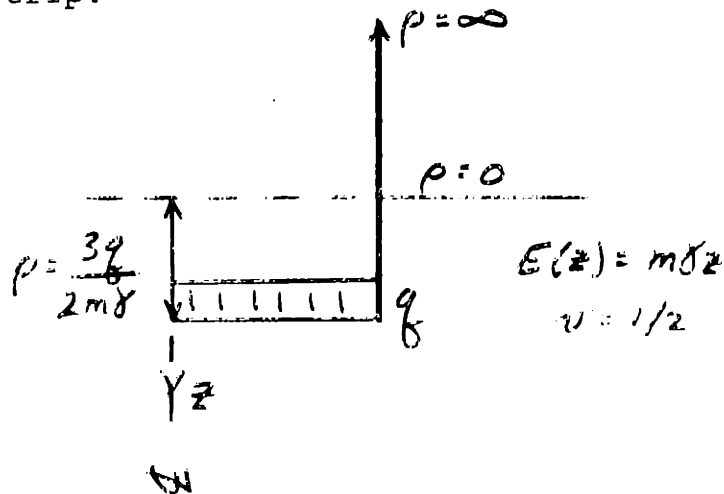
That is, he found that the displacement was uniform everywhere beneath the strip load and zero outside. Conversely, the author concluded that a smooth rigid strip footing will result in a uniform contact stress equal to the average stress applied to the strip.

This solution is remarkable in other ways as well. It was found that the components of stress were the same as those

for a uniform strip loading on a homogeneous halfspace. The work also showed that this halfspace is equivalent to a soil with a coefficient of subgrade reaction given by:

$$k_s = \frac{2}{3}m\gamma \quad \text{Eqn. 2.7}$$

As with the Boussinesq and the Zaretsky and Tsytovich solutions, the Gibson solution has a singular point at the edge of the strip:



All of the heave associated with the settlement of the strip is contained in an infinitesimally small element (which experiences infinite volumetric strain) at the edge of the strip on the surface of the halfspace. This of course is a physical impossibility for real soil. On the other hand, the settlement of the strip is finite, which is closer to reality.

#### PLASTICITY THEORY

Plasticity theory is used in soil mechanics to analyze situations in which a continuous yielded zone exists within the soil mass and extends to the surface. In the case of a rigid footing, the theory would be used to predict the stresses (but not the displacements) at the ultimate bearing capacity, or when the factor of safety is approximately 1.

Plasticity theory is far more complicated than elastic theory and as a result, a completely rigorous closed solution for a strip on a frictional soil has not been possible. There are two major theoretical groups: those who improve the statically correct solutions (lower bounds) and those who improve the kinematically acceptable solutions (upper bounds). The second group has not met with great success, as the assumed slip surfaces are not statically correct and the computed bearing capacity is very sensitive to small changes in the shape of the slip surface (DeBeer, 1965). Since this approach yields an upper bound and is thus unconservative, most engineers prefer the lower bound solutions, which will be discussed below.

Before bearing capacity theory is discussed, it is necessary to mention the yield criterion; that is, the point at which failure of a soil element occurs. The first criterion and by far the most popular is that due to Coulomb (1773):

$$\tau_{ff} = C + \sigma_{ff} \tan \phi \quad \text{Eqn. 2.8}$$

where

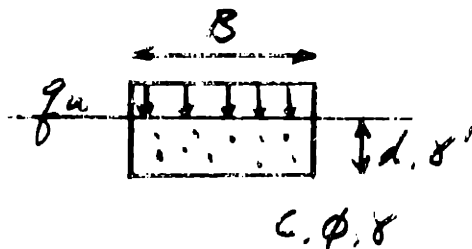
- $\tau_{ff}$  = shear stress on the failure plane at failure
- $\sigma_{ff}$  = normal stress on the failure plane at failure
- C = cohesion intercept
- $\phi$  = friction angle

This criterion was used by all the investigators to be discussed in this section. Much research, however, has been spent on developing new criteria.

### TERZAGHI

Terzaghi (1943) derived the following equation for the ultimate bearing capacity of a strip on soil:

$$q_u = cN_c + \frac{1}{2}\gamma BN_\gamma + \gamma' dN_q \quad \text{Eqn. 2.9}$$



$q_u$  = unit pressure applied to strip which causes failure

$c$  = cohesion of soil

$\phi$  = friction angle of soil

$\gamma$  = unit weight of soil below base of strip

$\gamma'$  = unit weight of soil above base of strip

$N_c, N_\gamma, N_q$  = Terzaghi bearing capacity factors which depend only on value of  $\phi$

Terzaghi recognized that the smoothness of the base of the strip would affect the value of  $N_c$ ,  $N_\gamma$ , and  $N_q$ . He determined that the factors would decrease in magnitude with increasing smoothness. However, he also found that a strip would behave as if it were perfectly rough even if the angle of base friction were very much smaller than the friction angle of the soil. And so Terzaghi made all his computations assuming a rough base.

For the case of  $c = 0$ ,  $d = 0$ , the Terzaghi method for determining  $N_\gamma$  is shown in Fig. 2.1. An elastic wedge and a passive Rankine wedge are assumed with the dimensions shown and a logarithmic spiral is assumed between points A and C with its origin at O. (Terzaghi neglected the fact that at point A, the spiral is not tangent to the Elastic wedge; he felt that the error was unimportant.)  $N_\gamma$  is then calculated by balancing the moments about O. (The value of the logarithmic spiral now becomes apparent, for along this curve the moment about O due to the friction forces  $F$  is zero.) It can be shown that  $\gamma$  and  $B$  divide out of the equation and thus  $N_\gamma$  is found to be a function only of  $\phi$ .  $N_\gamma$  vs.  $\phi$  is shown in Fig. 2.2.

The Terzaghi solution for  $N_\gamma$  as well as  $N_c$  and  $N_q$  assumes that the maximum shear strength of the soil (given by Eqn. 2.8) is developed all along the failure surface. Expressed another

way, this implies that the soil must be nearly incompressible or expand during shear. This is true only of dense soils; loose soils compress during shear. Terzaghi also realized that the deformation characteristics of the soil would affect the ultimate bearing capacity. For loose soils, he recommended that  $\phi$  and  $c$  be reduced to  $\phi'$  and  $c'$ ; he suggested lower limiting values of:

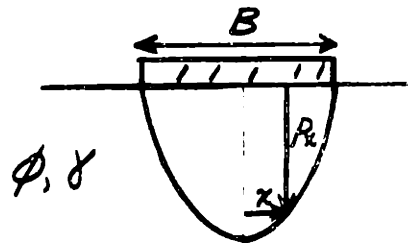
$$c' = \frac{2}{3}c$$

$$\phi' = \tan^{-1} \left( \frac{2}{3} \tan \phi \right) \quad \text{Eqn. 2.10}$$

Using the same approach by which he calculated  $N_\gamma$ , Terzaghi concluded that the contact pressure between a rough strip resting on the surface of cohesionless soil at the ultimate load would be "roughly parabolic", with the edge stress equal to zero.

Assuming a parabolic distribution, the contact stress is then given by:

$$p_x = 3\gamma N_\gamma \left( \frac{B}{4} - \frac{x^2}{B} \right) \quad \text{Eqn. 2.11}$$



### MEYERHOF

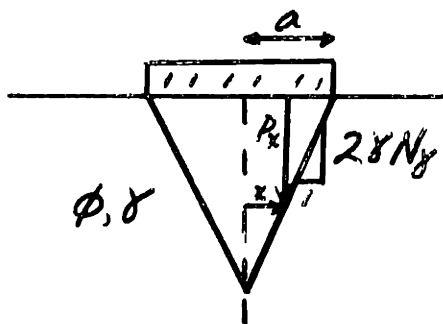
The most comprehensive review of bearing capacity is that of Meyerhof (1952). Meyerhof used essentially the same approach as Terzaghi to evaluate  $N_\gamma$ , with one important difference. Whereas Terzaghi restrained the origin of the logarithmic spiral to be located at the edge of the strip, Meyerhof permitted the origin to vary and solved for the minimum value of  $N_\gamma$ . As mentioned

above, Terzaghi felt that the error would be small, and Fig. 2.2 ( $N_\gamma$  vs.  $\phi$ ) indicates that he was right.

Meyerhof, besides evaluating  $N_\gamma$  for a strip on the surface of a soil, calculated  $N_c$ ,  $N_q$ , and  $N_\gamma$  for foundations on slopes and at depth. In the case of a purely cohesive soil, he found  $N_c$  and  $N_q$  for circular, square and rectangular foundations, as well as considering the effect of the deformation characteristics of the soil. In addition, Meyerhof found that for a smooth strip, the value of  $N_\gamma$  would be exactly half that for a rough strip; this is also shown in Fig. 2.2.

Although Meyerhof used the same approach as Terzaghi in calculating  $N_\gamma$ , he arrived at a different distribution for the contact stress beneath a rough strip at the ultimate load. Meyerhof determined that the stress distribution would be triangular in shape:

$$p_x = (a - |x|) 2\gamma N_\gamma \quad \text{Eqn. 2.12}$$



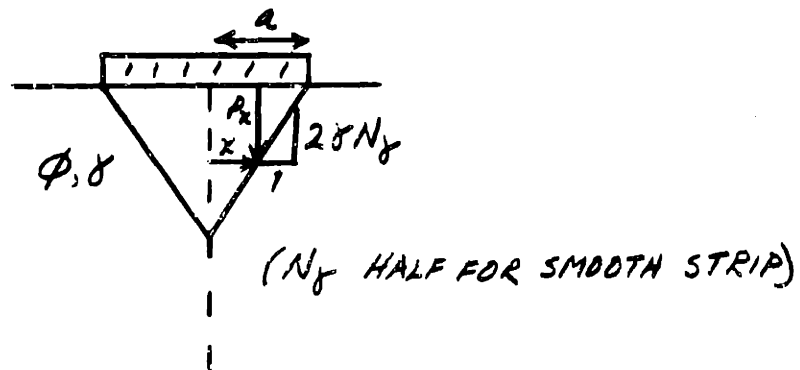
#### SOKOLOVSKII

Another solution to the bearing capacity problem is that of Sokolovskii (1965), who has developed a comprehensive approach to plasticity theory based on the method of characteristics. Sokolovskii has calculated  $N_\gamma$  vs.  $\phi$  for a smooth strip on incompressible soil; this is shown in Fig. 2.2. As can be seen, Sokolovskii's  $N_\gamma$  differs only slightly from the  $N_\gamma$  calculated by Meyerhof (smooth strip).

The method of characteristics involves calculating the stresses in the entire yielded zone (whereas the method of Terzaghi and Meyerhof only requires the stresses in the Passive Zone); as a result, a very accurate determination of the contact stress beneath a strip at the ultimate load is obtained.

Sokolovskii found that the distribution would be triangular in shape (as did Meyerhoff):

$$p_x = (a - |x|) 2\gamma N_\gamma \quad \text{Eqn. 2.13}$$



### 2.3 ELASTIC-PLASTIC THEORY

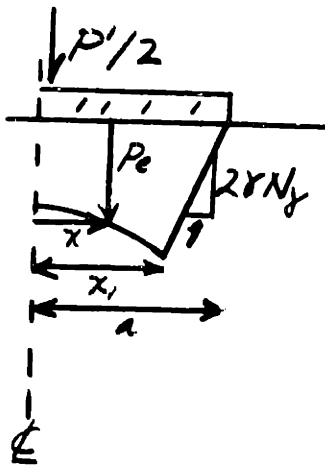
Elastic Theory is used to analyze situations far from failure; Plasticity Theory is used to analyze situations at incipient failure. But the most interesting cases are those which are somewhere between these two extremes. With the advent of the electronic computer, it has now become possible to analyze the wide range of elastic-plastic problems.

Christian (1966) has developed computer programs for the analysis of soils with different yield criteria, such as Tresca and Drucker-Prager (1952), but not Mohr-Coulomb (Eqn. 2.8). To date, the only solutions have been for a uniform strip load on homogeneous elastic-plastic soils, and thus Christian's results are not directly applicable to this work. Clearly, however, a similar approach is required before a rigid plate resting on an elastic-plastic soil can be adequately analyzed.



SCHULTZE

Without benefit of a computer solution, Schultze (1961) attempted to combine the Boussinesq solution (Eqn. 2.1) with the Meyerhof solution (Eqn. 2.12). Schultze recognized that the Boussinesq solution is impossible for real soil, and that failure would occur at the edge. He assumed that the distribution in the interior of the plate would adjust to pick up the stress lost at the edge, but would retain a shape similar to that given by Boussinesq. The result for a cohesionless soil is shown below.



$$P'/2 = P'_e + P'_p$$

$$P'_p = a^2 \gamma N_\gamma (1-\beta)^2$$

$$\beta = x_1/a$$

$$f(\beta) = \frac{P'}{2a^2 \gamma N_\gamma} = 2(1-\beta)(1-\beta^2)^{1/2} \sin^{-1} \beta + (1-\beta)^2 \quad \text{Eqn. 2.14}$$

$$P_e = \frac{P'_e}{\sin^{-1} \beta (a^2 - x^2)^{1/2}} \quad \text{Eqn. 2.15}$$

The Schultze Model is not rigorous, as it involves a number of simplifying assumptions, but it appears to be a rational approach to the problem. Also, Schultze presented field data to support his conclusions.

## CHAPTER 3

### NON-HOMOGENEOUS ELASTIC HALFSPACE

It was originally intended that a finite element analysis be made for a rigid plate resting on an elastic-plastic soil. When the numerical difficulties proved insurmountable, the author ran a series of computer runs (Appendix D) considering the soil to be only elastic. Since Zaretsky and Tsytovich (1965) and Gibson (1967) have already begun the analysis of a non-homogeneous incompressible halfspace in which  $E$  increases linearly with depth, it was decided to extend these solutions for other values of  $\nu$  and to consider plate roughness as well.

Since failure occurs at the edge of a real plate on soil, the solutions herein can only be used at high factors of safety, for which the edge failure can be neglected, but certain of the results have important consequences on the experimental investigation described in Chapter 4. It was found that the value of  $\nu$  strongly affects the settlement of the strip, as well as the distribution of horizontal stress in the soil mass. It was found that plate roughness did not affect the distribution of vertical and horizontal stresses in the soil, nor did it change the magnitude of the settlement. Also, very importantly, it was found that the contact shear stresses beneath the plate are of such small magnitude that any real plate would necessarily be rough. And further, the solution indicates that the distribution of contact stress in the interior of a real plate (where the soil is still elastic) will be uniform.

### 3.1 FINITE ELEMENT GRID

The grid that was employed in the analysis is shown in Fig. 3.1. Since the conditions beneath the rigid plate are symmetrical with respect to the centerline, it is only necessary to find half of the solution. It must be recognized that the mathematical model is not a halfspace nor is it infinite in breadth. However, the dimensions were chosen such that the effect of the rigid boundaries would be small near the plate.

### 3.2 NON-HOMOGENEITY

A non-homogeneous soil is one whose properties vary from point to point. As a first simplification, most analyses assume the soil properties vary only in the vertical direction and are constant in any horizontal direction; this was also assumed here. In addition, a common assumption is that the stress-strain curves for soils are approximately proportional to the confining stress, or

$$E = m\sigma \qquad \text{Eqn. 3.1}$$

This was assumed in the present analysis; and since the confining stress increases linearly with depth,

$$E = m\gamma z \qquad \text{Eqn. 3.2}$$

(Note that E is independent of the stresses imposed by the plate.) Finally, it has been observed that the volumetric strain vs. the major principal strain is independent of the confining stress, or

$$v = \text{const.} \qquad \text{Eqn. 3.3}$$

This was also assumed.

### 3.3 EFFECT OF $v$ - SMOOTH PLATE

A series of computer runs were made in which a smooth plate was pushed into the layer 0.0001 M; only the value of  $v$  was

varied from run to run. The results are shown in Fig. 3.2; the halfspace solution from Gibson (1967) is also shown. Several conclusions can be drawn from Fig. 3.2: (1) The rigid boundary at the bottom of the finite element grid has increased the contact stress at the plate approximately 16% over the theoretical solution for a halfspace. (2) Numerical error has caused a "blip" in the distribution of stress at the edge; this is unavoidable with the finite element method since the theoretical solution predicts infinite volumetric strain at the edge and this cannot be accounted for in the method. (3) Although the distribution of stress is generally uniform (as predicted by Gibson), the magnitude is seen to depend very greatly on the value of  $\nu$ .

This last observation deserves further attention, as it was quite an unexpected result. In the case of a rigid smooth circular plate on a homogeneous halfspace, the average contact stress is proportional to  $1/(1 - \nu')$ , which only varies from 1 to 1.33 ( $\nu = 0$  to  $\frac{1}{2}$ ). In the present case, it has been found that the effect of  $\nu$  is 1 to 4.38. What is more, the variation in contact stress is great even for the common range of interest of  $\nu$  ( $\nu = .3$  to  $.5$ ). In the past, more experimental effort has been spent on evaluating  $E$  than on  $\nu$ , since little importance was attached to the value of  $\nu$ . Now it would appear that  $\nu$  is far more important than was suspected. However,  $\nu$  is at least as difficult to evaluate as  $E$ : for a medium-dense sand, the secant value of  $\nu$  can vary from  $1/3$  to  $> 1/2$ . Clearly, if we expect to make meaningful predictions of behavior, all of the soil properties must be evaluated very carefully.

#### 3.4 SMOOTH VS. ROUGH PLATE

A series of computer runs were also made to determine the effect of a rough plate. It was found that for  $\nu \leq .45$ , the rough and smooth solutions for the contact stress were identical (See Fig. 3.3). For  $\nu > .45$ , the contact stress beneath a

rough plate was found to be slightly greater than beneath a smooth plate. These results will be discussed further in Sec. 3.5 .

### NUMERICAL STABILITY

For  $\nu > .4$ , the contact stress beneath a rough plate becomes very erratic; the results for  $\nu = .499$  are shown in Fig. 3.4. However, if an average stress is plotted between the extremes, the distribution is seen to be similar to that for a smooth plate, but of greater magnitude. It appears that the erratic distribution is due to the size of the elements next to the plate; until more accurate solutions are obtained, it is recommended that the average contact stress be used.

Expressed in terms of  $K/G = 2(1 + \nu)/3(1-2\nu)$ ,

<u>Plate</u>	<u><math>\nu</math></u>	<u>K/G</u>	<u>Solution</u>
Rough	.4	4.7	Stable
Rough	.48	24.7	Unstable
Smooth	.499	500	Stable

This suggests that to obtain a stable solution for a rough plate for  $\nu = .499$  will require a much finer mesh beneath the plate than was used in this investigation.

It is well-known that the finite element technique does not work for  $\nu = \frac{1}{2}$ , as the terms in the stiffness matrix go to infinity. Less well-known is how close  $\nu$  can go to  $\frac{1}{2}$ . A series of runs were made for a smooth plate in which input  $\nu$  varied from .4990 to .4999. Then  $\nu$  was back-calculated from the value of the intermediate principal stress (in plane strain,  $\sigma_2 = \nu(\sigma_1 + \sigma_3)$ ). It was found that

<u>Input <math>\nu</math></u>	<u>Back-Calculated <math>\nu</math></u>
.4990	.4989
.4995	.4997
.4998	.4959
.4999	.5019

As input  $\nu$  is increased above .4995, the back-calculated  $\nu$  changes and the compressibility decreases; the contact stresses also decrease below the value obtained for  $\nu = .4990$ . Thus, a value of .499 is sufficiently close to  $\frac{1}{2}$ .

### 3.5 STRESSES AND STRAINS

In the previous sections, we have dealt with the general results of the computer analysis. In this section, the solution will be considered in more detail.

$I_\rho$

The settlement of a rigid plate can be expressed as:

$$\rho = I_\rho \frac{q}{m\gamma} \quad \text{Eqn. 3.4}$$

where  $I_\rho$  is an influence factor, dependent on  $\nu$  and plate roughness.

$I_\rho$  has been calculated and is shown graphically in Fig. 3.5. (The value of  $q$  has been taken as the magnitude of contact stress for the innermost element of the finite element grid, rather than an average stress along the plate; the result is to ignore the blip at the edge.) It can be seen that the difference between a rough and smooth plate is really quite small. In fact, it suggests that the difference is due only to the erratic distribution of stress for rough plates at high values of  $\nu$  (Sec. 3.4) and that if a more accurate solution were available, there would be no difference at all. This result was wholly unanticipated, as it was expected that the shear stresses induced by a rough plate would markedly affect the vertical contact stress. For instance, in Sec. 2.2 it was found that the bearing capacity factor  $N_\gamma$  for a rough plate was twice that for a smooth plate. It was expected that roughness would also strongly alter the elastic solution.

Fig. 3.5 also shows that the Gibson solution for a half-space agrees quite well with the computer solution.

Gibson also calculated the settlement of various points along the centerline beneath the rigid plate; Fig. 3.6 was prepared to compare his solution with the computer's. It can be seen that agreement with the  $\nu = .499$  curve is satisfactory; the reason for the difference is of course the rigid boundary at  $B/z = 3.5$ . Fig. 3.6 also shows the importance of the value of  $\nu$ .

$$\underline{I_{\sigma_v}, I_{\sigma_h}, \text{ and } I_{\tau_h}}$$

The stress distribution in the soil mass beneath a rigid plate may be expressed as:

$$\begin{aligned} \Delta\sigma_v &= I_{\sigma_v} q \\ \Delta\sigma_h &= I_{\sigma_h} q \\ \Delta\tau_h &= I_{\tau_h} q \end{aligned} \qquad \text{Eqn. 3.5}$$

where the I's are influence factors, dependent on  $\nu$ ,  $B/x$ , and  $B/z$ . ( $q$  was defined above.)

$\Delta\sigma_v$  and  $\Delta\sigma_h$  for different values of  $\nu$  are plotted in Fig. 3.7. Of course, the magnitude of the stresses are quite different, but the distributions are also different.

$I_{\sigma_v}$  was calculated from Fig. 3.7 and plotted in Fig. 3.8. The first thing to be observed is that for  $\nu = .499$ ,  $I_{\sigma_v}$  along the centerline agrees quite closely with that for a uniform strip load on a homogeneous halfspace (as predicted by Gibson), but that  $I_{\sigma_v}$  along the edge is very erratic and agrees only in a general way with the homogeneous solution. This latter effect is attributed to the blip at the edge. In addition, it is seen that  $\nu$  affects the value of  $I_{\sigma_v}$  slightly. This was unexpected, as  $\nu$  does not affect homogeneous halfspace solutions for  $I_{\sigma_v}$  for a uniform strip load nor for a uniform smooth rigid plate (Schiffman and Aggarwala, 1961).

$I_{\sigma_h}$  has been calculated along the centerline and is shown in Fig. 3.9. As with  $I_{\sigma_v}$ , the solution for  $\nu = .499$  agrees almost exactly with the homogeneous halfspace solution for  $\nu = 1/2$  (Jurgenson, 1934). The value of  $\nu$  is seen to have a profound effect on the value of  $I_{\sigma_h}$ . The rough rigid boundary in the computer solution causes the curves to turn up at small values of  $B/2$ .

For  $\nu > .4$ , the rough solutions for  $I_{\sigma_v}$  and  $I_{\sigma_h}$  are erratic, but when  $\Delta\tau_h$  was calculated along the bottom of the plate, it was found that the stresses were stable and consistent. Thus,  $I_{\tau_h}$  has been plotted for the whole range of  $\nu$  in Fig. 3.10. Several important conclusions can be drawn from this plot. (1) At about  $\nu = .3$ , no shear stresses are applied; for  $\nu < .3$ , the stresses are inward toward the centerline of the plate; for  $\nu > .3$ , the stresses are outward. (2) The absolute value of the stresses are quite small, which explains why there was no difference between rough and smooth plate solutions. Also, the absolute shear stress for  $\nu = 0$  is greater than that for  $\nu = .499$ , and since the rough and smooth solutions are identical for the former, this lends evidence to the suspicion that the same is true for the latter. (3) Finally, it can be seen that for most soils ( $\nu \geq .3$ ), the angle of friction required to produce a rough plate is less than  $8^\circ$ , even at the edge. It now becomes clear that Terzaghi and Meyerhof (Sec. 2.2) were correct when they assumed any real footing would be rough.

$I_\lambda$

As a counterpart to  $I_{\tau_h}$  for rough plates, the influence factor  $I_\lambda$  for smooth plates was defined:

$$\lambda = I_\lambda \rho \quad \text{Eqn. 3.6}$$

where  $\lambda$  is the horizontal displacement of a point beneath the plate.

$I_\lambda$  has been plotted in Fig. 3.11. The main point here is that the horizontal displacements near the edge of the plate are



large and in the case of  $\nu = .499$  are greater than the settlement.

#### VERTICAL STRAIN

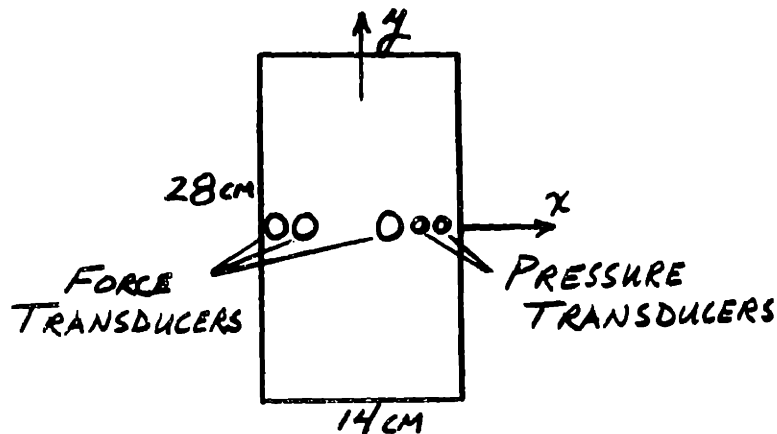
The vertical strain beneath the centerline has been plotted for  $\nu = .4$  and  $.499$  in Fig. 3.12. It can be seen that the distribution of strain is strongly affected by the value of  $\nu$ ; if this plot were for equal average applied stress rather than equal displacement, the contrast would be even greater. Furthermore, it is clear that in model tests, the soil surface is extremely important and care must be taken to avoid over-compaction or hills and valleys.

## CHAPTER 4

### EXPERIMENTAL INVESTIGATION

As explained in Chapter 3, the solution for the non-homogeneous elastic halfspace solution cannot be used directly for comparison with the experimental stress measurements, since the model does not consider failure at the edge. However, the results did show that any real plate would be a rough plate, and that roughness would not affect the elastic portion. In addition, the solution showed that the stresses would be uniform in the central portion of the plate where conditions are still elastic; this is also predicted by the Schultze Model, and as will be shown below, this was observed.

To measure the contact stress distribution beneath a rigid plate (and from this to back-calculate the friction angle of the sand), a scheme was devised which involved a stainless steel loading plate (14 x 28 x 1cm) instrumented with 3 force transducers and 2 pressure transducers (Appendix B; Photographs of the Apparatus). The sensing elements were placed along the short axis of the plate flush with the bottom as shown:



These transducers are similar to those used to measure pore pressure response in undrained triaxial and plane strain tests; they are extremely rigid and the author feels that "arching" was not a problem.

The plate was loaded in stages and pushed into a prepared bed of sand at known densities and strengths (see Table 4.1 and 4.2). The signals from the transducers were recorded on the Remote Data Acquisition system. A computer program was specially written by the author to take the raw data, convert them to stresses, and plot them on a Calcomp plotter attached to an 1130 IBM computer. (Appendix C). The results of these tests are shown in Figs. 4.1 to 4.10. A few comments are necessary to explain what is shown in these figures. The Soil No. in the upper right-hand corner identifies the run in Table 4.1. The numbers in the plots serve two purposes: the location shows the stress at a point beneath the plate; the value of the number refers to the stage number. The solid curves are the predicted stresses for each stage based on the Schultze Model, as modified below. Transducer 1 was accidentally damaged and the data have been neglected in all the analyses. However, in earlier runs (Appendix E), before the transducer was damaged, the stresses were measured near the center line of the plate and found to agree quite well with the predicted stresses.

It should also be noted that Transducers 2 and 4 are on the opposite half of the plate from Transducers 1, 3 and 5. In certain of the runs, it appears the plate tilted slightly, although great care was taken to avoid this. Evidently, in the interior of the plate, where the stresses are "elastic" and thus relatively uniform, tilting did not significantly affect the stresses measured by Transducer 2 (in the interior, the magnitude of the tilting is also less); but near the edge (Transducer 4), it had an important effect, as seen in Figs. 4.1 and 4.3.

Another important problem is local variations in the compactness of the surface of the sand. An extreme case is shown in Fig. 4.4: Transducers 3 and 5 are approximately 1cm apart and yet registered completely different stresses. A new design is proposed in Chapter 5 which would help eliminate this effect.

Despite these difficulties, general agreement with the Schultze Model was obtained, with two notable exceptions. A peak in the distribution was observed near the edge, but did not appear to be as sharp as predicted by Schultze. This transition zone between the elastic portion and the plastic portion needs to be measured more accurately and compared with better theoretical models. In addition, the following phenomenon was observed: at the edge, the stress would usually build up to a maximum and then "slip" to a lower value, where it would sometimes continue to decrease and other times increase, as more load was added to the plate. The Schultze Model predicts that the edge stresses should increase to the failure stress and then remain constant. The author does not know what caused slips to occur; but he believes that the stresses were correctly measured and that the slip phenomenon is due to complex aspects of particulate materials that are not considered in existing soil models.

To back-calculate  $N_c$  from the distribution of stress near the plate edge, it is necessary to determine when the failure stress has been reached. The Schultze Model predicts that this occurs when the contact stress at a point stops increasing and remains constant while more load is added to the plate. Experimentally, however, it has been observed that the contact stress increases to a maximum and then decreases when more load is applied. Clearly, the failure stress is related to this slip; and an algorithm was devised for interpreting these slips, although a comprehensive approach will require far more experience with this technique. Nonetheless, the values of  $N_c$  and  $\phi$  back-calculated by means of the algorithm are remarkably close to the values determined from laboratory shear tests.

#### 4.1 PREVIOUS EXPERIMENTAL INVESTIGATIONS

Although many investigators have predicted the contact stress beneath a rigid plate, few have attempted to measure it; and to the author's knowledge, no one has suggested that the strength of the soil could be back-calculated from the stress distribution.

##### BOND

Bond (1956) ran a series of footing tests on sand while in Uganda and measured the distribution of contact stress beneath different shaped footings. He found the distribution to be roughly uniform, contrary to the results obtained in this work. In a few cases, a slight peak developed, but not of the magnitude observed here. The phenomenon of slippage did not occur at all. The explanation for the contradiction would seem to lie in the measuring system. As no electrical measuring devices were available in Uganda, Bond was forced to use a scheme similar to that employed by Terzaghi in his famous study of the horizontal pressure of soil against a retaining wall. The system consisted of strips embedded in the face of the footings; by measuring the tensile force required to pull these strips and knowing the coefficient of friction between the strip and the sand, the normal pressure could be computed. The author feels that the movement of the strips would change the actual stress beneath the footing and cause erroneous readings.

##### SCHULTZE

Already described in Sec. 2.3 is Schultze's work (1961). He collected data from many field tests which generally tended to support his model. However, most of the tests date from the '30's, before the advent of modern pressure gages. Furthermore, no soil properties were available to predict the stress distribution and compare with the measured values.

##### BARDEN

Barden (1962, 1963) has spent considerable effort in the analysis of flexible plates on an elastic halfspace (including

anisotropy). His theoretical work was not reviewed in Chapter 2, because his approximate solution for a rigid plate is the same regardless of what soil model is selected.

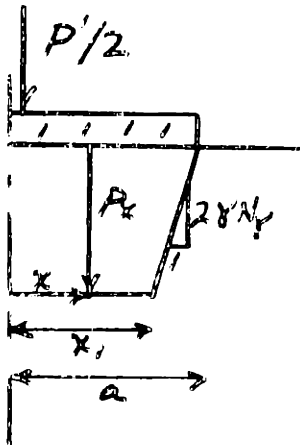
Barden also ran laboratory experiments with an instrumented plate with different flexibilities. The plate was 4 in X 36 in and 11 sensors were mounted along the long axis (opposite to the present tests; he found good agreement with his elastic model.

#### CHAE, HALL and RICHART

Chae, Hall and Richart (1965) measured the static distribution beneath a circular plate as a by-product of their dynamic investigation. The plate was 12 in in diameter and consisted of independent concentric rings. They found the distribution to be roughly parabolic, with zero stress at the edge and maximum stress at the center. However, the average stress applied to the soil was about 5 psi (3500 nwt/m), which is well below failure. As a result, they did not observe the effects described in this thesis.

#### 4.2 SELECTION OF MODEL TO COMPARE WITH DATA

In Chapter 3, the solution for a rigid plate resting on a non-homogeneous elastic halfspace was examined in detail. Although this model is only an approximation to soil behavior, it is an improvement over a homogeneous halfspace. As we saw in Fig. 3 2, the contact stress for the non-homogeneous halfspace is uniform. Of course, for a real soil, this would only be true at high factors of safety, where the behavior is still close to elastic. As the load is increased on the plate, failure occurs at the edge, modifying the distribution. By using the same approach as Schultze (1961), the uniform distribution for the elastic part was combined with the triangular distribution for the plastic part to obtain:



$$\beta = x/a$$

$$\frac{P'}{2a'\gamma N_\gamma} = 1 - \beta' \quad \text{Eqn. 4.1}$$

$$P_x | x \leq a\beta = 2a\gamma N_\gamma (1-\beta) \quad \text{Eqn. 4.2}$$

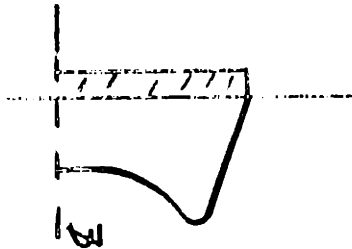
(Compare Eqn. 4.2 with Eqn. 2.14)

Figs. 4.1 to 4.10 show that the measured stresses are relatively uniform beneath the plate at high factors of safety, but at higher loads, a peak usually develops which is not predicted by Eqn. 4.2, but which is predicted by the Schultze Model.

The explanation for this behavior would appear to be due to

the following: for the non-homogeneous elastic halfspace analyzed in Chapter 3, the value of  $E$  is a material property, independent of the loading geometry; for a real soil, the value of  $E$  is very dependent on the imposed loads. As the plate is pushed into the sand, it imposes confining stresses on the soil, resulting in an increase in the value of  $E$  directly beneath the plate. Thus, the soil becomes more homogeneous, and the contact stress distribution in the interior of the plate is similar to that given by Boussinesq. Schultze's assumption of a homogeneous elastic soil has thus resulted in a predicted distribution which is close to the measured one.

It is suspected that the peak in the distribution is actually rounded, rather than sharp:



However, theoretical analyses of elastic-plastic soils are required to predict the stresses and better instrumented plates are required to measure the stresses before it will be possible to improve the Schultze Model.

#### 4.3 VALUE OF $m$ BACK-CALCULATED FOR WHOLE PLATE

In Sec. 4.2 above, it was found that the non-homogeneous solution is better than the homogeneous solution, but that there was no way yet to combine the former with the plastic solution for failure at the edge. On the other hand, at high factors of safety, the fact that failure is occurring at the edge may be neglected and the non-homogeneous solution is a good approximation. Accordingly, the settlement of the whole plate was analyzed; the value of  $m$  (the ratio between  $E$  and  $\sigma$ ) was back-calculated from the settlement data for the first stage of loading. The value of  $I_\rho$  was obtained from Fig. 3.5, assuming  $\nu = .4$ , a typical value for sands. (Actually,  $\nu$  is dependent on relative density, but in this analysis, it was



assumed to be constant ) The result of these calculations is shown in Fig. 4.11 .

The results of triaxial tests run on the soil used in the plate bearing tests are summarized in Figs. A.6 to A.8. It can be seen that the value of  $m$  is almost independent of the relative density, whereas  $m$  from the plate load tests showed a strong dependence on relative density. Furthermore, the value of  $m$  from the plate is 1.5 to 4 times greater than the  $m$  determined from the triaxial tests. There are several reasons for these discrepancies: the tests were triaxial, while most of the plate experienced plane strain; the tests started from isotropic consolidation, while the tests were run at significantly higher stresses than were imposed by the loading plate. In addition, the initial tangent modulus in standard soil mechanics tests is usually inaccurate, since the modulus begins to decrease at very small strains. It is clear, then, that a plate-load test is much more valuable than standard laboratory tests for a settlement prediction of a footing on sand. The value of  $m$  back-calculated from a plate-load test also provides a parameter for comparing the deformation characteristics of soil deposits.

#### 4.4 MODIFICATION OF SCHULTZE MODEL

Schultze's equations were derived for the case of plane strain, whereas the actual plate dimensions are 2 to 1. The end effects change the value of  $\beta$  (and thus the elastic portion) but the slope of the plastic portion remains unchanged (assuming the central portion of the plate is in plane strain; this is discussed in Appendix B). It thus became necessary to modify Schultze's equations. First, it was assumed that the width of the plastic zone would be the same everywhere beneath the plate; that is,  $\beta = \text{const}$ . Next, it was assumed that the elastic distribution was dependent only on  $x$ , and not on  $y$ . Eqn. 2.14 then becomes:

$$f(\beta) = \frac{P'}{2a^2 \gamma N_\gamma} = \frac{2(1-\beta)(k+\beta-1)}{k} \sin^{-1} \beta (1-\beta^2)^{\frac{1}{2}} + (1-\beta)^2 \left(\frac{k+\beta}{k}\right)$$

Eqn. 4.3

where  $k = L/B$

for the experimental plate,  $k = 2$  and Eqn. 4.3 is plotted in Fig. 4.12. It can be seen that the correction is only important for low values of  $\beta$ , or very near failure. Eqn. 4.3 was input into the computer and the solid curves in Figs. 4.1 to 4.10 are based on this correction.

#### 4.5 SELECTION OF $\phi$ AND $N_\gamma$

##### $\phi$ - PLANE STRAIN

In Sec. 4.4 above, it was assumed that the transducers would experience stresses due to plane strain. It has been found that the plane strain  $\phi$  is different from the  $\phi$  found from triaxial compression tests. However, as very limited plane strain data were available for this soil, it was necessary to use other tests and attempt to predict the plane strain behavior.

A series of direct shear tests were run, but were found to be uninterpretable in terms of the Davis-factors  $N_{\phi f}$  and  $\mu$  (Davis, 1968; Appendix F). The results are presented in Table A.1 and Figs. A.3 to A.5. This necessitated running a series of triaxial compression tests (isotropic consolidation); the results are summarized in Table A.2 and Figs. A.6 to A.8. It was found that these tests could be used to find the Davis-factors (see below). Furthermore, it was found that the friction angle ( $c = 0$ ) in the triaxial tests was less dependent on the normal stress than in the direct shear tests; in addition, the triaxial tests were more internally consistent than the direct shear tests. For these reasons, it was decided to discard the direct shear test results and deal solely with the triaxial compression tests.

The triaxial data are presented in terms of the Davis factors in Fig. 4.13 . To calculate  $N_{\phi_f}$  and  $\mu$ , the maximum values of  $(\sigma_1/\sigma_3)$  and  $(d\varepsilon_{vol}/d\varepsilon)$  were used. (See Table A.2) A straight line was fitted through the data points and  $\phi$  (triaxial) was back-calculated as shown in Fig. 4.14 for comparison. Then, since  $N_{\phi_f}$  and  $\mu$  are supposed to be independent of the lab test, the plane strain  $\phi$  was calculated (Fig. 4.15).  $\phi_{ps}$  calculated in this way seemed too large and so it was decided to compare these results with those of Bishop (1957). Bishop found that  $\phi_{ps}$  for dense sands is about 10% greater than  $\phi_{tri}$ ; this was plotted in Fig. 4.16 . It can be seen that the Davis-factors lead to much larger values of  $\phi_{ps}$  than those obtained by increasing  $\phi_{tri}$  10%, and so it was decided to use a  $\phi_{ps}$  10% greater than  $\phi_{tri}$ ; the final result is shown in Fig. 4.17 as well as Table 4.2 .

#### $\phi$ - CURVATURE AND LOCAL SHEAR

In Fig. 4.14, it was seen that  $\phi_{tri}$  was dependent on the normal stress. This phenomenon has long been recognized and contributes to the difficulty of interpreting bearing capacity tests with small plates (De Beer, 1965). In arriving at  $\phi_{ps}$ , this curvature of the Mohr-Coulomb envelope was neglected for a number of reasons. First, it is not yet possible to analyze what effect this would have on the contact stresses. Second, there is no way of telling how much curvature exists for  $\phi_{ps}$ , since all the tests were for  $\phi_{tri}$  .

In addition, an analysis was made for the bearing capacity of the plate as a whole. The load settlement curves for the tests are plotted in Fig. 4.18. The ultimate load was then predicted, employing various empirical corrections, including De Beer's correction for curvature. These predictions are given in Fig. 4.19; the actual failure load (at  $\rho = 10\% B$ ) is also shown for comparison. It can be seen that De Beer's simple correction for shape gives the best agreement, and that including curvature greatly overestimates the failure load. Also, it was

found that to use the curvature correction for small plates, it is necessary to run the tests at extremely low stresses.

Also plotted on Fig. 4.19 is the predicted failure load if the soil were to fail in local shear (Eqn. 2.10). As we would expect, as the relative density decreases, the actual failure load approaches this limiting value.

$N_{\gamma}$

Although it is clear local shear effects were occurring in the lower densities, it was decided to use Meyerhof's solution for  $N_{\gamma}$ , shown in Fig. 2.2. In Fig. 4.20, the load-settlement curves are normalized. The fact that the curves bunch together, even for the loose soils, lends support to the decision to neglect local shear.

#### 4.6 EVALUATION OF RESULTS

While examining the results of the tests, it became apparent that the predicted and measured stresses were in better agreement in the interior of the plate than at the edge. For purposes of an error analysis, it was decided to divide the plate into two zones; Elastic and Plastic.

##### ELASTIC ZONE

The results of an error analysis of the stresses in this zone are shown in Fig. 4.21. The data include results from two earlier series of runs as well (Appendix E). These data show that the predicted stresses are within 15% of the measured stresses, and the error tends to decrease with increasing relative density and increasing average plate stress. It also shows the tests are repeatable within 10% or less.

Although there is a marked tendency to overestimate the stresses in the elastic zone, this was not true in all cases. There are insufficient data at this time to attempt to empirically improve the model.

## PLASTIC ZONE

The good agreement between predicted and measured stresses in the Elastic Zone is due in part to the simple, almost uniform distribution in that portion of the plate. In the plastic zone, the predicted distribution is steep at the edge. As a result, the agreement is much worse. This is shown in Fig. 4.22. Not only is the error large, it is erratic and unrepeatabile.

### ALGORITHM FOR BACK-CALCULATING $N_Y$

Although the magnitude of the stresses in the plastic zone are often greatly in error, the slope of the distribution determined by the failure stresses is usually close and repeatable. Since this slope is equal to  $2\gamma N_Y$  (Sec. 2.3), this technique offers the possibility of back-calculating  $N_Y$ . An algorithm was devised to select an experimental value of  $N_Y$ .

In examining the results of the tests, it will be seen that at the edge the measured stress usually builds up to a maximum value and then "slips" to a lower value. The algorithm is based on these slips:

- (1) If no slips occur, the maximum stress registered by the transducer closest to the edge is used to calculate  $N_Y$ .
- (2) If slippage occurs, the stress measured immediately after the slip is used. If two or more slips occur, an average slope is taken as well.

Using this algorithm,  $N_Y$  was back-calculated for the series of runs and is shown in Fig. 4.23. The agreement with the predicted value, although not perfect, is remarkably good. (The one wild data point comes from Fig. 4.4 and was discussed in the introduction to this chapter.) Furthermore, if  $\phi_{ps}$  is then taken from  $N_Y$ , as shown in Fig. 4.24, very good agreement is also obtained.

It must be admitted that the algorithm that was chosen was based on a desire to achieve the best agreement between

prediction and measurement; a comprehensive method for interpreting the data has not been developed. For instance, the significance of the maximum stress before slip occurs is not completely understood. It will require many more tests on many different soils before as much faith can be placed in this technique as is placed in the bearing capacity test. On the other hand, Fig. 4.19 has shown that interpretation of the latter is also a difficult task.

## CHAPTER 5

### IN SITU TESTING DEVICES FOR THE LUNAR SURFACE

The original impetus for this thesis was to develop a new in situ testing device for measuring the strength of the lunar soil. A new application of bearing capacity theory has been explored in the preceding chapters; this chapter contains specific recommendations for a device to be used on the moon. These recommendations are based on a review of existing terrestrial soil mechanics devices, and on the author's experiments with the instrumented plate.

It must be recognized that the selection of a device depends on lead time, required degree of sophistication, purpose of tests, time allotted for experiment, astronaut limitations, etc. For example, the astronaut is capable of applying only about 30lb. of force on the lunar surface; a hand-operated plate bearing test of any size is thus out of the question. With these problems in mind, the proposed measuring systems have been arranged below in order of decreasing desirability and are summarized in Table 5.1.

Not considered in this study is the very basic and important problem of determining the unit weight of the soil. On earth, various methods are employed, such as undisturbed sampling, sand displacement, and gamma ray (Meigh and Skipp, 1960). This problem must be thoroughly explored to select the method which is most compatible with the special constraints imposed by the lunar environment.

#### 5.1 INSTRUMENTED PLATE

The concept of measuring the stress distribution beneath a rigid plate to determine the strength parameters of soil has been found to be valid; and it is clearly more useful than just

a plate-bearing test. For these reasons, it is recommended that this technique be used. However, a far better design is possible. This is shown in Fig. 5.1; it would consist of twenty-four separate parallel strips which are constrained to move as a unit, but the force on each strip can be measured separately by means of load cells. (This is the same idea as the concentric rings of Chae, Hall, and Richart, 1965.) In addition, the "plate" would consist of three sections along the long axis: an inner section of the strips for the actual measurements in plane strain; and two outer sections (which move with the inner section but are independent), thus ensuring plane strain conditions in the central portion. This design would greatly reduce the effect of local variations, as well as permit a larger grain size than in the present investigation.

The design in Fig. 5.1 involves 56 load cells and will yield a very detailed description of the stress distribution beneath the plate; but it will also require a large data collection system. An alternate design has been devised (Fig. 5.2) which requires only 26 load cells. This design emphasizes the edge effect observed in the present tests, but less detail is obtained in the inner portions. This design is considered a minimum if this technique is to be used successfully on the lunar surface. The type of design employed in the present investigation is not recommended, as this approach is only useful in the laboratory where the soil surface can be carefully prepared.

### LOADING SYSTEM

There are several types of loading systems that could be used with the instrumented plate.

#### Roving Vehicle

To obtain the most information about the lunar surface, tests should be run at many different points. The best loading system for the instrumented plate would be



a strain-controlled jack mounted on a lunar roving vehicle. Periodically, the vehicles will be stopped for observations; a plate-load test could easily be included during each stop. Of course, the roving vehicle could be manned or unmanned. The total load applied to the plate would be limited of course by the location of the jack and the weight of the vehicle.

#### Lunar Excursion Module

Unfortunately, roving vehicles will not be sent to the moon for some time. Until such vehicles become available, it will be necessary to run plate bearing tests by jacking against the LEM (Lunar Excursion Module). This limits the area of investigation to the near vicinity of the LEM, which will undoubtedly be disturbed during the landing. This is an unfortunate situation, but can only be overcome by providing a sufficient resisting force at the test location.

#### 5.2 CONE PENETROMETER

The use of the instrumented plate is limited by the requirement for a large resisting force. Reducing the dimensions of the plate to a size which could be operated by the astronaut is not recommended for two reasons: a small instrumented plate would not be capable of detecting the stress distribution accurately enough to determine the soil strength; and a standard plate test on a very small plate is extremely difficult to interpret.

Since it is not possible to use a soil mechanics test based on theory, it is necessary to turn to tests which are based on empirical experience and which can be operated manually by the astronaut. A vane shear test has been suggested, but on earth, this test is valuable only for testing clays; in other soils, the stress system associated with the vane is so complex that it is impossible to interpret the results.

The cone penetrometer, on the other hand, has been found useful for testing a variety of terrestrial soils and its use is recommended on the lunar surface. It must be recognized that the cone penetrometer has a limited value for determining the strength parameters of the lunar surface, but it will give a qualitative measure of the strength and it offers a simple, rapid method for measuring the spatial non-homogeneity of the lunar surface, as well as for comparing the results with terrestrial soil deposits.

One important improvement can be made on the standard hand-held cone penetrometer test. Usually, the cone is forced into the soil a given distance and the force measured; thus, only one data point is obtained for each test. The complete force-displacement curve would be far more valuable for making comparisons. A reference system is necessary for measuring the displacement of the cone; one possibility is double integration of the signal from an accelerometer mounted on the cone.

### 5.3 LEM FOOTPADS

Regardless of whether the above tests are run, the force on all four of the LEM footpads should be measured during and after landing. Such data will aid in the analysis of the dynamic and static bearing capacity of the lunar surface, as well as providing a comparison between different sites.

This type of instrumentation was used on the Surveyor probes and was planned for the LEM at one time, but apparently has now been removed. The need for this instrumentation cannot be overstated.

### 5.4 ASTRONAUT FOOTPRINT

It has been suggested that photographs of the astronaut footprints would be a simple, easy method to test the soil surface. A "controlled" footprint, without eccentricity and

dynamic effects, would be difficult to achieve. Furthermore, the astronaut can apply only a very small stress: less than 1 psi. But footprints would give an estimate of the non-homogeneity of the lunar surface.

## CHAPTER 6

### CONCLUSIONS AND RECOMMENDATIONS

1. Measurements of the contact stress distribution beneath a rigid plate resting on a quartz sand have indicated that the stresses are close to those predicted by the Schultze Model. However, there are still many facets of bearing capacity which are understood too well. This investigation has left many questions unanswered, and raised more questions as well. The technique is not sufficiently developed to replace a standard bearing capacity test, but it has been shown to have great promise as a new tool, and more work in this area is strongly recommended.

2. It has become clear that a far better design for the instrumented plate is possible. This would consist of separate parallel strips which are constrained to move as a unit, but the force on each strip can be measured separately. In addition, the "plate" would consist of three sections along the long axis: an inner section of the strips for the actual measurements in plane strain; and two outer sections (which move with the inner section but are independent), thus ensuring plane strain conditions in the central portion. This type of design would greatly reduce the effect of local variations, as well as permit a grain size larger than in the present investigation. Improvements in the load frame, soil bin, etc., are described in Appendix B.

3. A great deal of theoretical work is required in this area. Finite element computer programs should be developed to handle elastic-plastic soils with different yield criteria. (It should be mentioned that several months were spent unsuccessfully attempting to modify the finite element program of Appendix D to analyze a Mohr-Coulomb soil; but the author is confident that a solution can be obtained.) Special areas of interest are the phenomena of curvature and local shear. These effects are poorly understood and deserve far more work. In

addition, other non-homogeneous models for the elastic behavior should be investigated (such as  $E$  proportional to  $\sqrt{\sigma}$ ), as well as the effect of imposed stresses on the value of  $E$ .

4. A lunar in situ testing device consisting of the improved instrumented plate above is recommended. However, since the plate cannot be operated manually, it will be necessary to jack against the LEM or a roving vehicle. A hand-held cone penetrometer should also be used for making comparisons between lunar sites and with terrestrial soils. The LEM footpad instrumentation should be reinstated.

5. The whole area of cohesive soils has been neglected in this study. The Schultze Model can be modified to include cohesion, and the theoretical work above should also consider this in detail. Experiments should be run and the results compared with theoretical predictions. Included in this study should be brittle materials which lose their cohesion during shear.

6. Another major problem that must be considered is the in situ determination of the unit weight. In order to interpret the results of the plate bearing tests, measurements of the unit weight of the soil must also be made.

7. It is recommended that in future studies, a comprehensive series of plane strain tests be made on the soil used in the experiments. This avoids the problem of using other tests (such as triaxial) to determine the plane strain soil properties.

8. The concept of the instrumented plate can be used in other areas of soil mechanics also: bearing capacity of normally consolidated clays (this might include pore pressure measurements at the contact as well); effect of eccentricity; repeated load tests; time-dependent phenomena in soils.

## REFERENCES

- Barden, L. (1962), "Distribution of Contact Pressure Under Foundations," Geotechnique, Vol. 12, pp. 181-198.
- Barden, L. (1963), "Stresses and Displacements in a Cross-Anisotropic Soil," Geotechnique, Vol. 13.
- Barden, L. (1963), "Winkler Model and its Application to Soil," The Structural Engineer, Vol. 41, pp. 279-280.
- Bishop, A. and N. Janbu (1957), Discussion on "Soil Properties and Their Measurements," Proc., 4th ICSMFE, London, Vol. 3, p.103.
- Bishop, A. and D. Henkel (1962), The Measurement of Soil Properties in the Triaxial Test, Edward Arnold, London.
- Bond, D. (1956), "The Use of Model Tests for the Prediction of Settlement Under Foundations in Dry Sand," A Thesis submitted for the External Degree of Doctor of Philosophy in the Faculty of Engineering, University of London.
- Boussinesq, J. (1885), Application des Potentiels a l'Etude de l'Equilibre et du Mouvement des Solides Elastiques, Gauthier-Villard, Paris.
- Chae, Y.S., J.R. Hall, Jr., and F.E. Richart, Jr. (1965), "Dynamic Pressure Distribution Beneath A Vibrating Footing," Proceedings, 6th ICSMFE, Vol. II, pp. 22-26.
- Christian, J.T. (1966), "Two-Dimensional Analysis of Stress and Strain in Soils," Contract Report No. 3-129 Conducted for US Army Engineer Waterways Experiment Station.
- Coulomb, C.A. (1773), "Essai Sur Une Application des Regles Maximis et Minimis a quelques Problems de Statique, Relatifs a l'Architecture," Memoirs de Mathematique et de Physique, Paris, pp. 343-381.
- Cox, A.D. (1963), "The Use of Non-Associated Flow Rules in Soil Plasticity," Royal Armament Research and Development Establishment Report (B)2/63.
- D'Appolonia, D.J. (1968), "Prediction of Stresses and Deformations in Soil Bodies for Undrained Loading Conditions," Thesis submitted in partial fulfillment of the requirements for the degree of Doctor of Science, MIT.
- Davis, E.H. (1968), "Theories of Plasticity and the Failure of Soil Masses," Chap. 6 from Soil Mechanics, Selected

Topics, ed. by I.K. Lee, to be published by Butterworths, London.

- De Beer, E.E. (1965), "Bearing Capacity and Settlement of Shallow Foundations on Sand," Proceedings, Duke University Conf. on Bearing Capacity and Settlement of Foundations.
- Drucker, D.C. and W. Prager (1952), "Soil Mechanics and Plastic Analysis or Limit Design," Quarterly of Applied Mathematics, Vol. 10, No. 2, pp. 157-165.
- Drucker, D.C., R.E. Gibson, and D.J. Henkel (1957), "Soil Mechanics and Work-Hardening Theories of Plasticity," Transactions, ASCE, Vol. 122, pp. 338-346.
- Eggestad, A. (1963), "Deformation Measurements Below a Model Footing on the Surface of Dry Sand," Proceedings, European Conf. on SMFE, Vol. I, pp. 233-239.
- Feda, J. (1961), "Research on the Bearing Capacity of Loose Soils," Proceedings, 5th ICSMFE, Vol. I, pp. 635-642.
- Feda, J. and L. Pruska (1965), "Bearing Capacity and Critical Loads - Two Comments," Proceedings, 6th ICSMFE, Vol. II, pp. 46-50.
- Gibson, R.E. (1967), "Some Results Concerning Displacements and Stresses in a Non-Homogeneous Elastic Half-Space," Geotechnique, Vol. 17, pp. 58-67.
- Hansen, B. (1961), "The Bearing Capacity on Sand, Tested by Loading Circular Plates," Proceedings, 5th ICSMFE, Vol. I, pp. 659-664.
- Jurgenson, L. (1934), "The Application of Theories of Elasticity and Plasticity to Foundation Problems," Journal of the Boston Society of Civil Engineers.
- Lambe, T.W. (1951), Soil Testing for Engineers, John Wiley & Sons, Inc., New York.
- Livneh, M. (1965), "The Theoretical Bearing Capacity of Soils on a Rock Foundation," Proceedings, 6th ICSMFE, Vol. II, pp. 122-126.
- Meigh, A.C., and B.O. Skipp (1960), "Gamma-Ray and Neutron Methods of Measuring Soil Density and Moisture," Geotechnique, Vol. 10, pp. 110-126.

- Meyerhof, G.G. (1952), "The Ultimate Bearing Capacity of Foundations," Geotechnique, Vol. 2, pp. 301-332.
- Meyerhof, G. (1963), "Some Recent Research on the Bearing Capacity of Foundations," Canadian Geotechnical Journal, Vol. 1, No. 1, pp. 16-26.
- Roscoe, K.H., A.N. Scofield, and A. Thurairajah (1963), "Yielding of Soils in States Wetter than Critical," Geotechnique, Vol. 13, No. 3, pp. 211-240.
- Schiffman, R.L., and B.D. Aggarwala (1961), "Stresses and Displacements Produced in a Semi-Infinite Elastic Solid by a Rigid Elliptical Footing," Proceedings, 5th ICSMFE, Vol. 1, pp. 795-801.
- Schultze, E. (1961), "Distribution of Stress Beneath a Rigid Footing," Proceedings, 5th ICSMFE, Vol. 1, pp. 807-813.
- Sokolovskii, V.V. (1965), Statics of Granular Media, Pergamon Press, New York.
- Sowers, G.F. (1962), "Shallow Foundations," Chap. 6 in Foundation Engineering, ed. by G.A. Leonards, McGraw-Hill, Inc., New York.
- Terzaghi, K. (1943), Theoretical Soil Mechanics, John Wiley and Sons, Inc., New York.
- Zaretsky, Yu K., and N.A. Tsytoovich (1965), "Consideration of Heterogeneity and Non-Linear Deformation of the Base in the Design of Rigid Foundations," Proceedings, 6th ICSMFE, Vol. II, pp 222-225.
- Sadowsky, Z. (1930), Z. angew Math. Mech., Vol 10, p. 77.



## BIOGRAPHY

William David Carrier, III was born on December 21, 1943 in Allentown, Pennsylvania. He received his high school diploma from Point Loma High School in San Diego, California in June, 1961. He entered the Massachusetts Institute of Technology in September, 1961 and received the SB degree in June, 1965 and the SM degree in September, 1966.

His professional experience includes a summer job with Dames & Moore (1967) in New York City as a Staff Engineer and part-time work with T. William Lambe & Assoc. during most of his graduate study at MIT.

He is a member of Sigma Xi and Chi Epsilon, honorary societies. He is also an Associate Member of the American Society of Civil Engineers.

## NOTATION

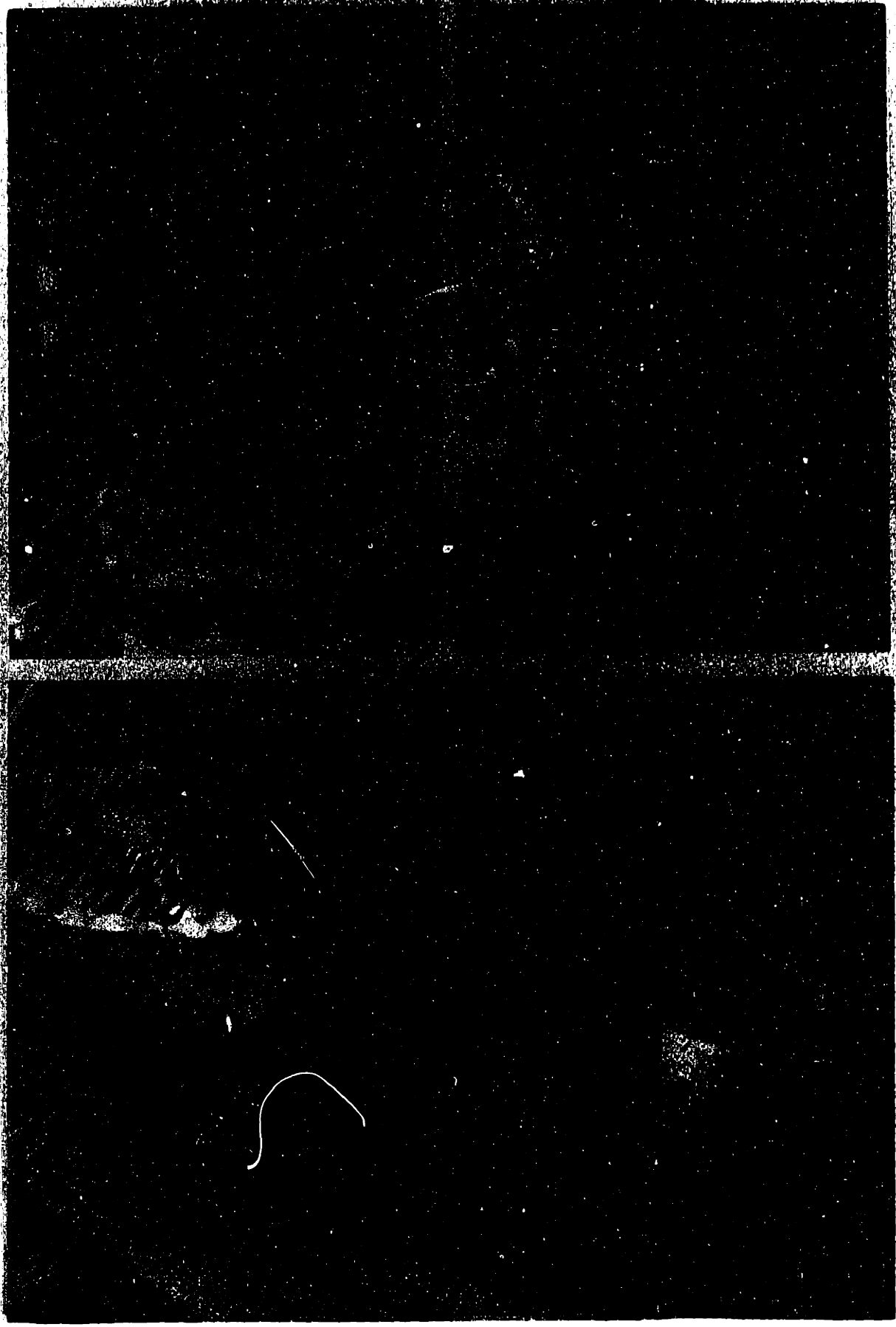
a	Plate Halfwidth
B	Plate Width
b	Plate Halfwidth
c	Cohesion Intercept on Mohr-Coulomb Failure Envelope
c'	Reduced Value of c to Account for Local Shear
$D_R$	Relative Density
E	Young's Modulus
e	Void Ratio
G	Shear Modulus; Specific Gravity
$I_\lambda$	Horizontal Displacement Influence Factor
$I_\rho$	Vertical Displacement Influence Factor
$I_{\sigma H}$	Horizontal Normal Stress Influence Factor
$I_{\sigma V}$	Vertical Normal Stress Influence Factor
$I_{\tau H}$	Horizontal Shear Stress Influence Factor
K	Bulk Modulus
k	Ratio of L/B
$k_s$	Modulus of Subgrade Reaction
L	Footing Length
m	Ratio of E/ $\sigma$
$N_\gamma$	Terzaghi Bearing Capacity Factor
$N_{\phi f}$	Davis Plasticity Factor
P	Total Force Applied to Plate
P'	Force/Unit Length Applied to Plate
$p_x$	Vertical Contact Stress Along the x - axis
$p_{xy}$	Vertical Contact Stress in the x - y Plane
q	Average Contact Stress
$q_u$	Ultimate Average Contact Stress
x	Distance in a Horizontal Direction
y	Distance in a Horizontal Direction
z	Distance in the Vertical Direction
$\alpha$	Zaretsky-Tsytoovich Parameter
$\beta$	Ratio of x/a in Schultze Model
$\gamma$	Unit Weight of Soil

$\gamma_{ij}$  Shear Strain on the  $i - j$  Plane  
 $\delta$  Non-Linearity Factor  
 $\epsilon_{ii}$  Normal Strain on the  $i - i$  Plane  
 $\eta$  Non-Homogeneity Factor  
 $\lambda$  Horizontal Displacement  
 $\mu$  Davis Plasticity Factor  
 $\nu$  Poisson's Ratio  
 $\rho$  Displacement; Vertical Settlement  
 $\sigma_{ii}$  Normal Stress on the  $i - i$  Plane  
 $\sigma_{vi}$  Initial Vertical Stress in Soil  
 $\tau_{ij}$  Shear Stress on the  $i - j$  Plane  
 $\phi$  Friction Angle on Mohr-Coulomb Failure Envelope  
 $\phi'$  Reduced Value of  $\phi$  to Account for Local Shear

EXPERIMENTAL APPARATUS



EXPERIMENTAL APPARATUS



SOLUTIONS FOR A RIGID PLATE RESTING ON AN ELASTIC SOIL - TABLE 2.1

SOURCE	EQUATIONS		ASSUMPTIONS	
	CONTACT STRESS	SETTLEMENT	SOIL	FOOTING
BOUSSINESQ (1885)	$P_x = \frac{P'}{\pi a} \left(1 - \frac{x^2}{a^2}\right)^{1/2} \quad (2.1)$	$\rho = \infty$	HOMOGENEOUS, ISOTROPIC LINEARLY ELASTIC HALFSPACE	SMOOTH STRIP
SCHIFFMAN AND AGGARWALA (1961)	$P_x y = \frac{P}{2\pi ab} \left(1 - \frac{x^2}{a^2} - \frac{y^2}{b^2}\right)^{1/2} \quad (2.2)$	$a = b; \rho = \frac{P(1-\nu^2)}{2\alpha E}$ $b \rightarrow \infty; \rho = \infty$	"	SMOOTH ELLIPSE
ZARETSKY AND TSYTOVICH (1965)	$P_x = \frac{\Gamma[(1-\alpha)/2] \Gamma(1+\frac{\alpha}{2})}{\sqrt{\pi}} \cdot \frac{P' \cos(\pi\alpha/2)}{\pi a \left(1 - \frac{x^2}{a^2}\right) \left(\frac{1-\alpha}{2}\right)} \quad (2.4)$	—	NON-HOMOGENEOUS; ISOTROPIC, NON-LINEAR; INCOMPRESSIBLE ELASTIC HALFSPACE	SMOOTH STRIP
GIBSON (1967)	$P_x = \frac{P'}{2a}$	$\rho = 1.5 \frac{P'}{2\pi \alpha \sigma} \quad (2.6)$	NON-HOMOGENEOUS, ISOTROPIC, LINEAR, INCOMPRESSIBLE ELASTIC HALFSPACE	SMOOTH STRIP

SOLUTIONS FOR A RIGID PLATE AT ULTIMATE LOAD - TABLE 2.2

<u>SOURCE</u>	<u>CONTACT STRESS</u>	SOIL	<u>ASSUMPTIONS</u> FOOTING
TERZAGHI (1943)	$P_x = 3\gamma N_c \left( \frac{B}{4} - \frac{x^2}{B} \right)$ (2.11)	HOMOGENEOUS, ISOTROPIC INCOMPRESSIBLE	ROUGH
MEYERHOF (1952)	$P_x = (a - 1/x) 2\gamma N_c$ (2.12)	"	"
SOKOLOVSKI (1965)	$P_x = (a - 1/x) 2\gamma N_c$ (2.13)	"	SMOOTH

TABLE 3.1SUMMARY OF FINITE ELEMENT COMPUTER RUNS

NON-HOMOGENEOUS ELASTIC HALFSPACE

$$E = 118 \times 10^9$$

$$\nu = \text{CONST.}$$

<u>RUN</u>	<u>M</u>	<u><math>\gamma</math></u> (NWT/M <sup>3</sup> )	<u><math>\nu</math></u>	<u>PLATE</u>
50	200	15500	.4	SMOOTH
53	"	"	.48	ROUGH
54	"	"	.2	"
57	"	"	.4	"
59	"	"	.0	"
60	"	"	.0	SMOOTH
61	"	"	.48	"
62	"	"	.499	"
66	"	1.55	.499	ROUGH
68	"	15500	.4999	SMOOTH
69	100	"	.40	"
70	200	"	.4995	"
71	"	"	.4998	"



TABLE 4.1SUMMARY OF PLATE LOAD TESTS

<u>SOIL No.</u>	<u>RUN No.</u>	<u>REL. DENSITY</u>	<u>UNIT WT.</u> (NWT/M <sup>3</sup> )	<u>NO. OF STAGES</u>
10	17	85%	16000	6
11	18	85%	16000	6
12	19	80%	15780	6
13	20	80%	15780	6
14	21	70%	15340	6
15	22	70%	15340	6
16	23	60%	14920	6
17	24	60%	14920	6
18	25	50%	14520	5
19	26	50%	14520	5

TABLE 4.1 - CONTINUED

$\bar{q}$ : AVE. PLATE STRESS APPLIED TO SOIL -  $\times 10^3$  NWT/M<sup>2</sup>

<u>SOIL NO.</u>	<u>STAGE NO.</u>					
	1	2	3	4	5	6
10	32.6	54.7	75.6	85.4	95.3	103.5
11	"	"	"	"	"	"
12	"	"	"	"	"	"
13	"	"	"	"	"	"
14	"	"	69.5	80.5	90.4	100.3
15	"	"	"	"	"	"
16	"	62.1	75.6	"	85.4	90.4
17	"	47.3	62.1	75.6	80.5	85.4
18	"	"	54.7	62.1	69.5	—
19	"	"	"	"	"	—

TABLE 4.2.

EXPERIMENTAL PARAMETERS SELECTED TO COMPARE  
WITH PLATE LOAD TEST DATA

<u>RELATIVE DENSITY</u>	<u>UNIT WEIGHT</u> (NWT/M <sup>3</sup> )	<u><math>\phi_{ps}</math></u>	<u><math>N_s</math></u>
85%	16000	46.2	490
80%	15780	45.7	420
70%	15340	44.7	330
60%	14920	43.6	270
50%	14520	42.7	225

SEE FIG. 4.16

TABLE 5.1  
IN SITU TESTING DEVICES  
FOR THE LUNAR SURFACE

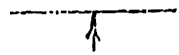

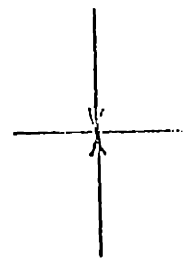
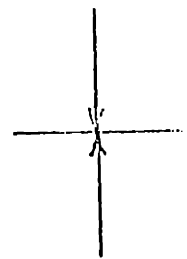
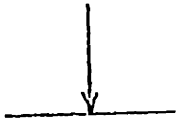
<u>DEVICE</u>	<u>EVALUATION</u>
INSTRUMENTED PLATE MOUNTED ON ROVING VEHICLE	 HIGHLY DESIRABLE
MOUNTED ON LEM	
CONE PENETROMETER	 VERY DESIRABLE
LEM FOOTPADS	 ABSOLUTE MINIMUM
ASTRONAUT FOOTPRINT	

TABLE A.1SUMMARY OF DIRECT SHEAR TESTS

<u>TEST</u>	<u><math>e_r</math></u>	<u><math>e_c</math></u>	<u><math>\sigma_c</math></u> ( <u>NO.2/IN<sup>2</sup></u> )	<u><math>T_{MAX}</math></u> ( <u>NO.2/IN<sup>2</sup></u> )	<u><math>(\tau/\sigma)_{MAX}</math></u>	<u><math>\phi_{DS}</math></u>
2A	.796	.796	16300	14,630	.851	40.4
2B	"	.782	72800	61,000	.800	39.6
2C	"	.775	152,500	126,500	.750	36.8
2D	"	.773	251,000	210,000	.723	35.8
3A	.700	.700	16300	203,000	1.200	50.2
3B	"	.687	72800	72,700	.949	43.5
3C	"	.676	152,500	134,000	.811	39.1
3D	"	.670	251,000	237,000	.834	39.8
4A	.892	.892	16300	12,800	.693	34.7
4B	"	.870	72800	49,600	.640	32.6
4C	"	.854	152,500	109,000	.638	32.5
4D	"	.840	251,000	185,500	.612	31.5

# TABLE A. 2

## SUMMARY OF CID TRAINING TESTS

TEST	$e_c$	$\sigma_c$ (NUT/IN)	$(\sigma_1 - \sigma_3)_{MAX}$ (NUT/IN)	$\phi_{TRI}$	$(\sigma_1/\sigma_3)_{MAX}$	$\frac{dE_{VOL}}{dE_1}$	$N_{eff}$	$\mu$
4	.617	49,000	228,000	44.3	5.65	-.633	3.46	.677
5	.695	"	199,000	42.0	5.06	-.421	3.56	.614
6	.727	"	179,000	40.1	4.65	-.284	3.62	.575
7	.620	98,000	408,000	42.5	5.17	-.530	3.38	.643
8	.620	245,000	911,000	40.5	4.71	-.384	3.40	.600
9	.673	98,000	365,000	40.5	4.72	-.350	3.50	.591
10	.652	245,000	882,000	39.9	4.59	-.324	3.47	.585
11	.690	98,000	358,000	40.2	4.66	-.280	3.64	.574
12	.657	245,000	892,000	40.1	4.63	-.327	3.49	.585
13	.773	98,000	323,000	38.4	4.30	-.0998	3.91	.525
2	.642	98,000	384,000	41.4	4.92	-.421	3.46	.612



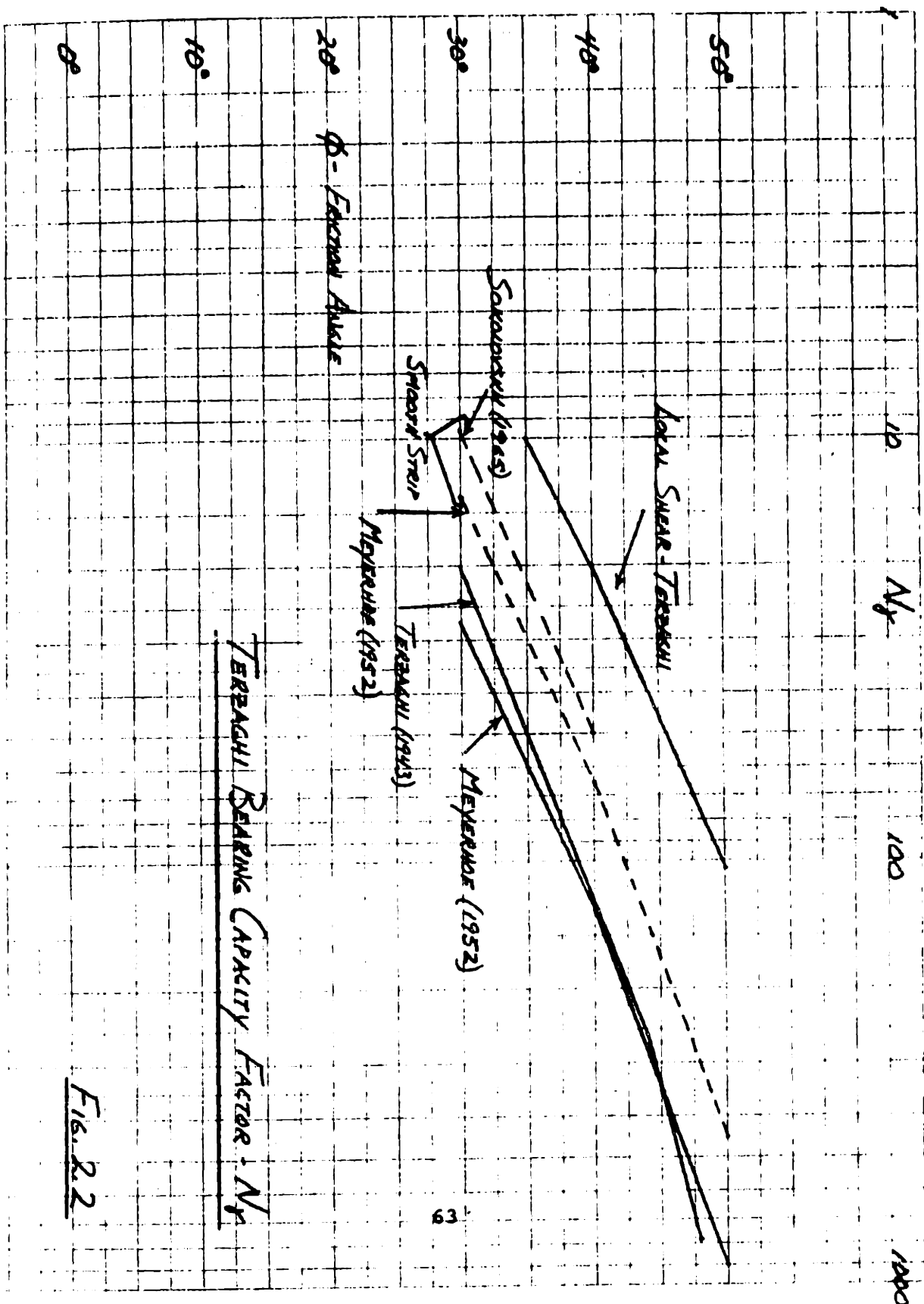
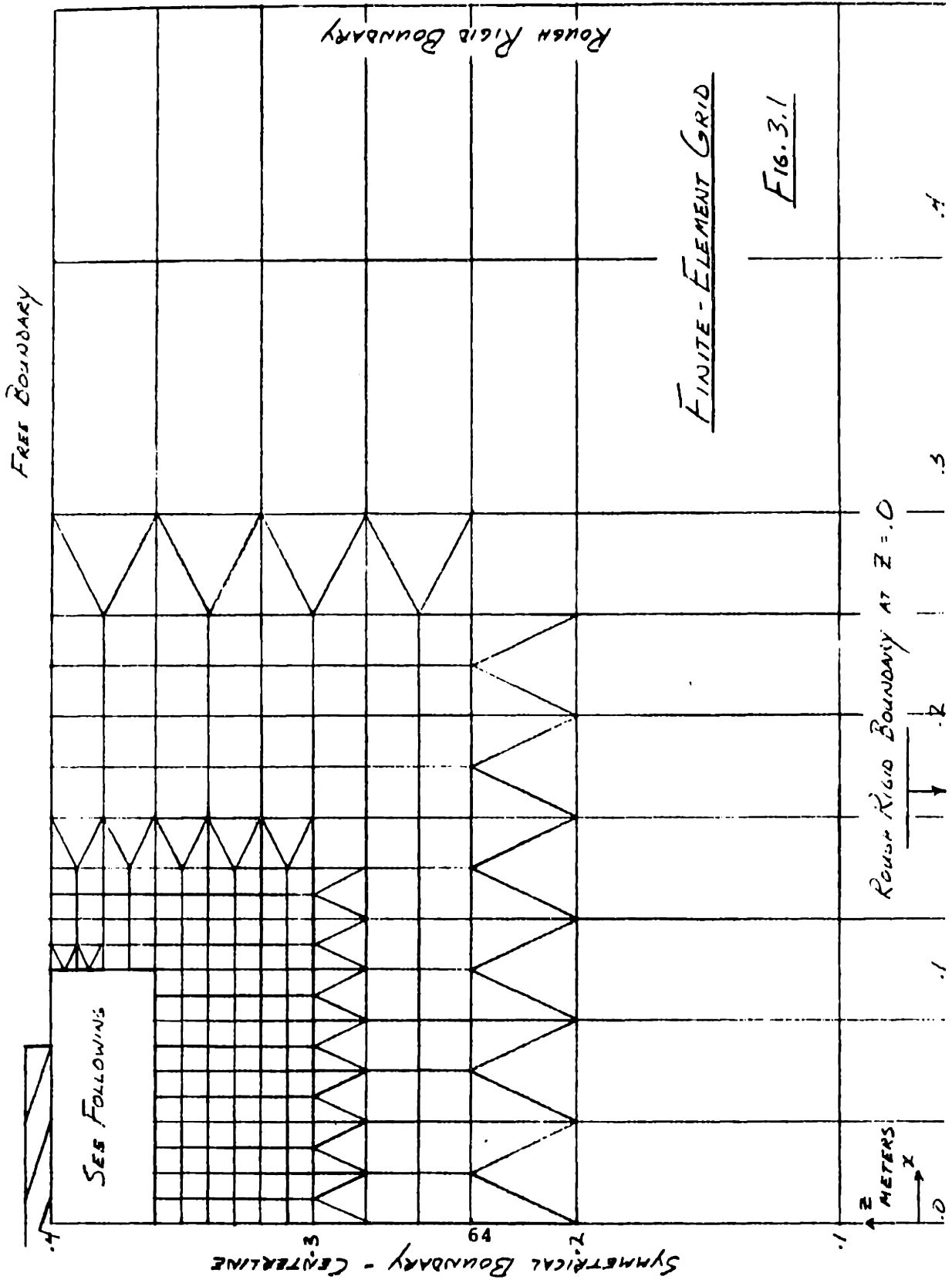
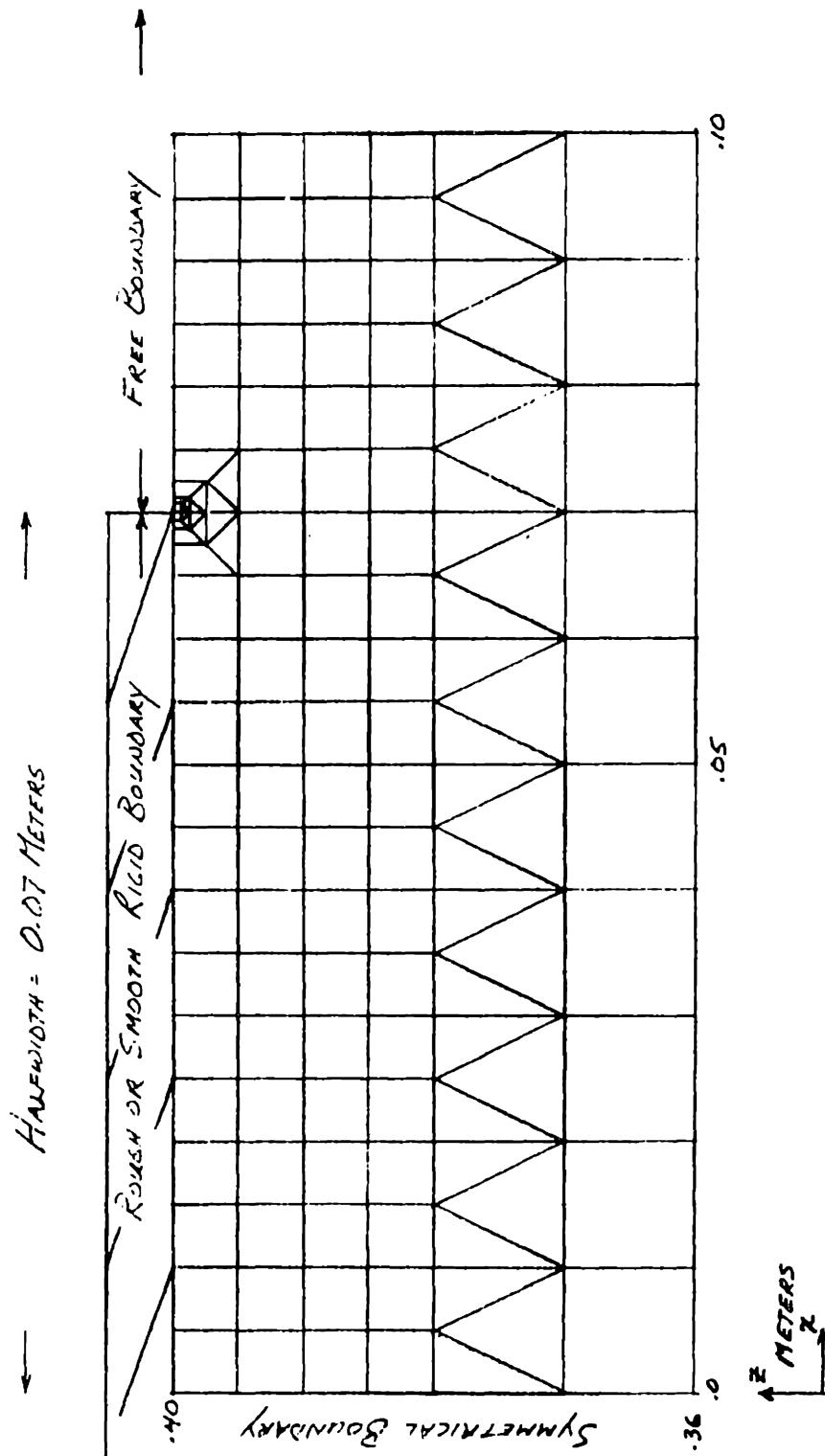


FIG. 2.2



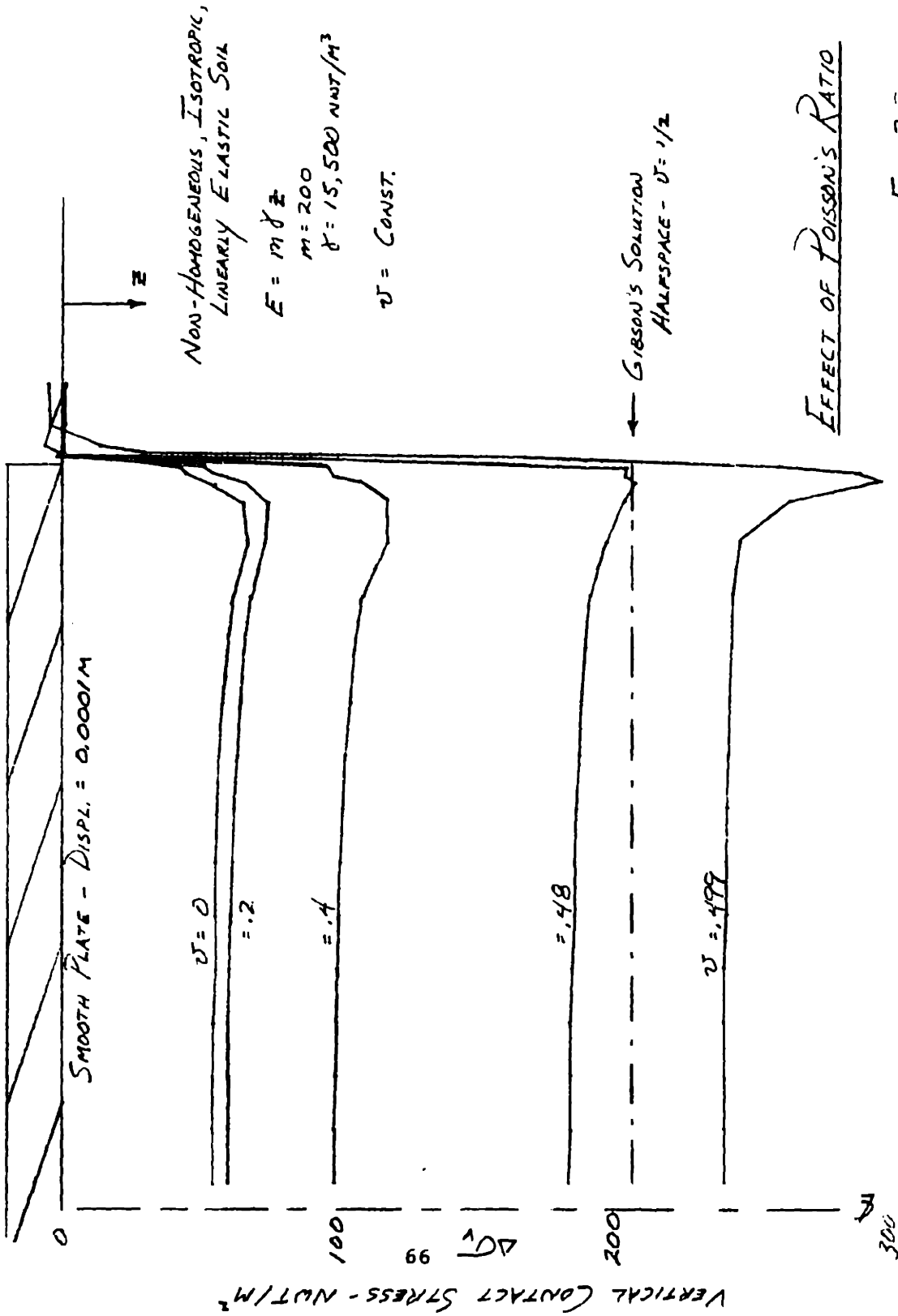




65

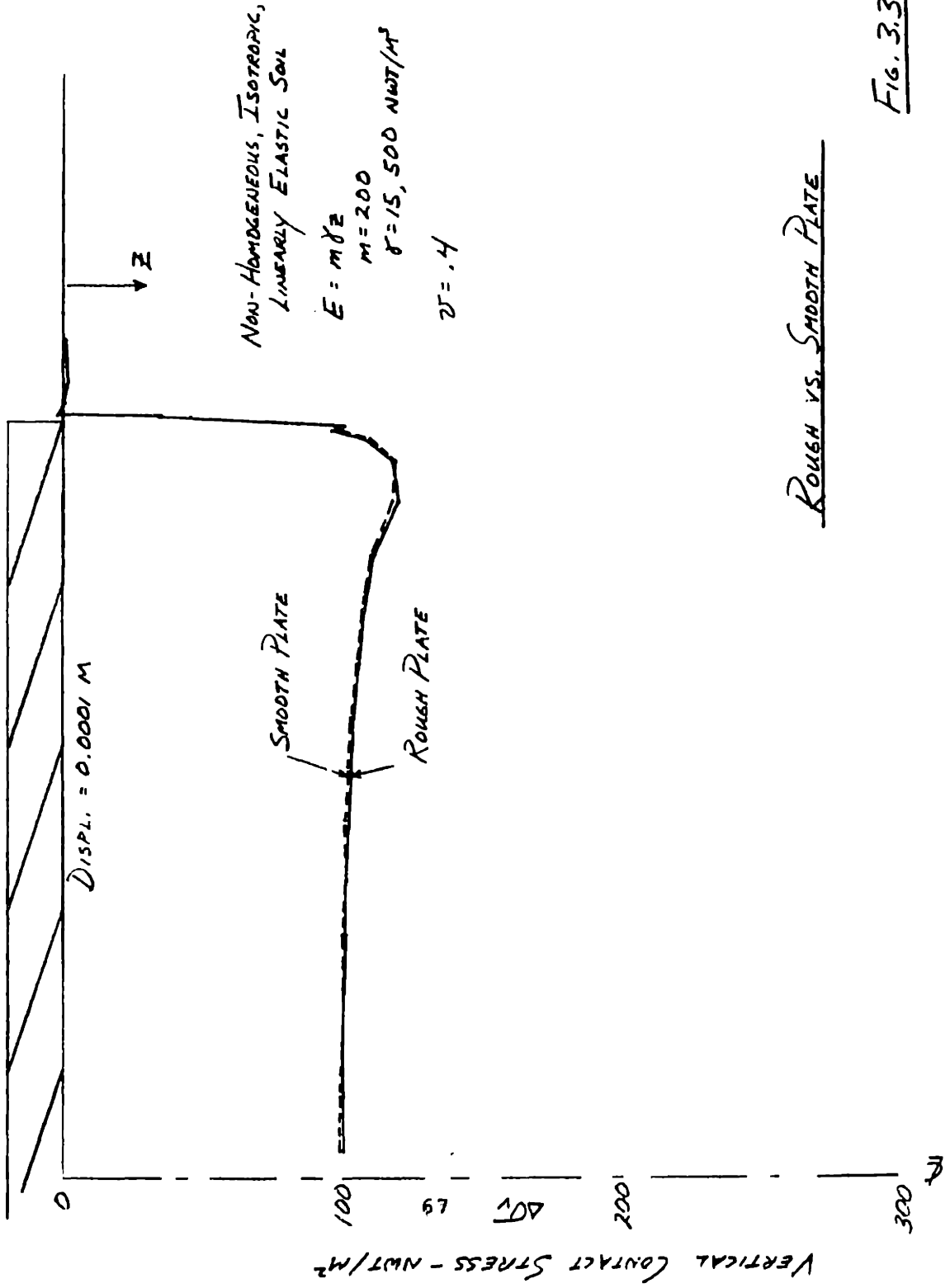
FIG. 3.1

- CONT.



EFFECT OF POISSON'S RATIO

FIG. 3.2



ROUGH VS. SMOOTH PLATE

FIG. 3.3

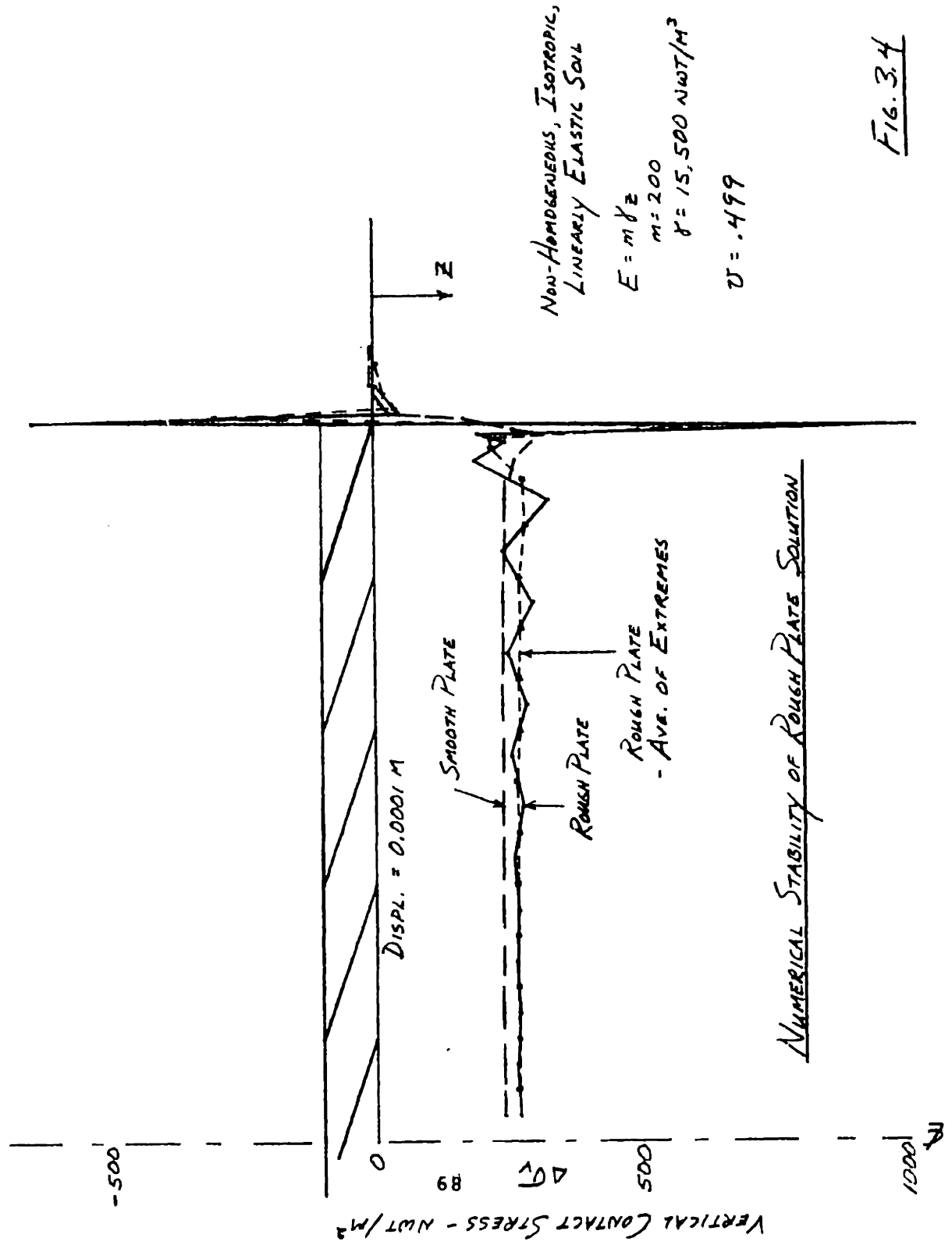
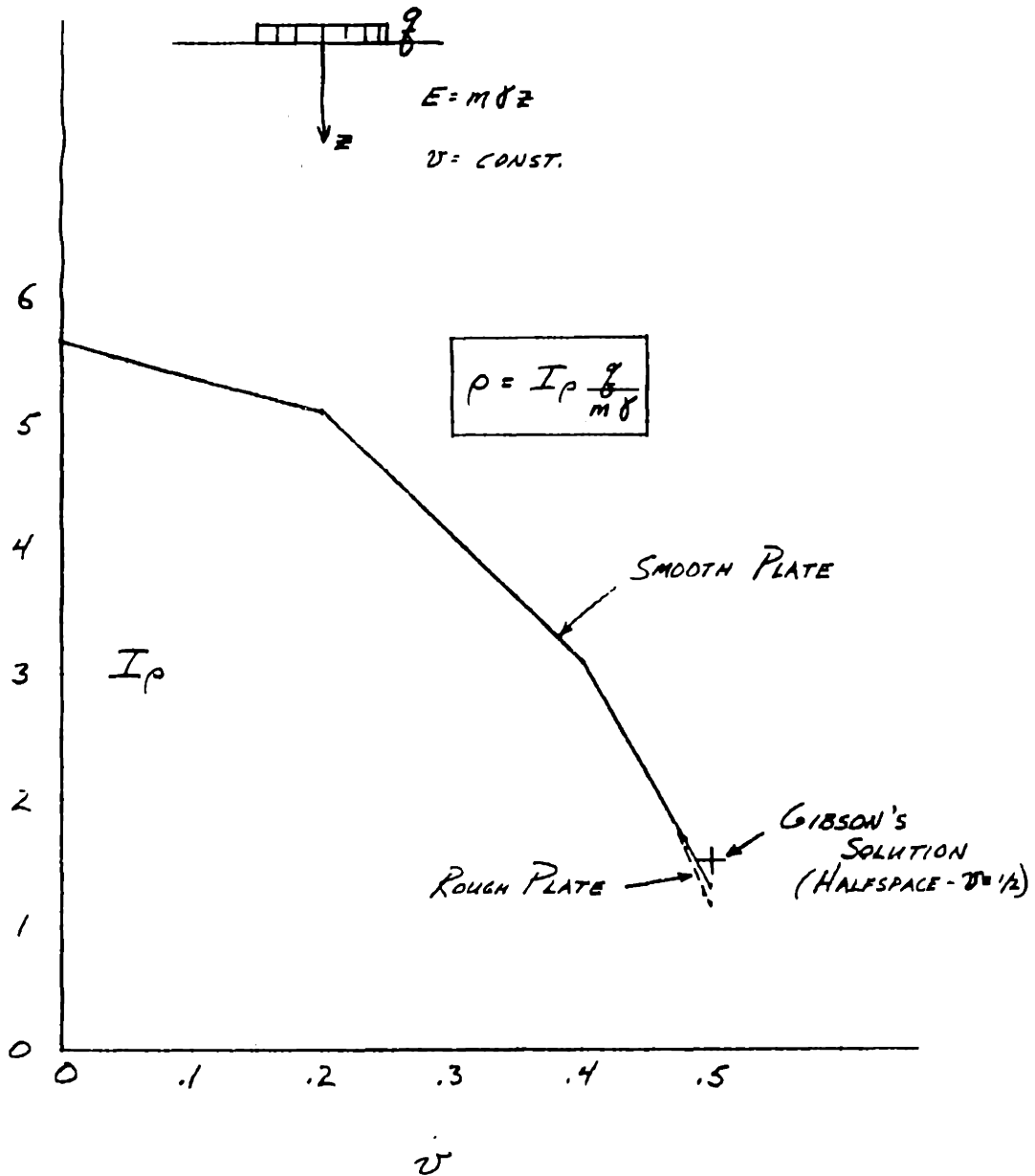


FIG. 34

FIG. 3.5

SETTLEMENT OF A RIGID PLATE



1000

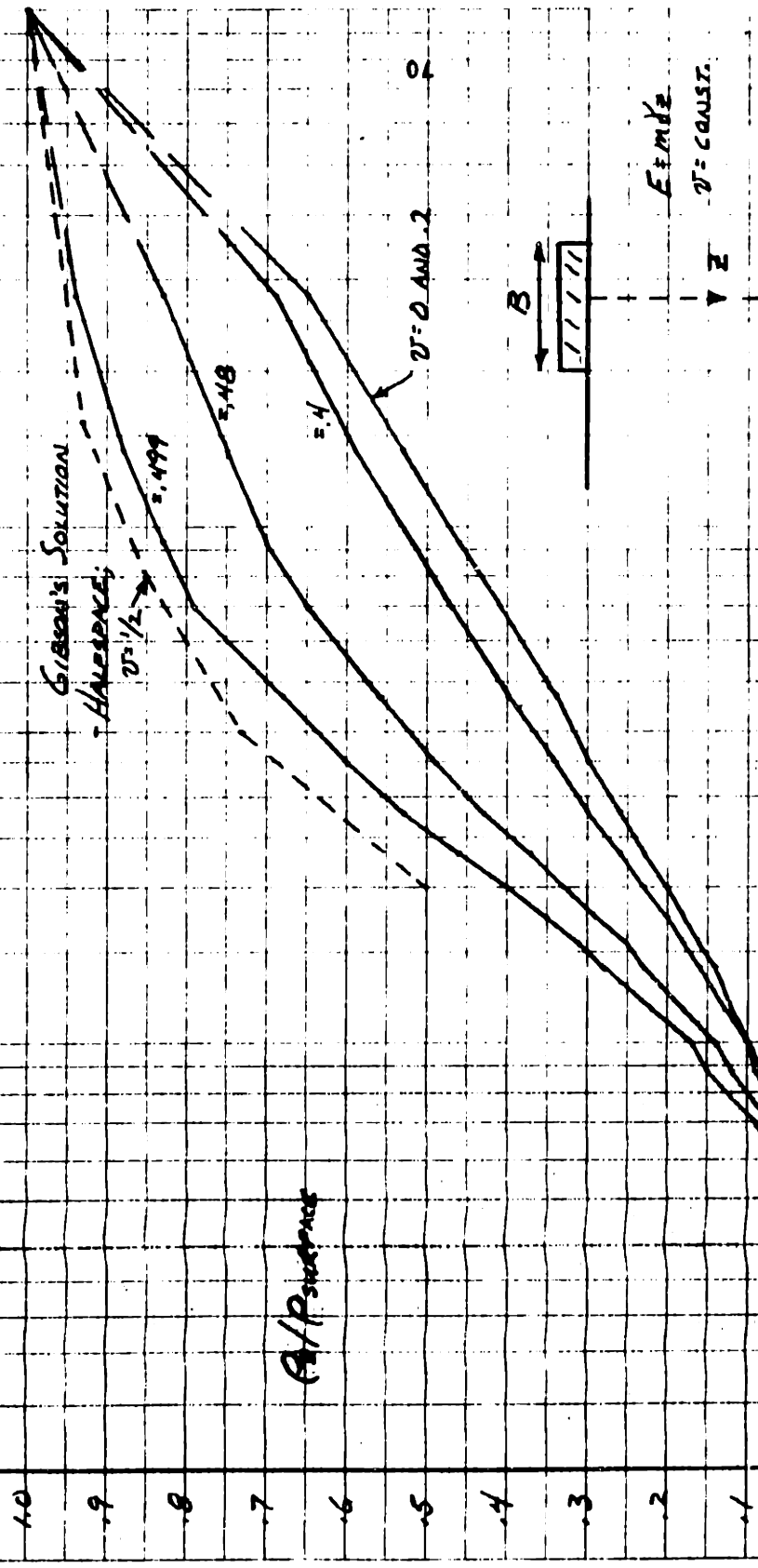
100

$B/z$

10

FIG. 3.6

CENTERLINE SETTLEMENT OF A RIGID PLATE



GIBSON'S SOLUTION

HAYES

$\nu = 1/2$

$\nu = 0.499$

$\nu = 0.4$

AND

$\nu = 0.2$

$\nu$

$B$

$E = \text{CONST.}$

$\nu = \text{CONST.}$

$z$

1.0

.9

.8

.7

.6

.5

.4

.3

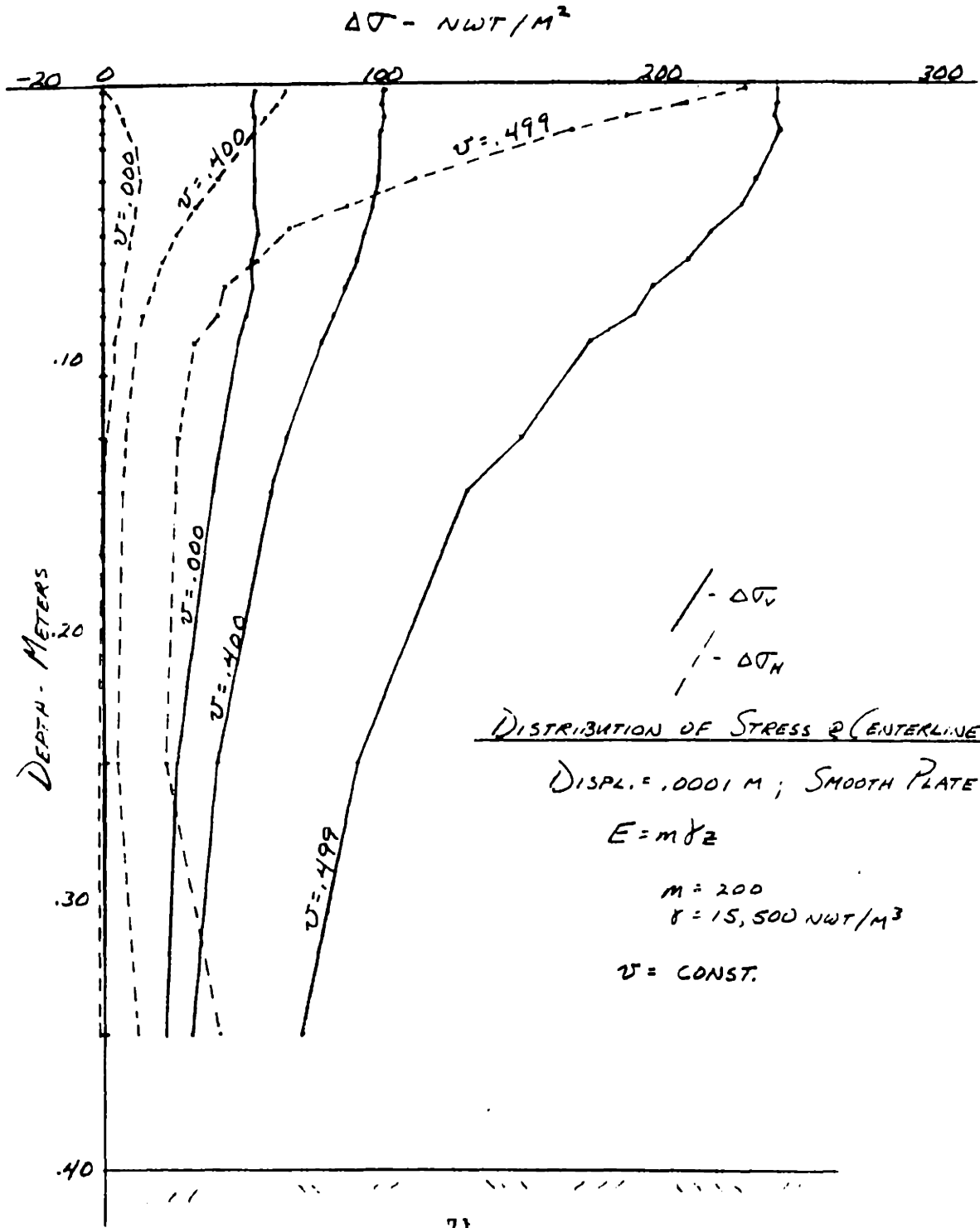
.2

.1

.0

$A/P$  settlement

FIG. 3.7





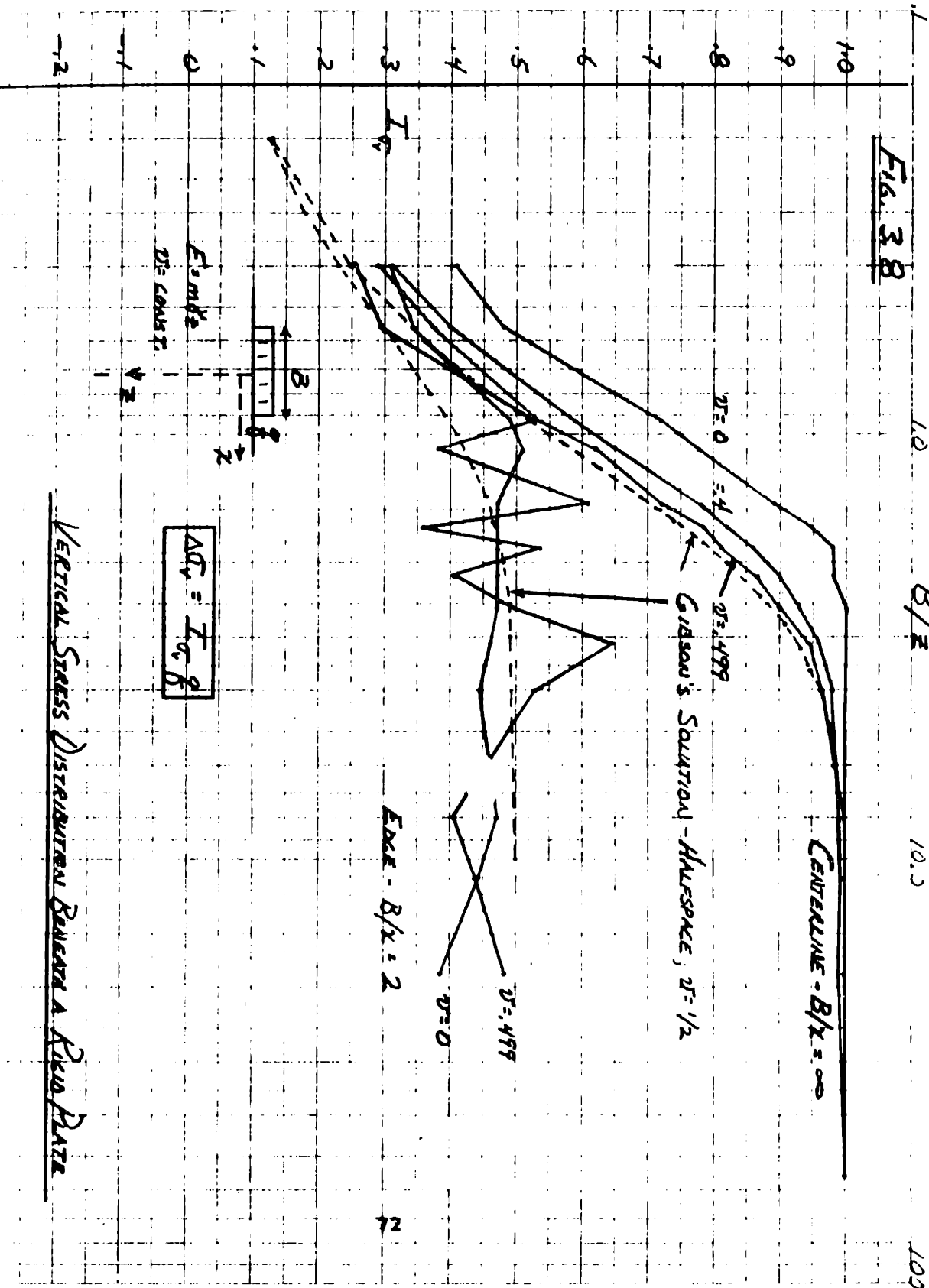
10

B/z

10.5

100.0

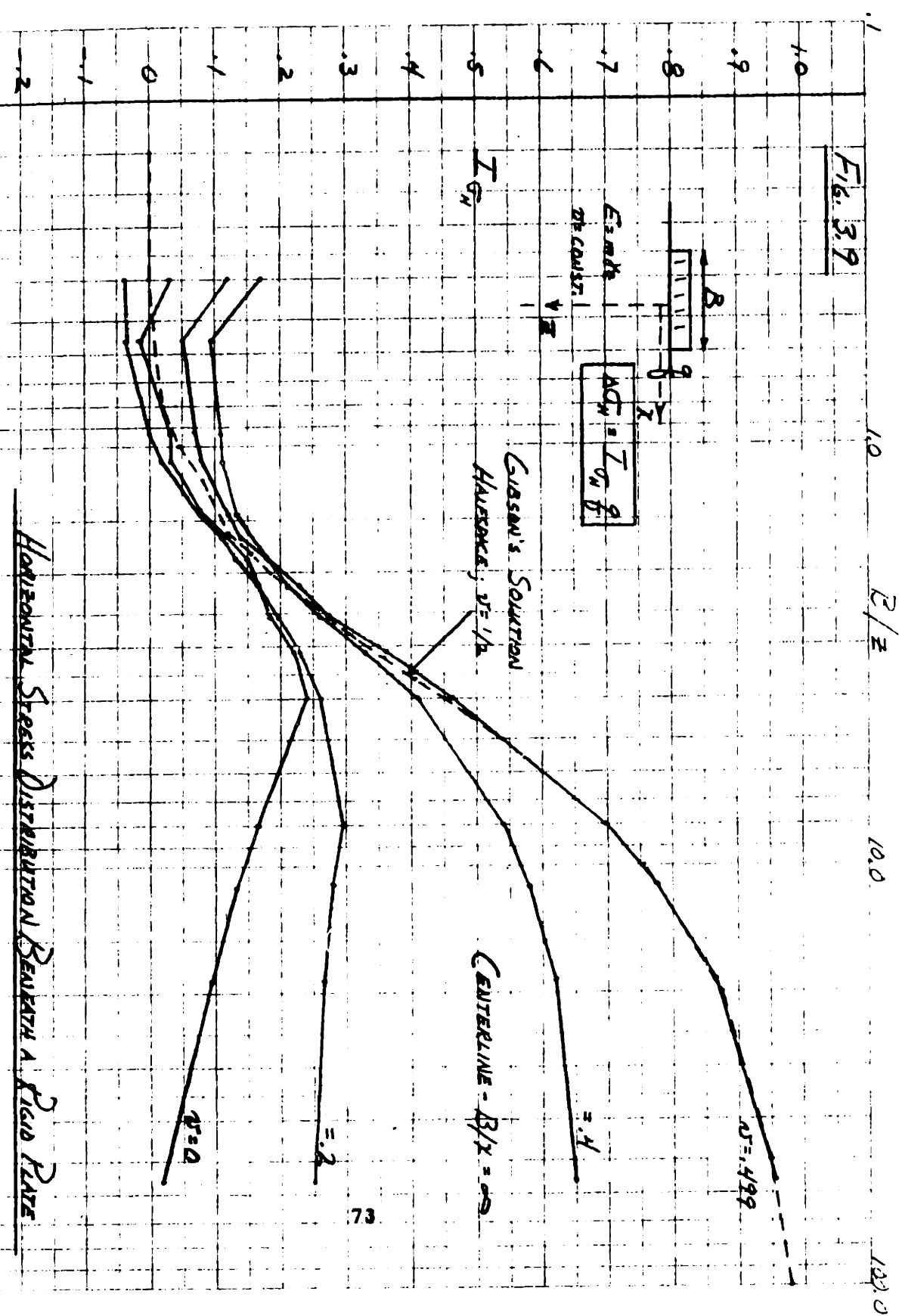
FIG. 38

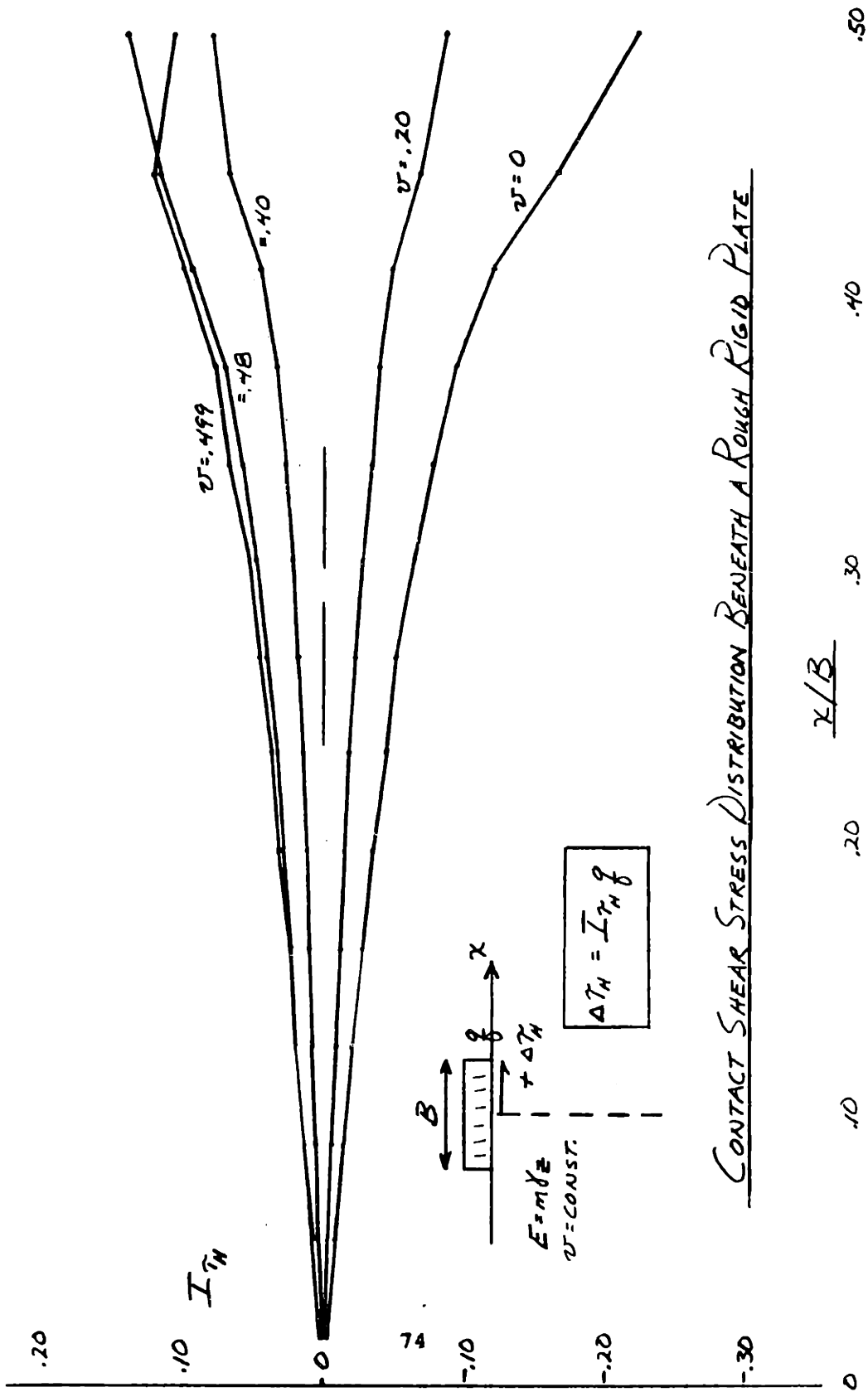


EDGE - B/z = 2

72

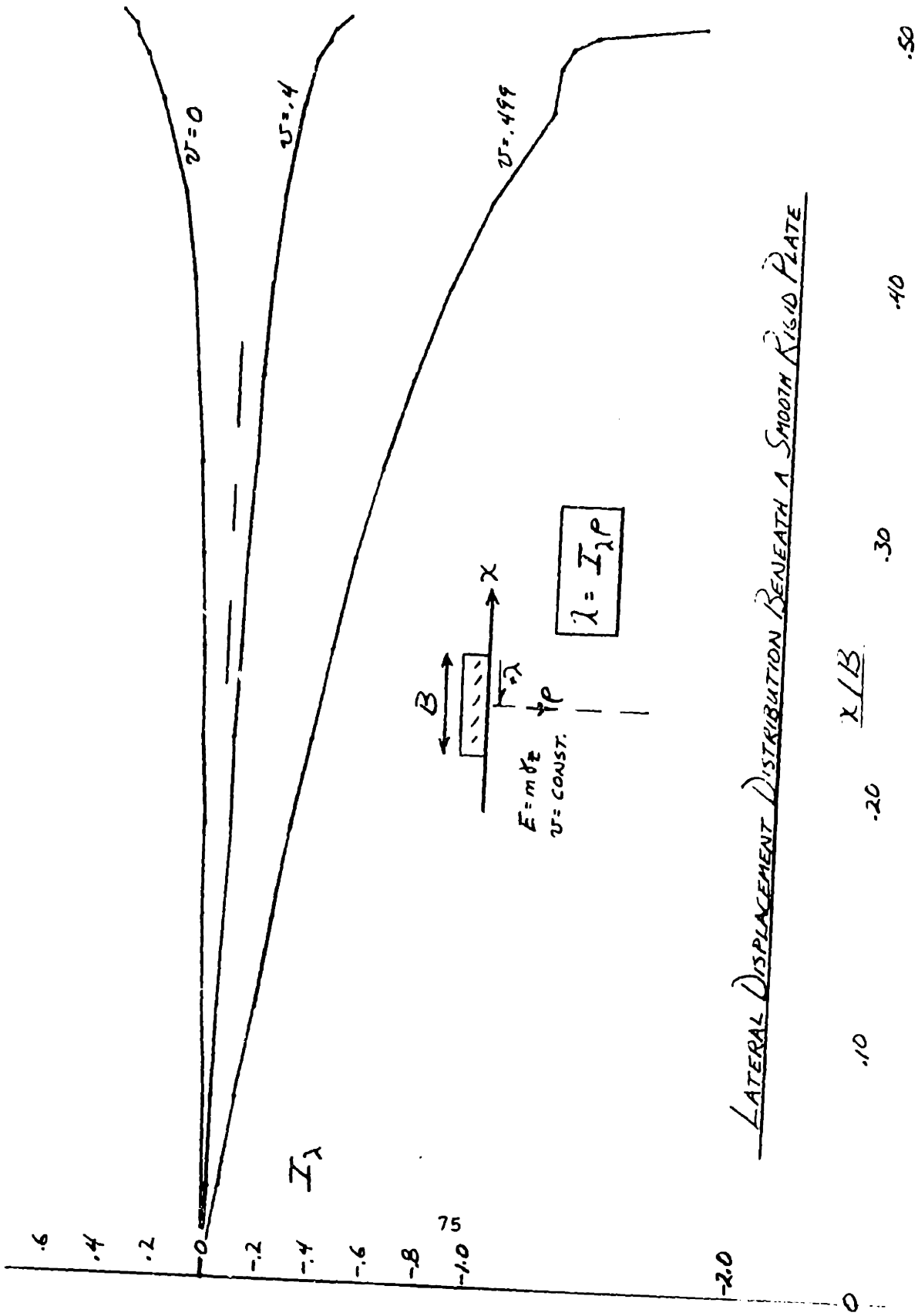
Fig. 3.9





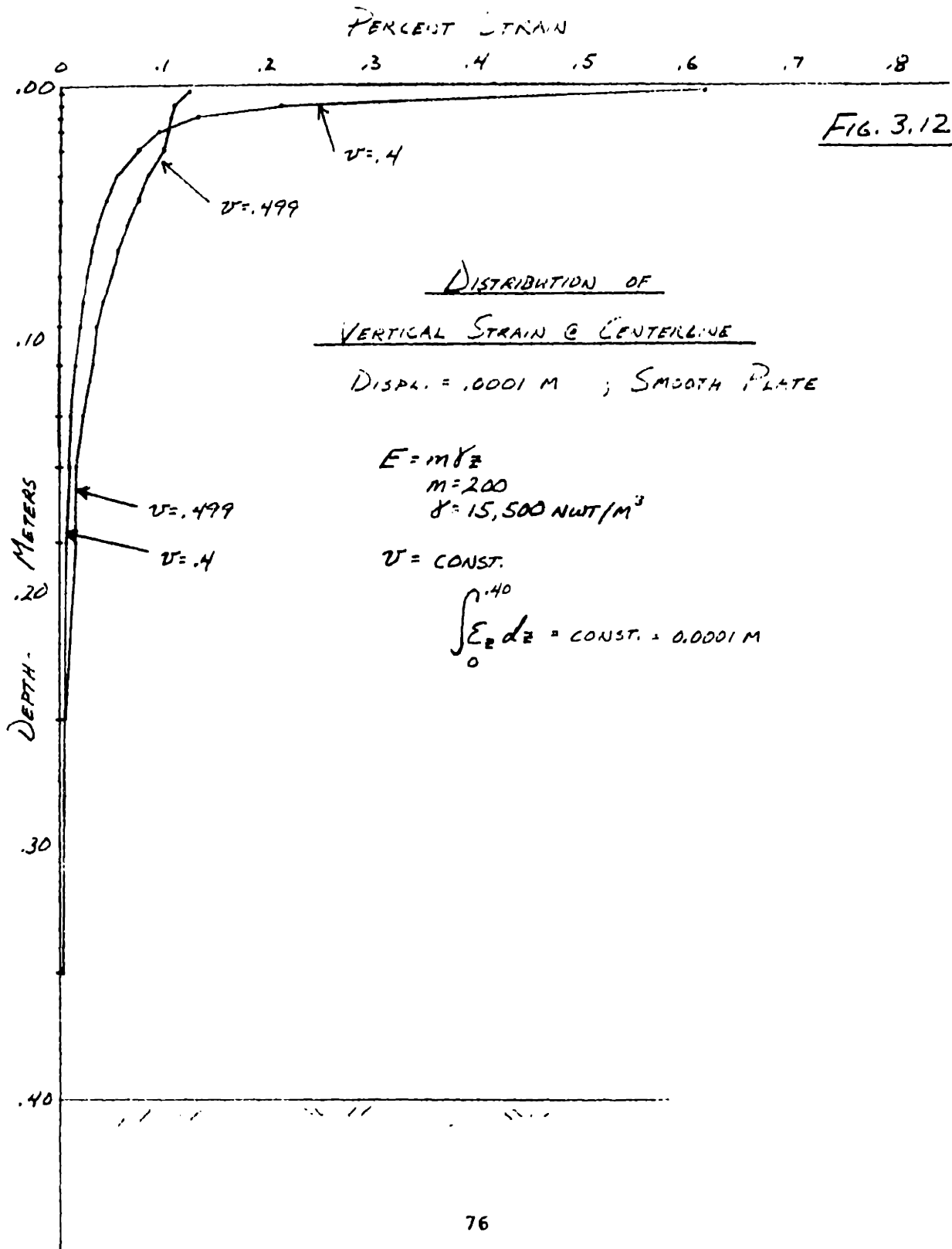
CONTACT SHEAR STRESS DISTRIBUTION BENEATH A ROUGH RIGID PLATE

FIG. 3.10

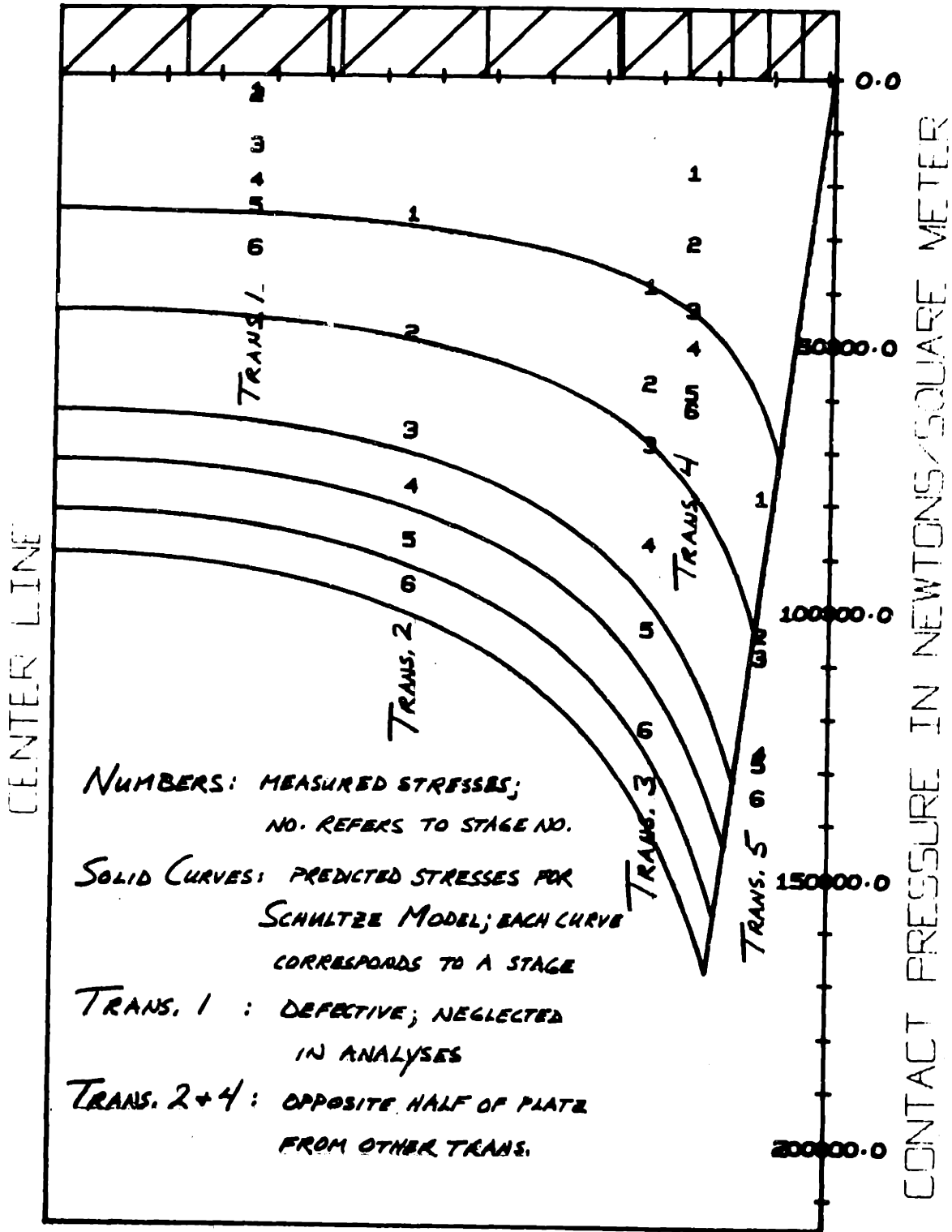


LATERAL DISPLACEMENT DISTRIBUTION BENEATH A SMOOTH RIGID PLATE

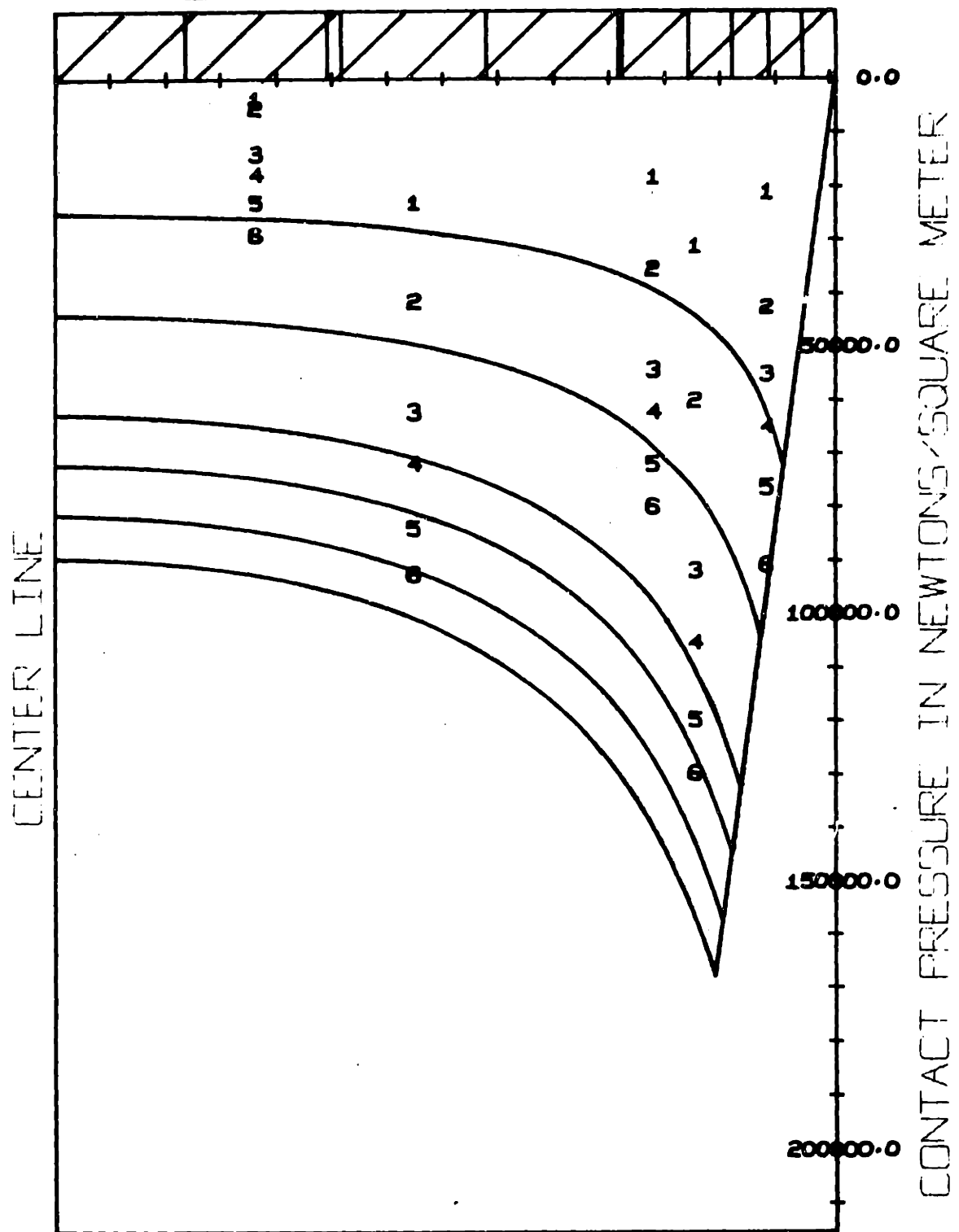
FIG. 3.11



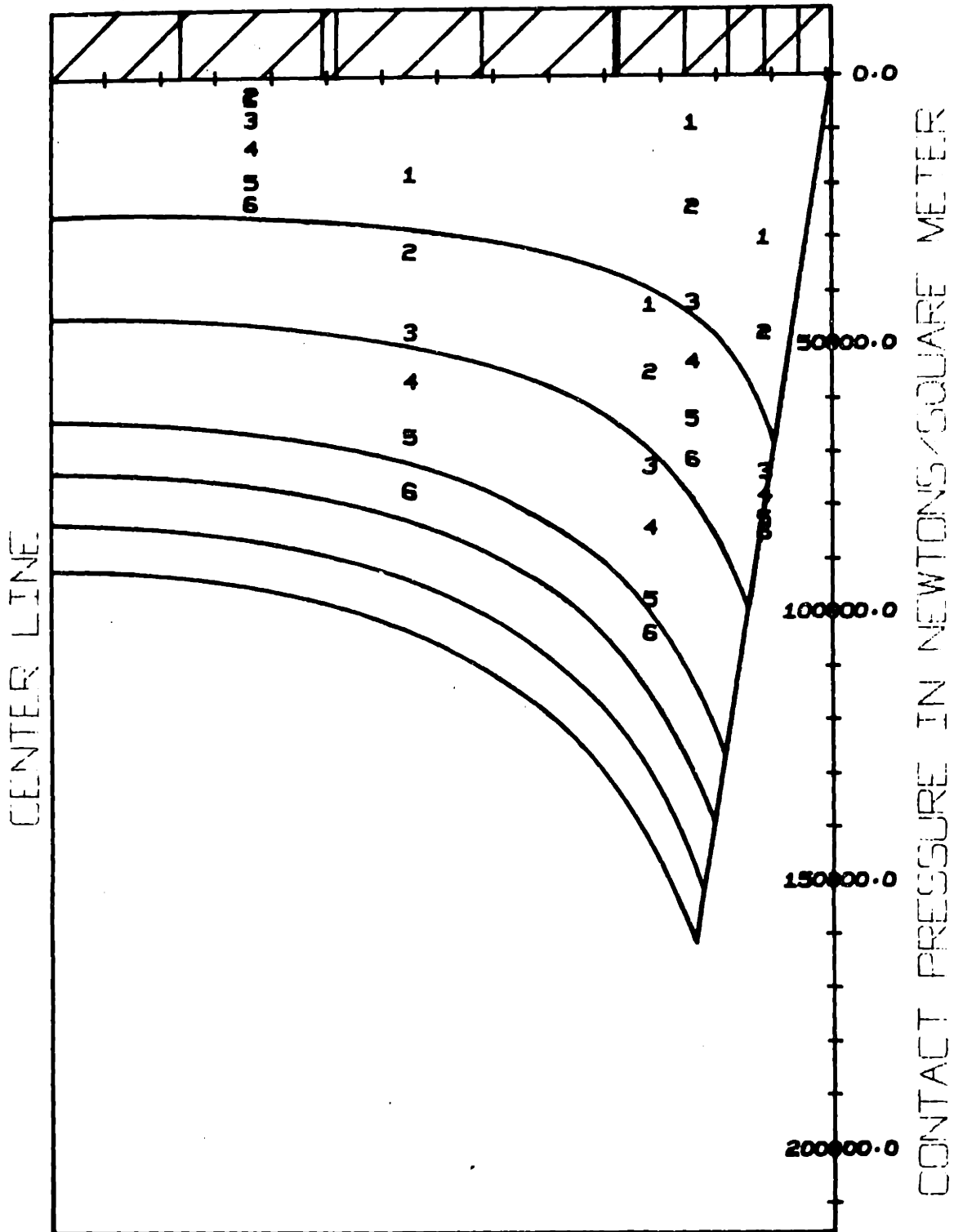
HALFWIDTH = 0.07 METERS



HALFWIDTH = 0.07 METERS

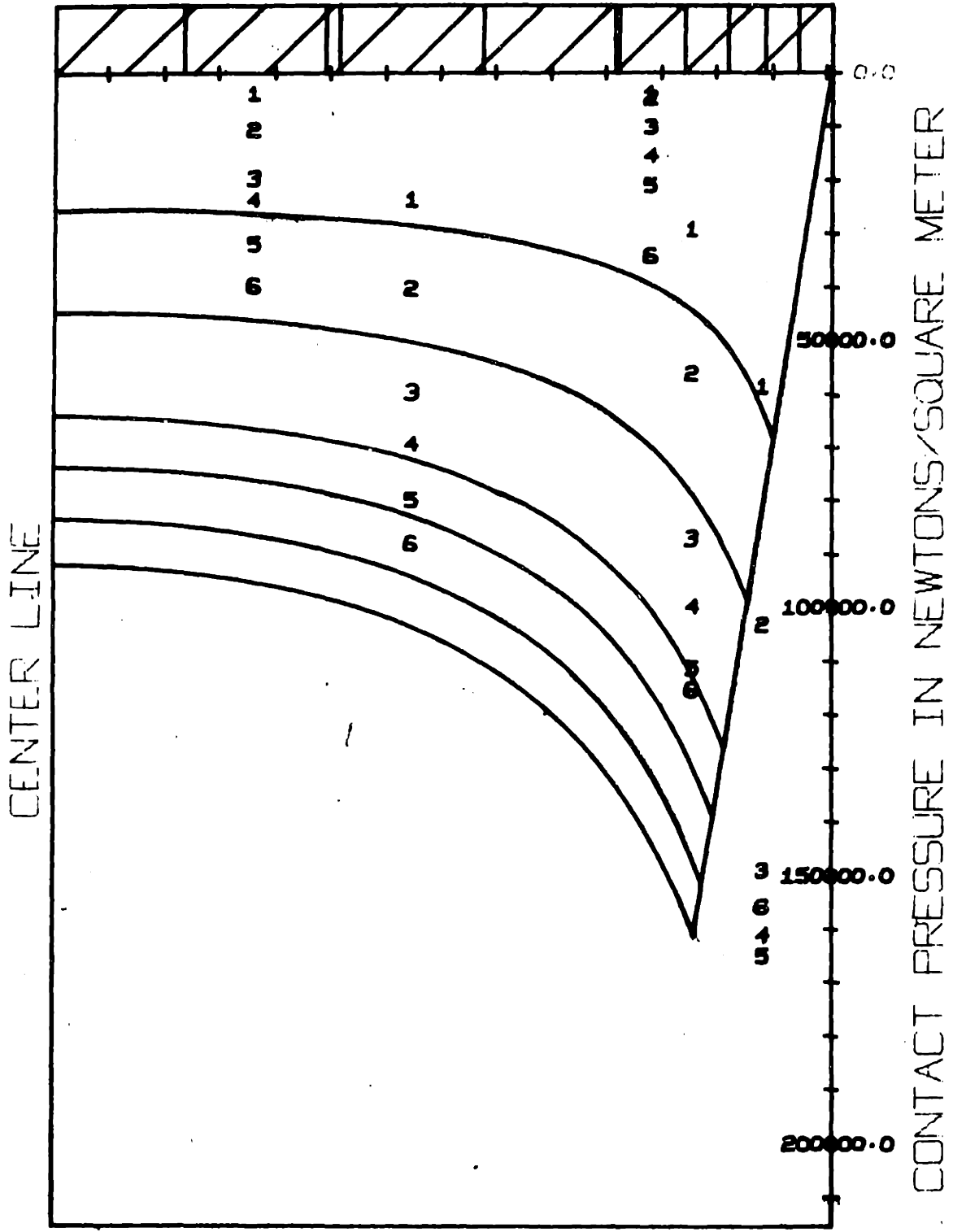


HALFWIDTH = 0.07 METERS

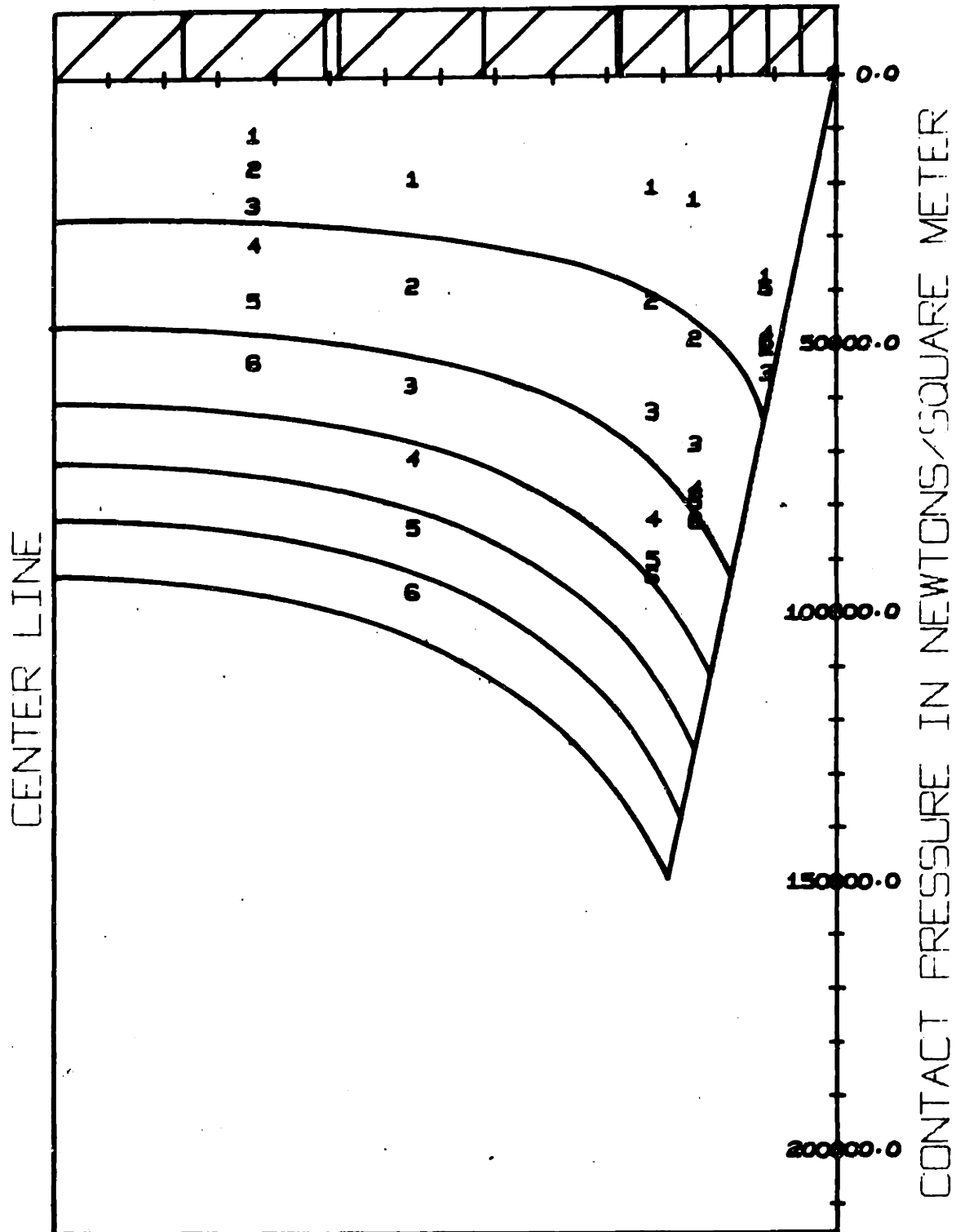




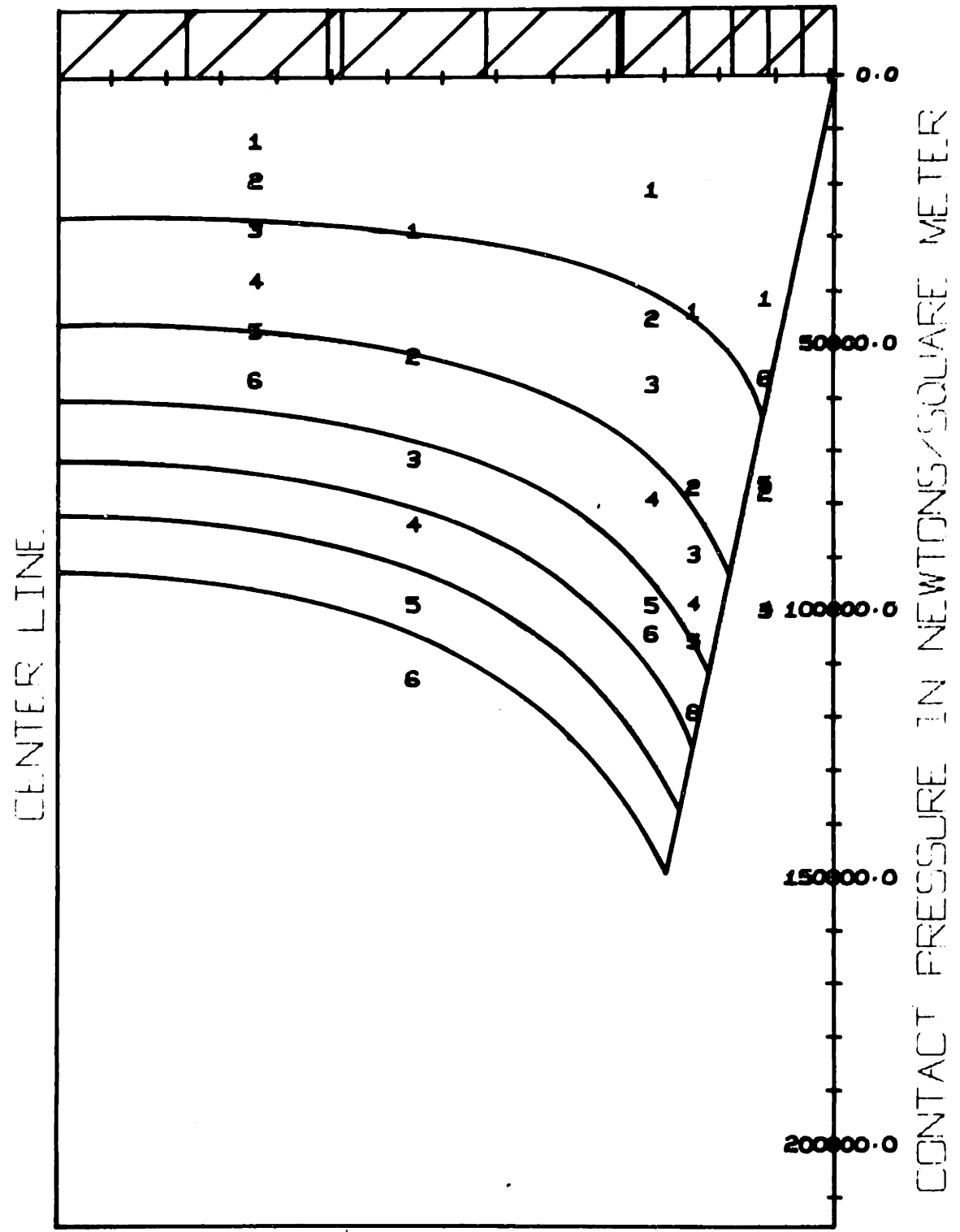
HALFWIDTH = 0.07 METERS



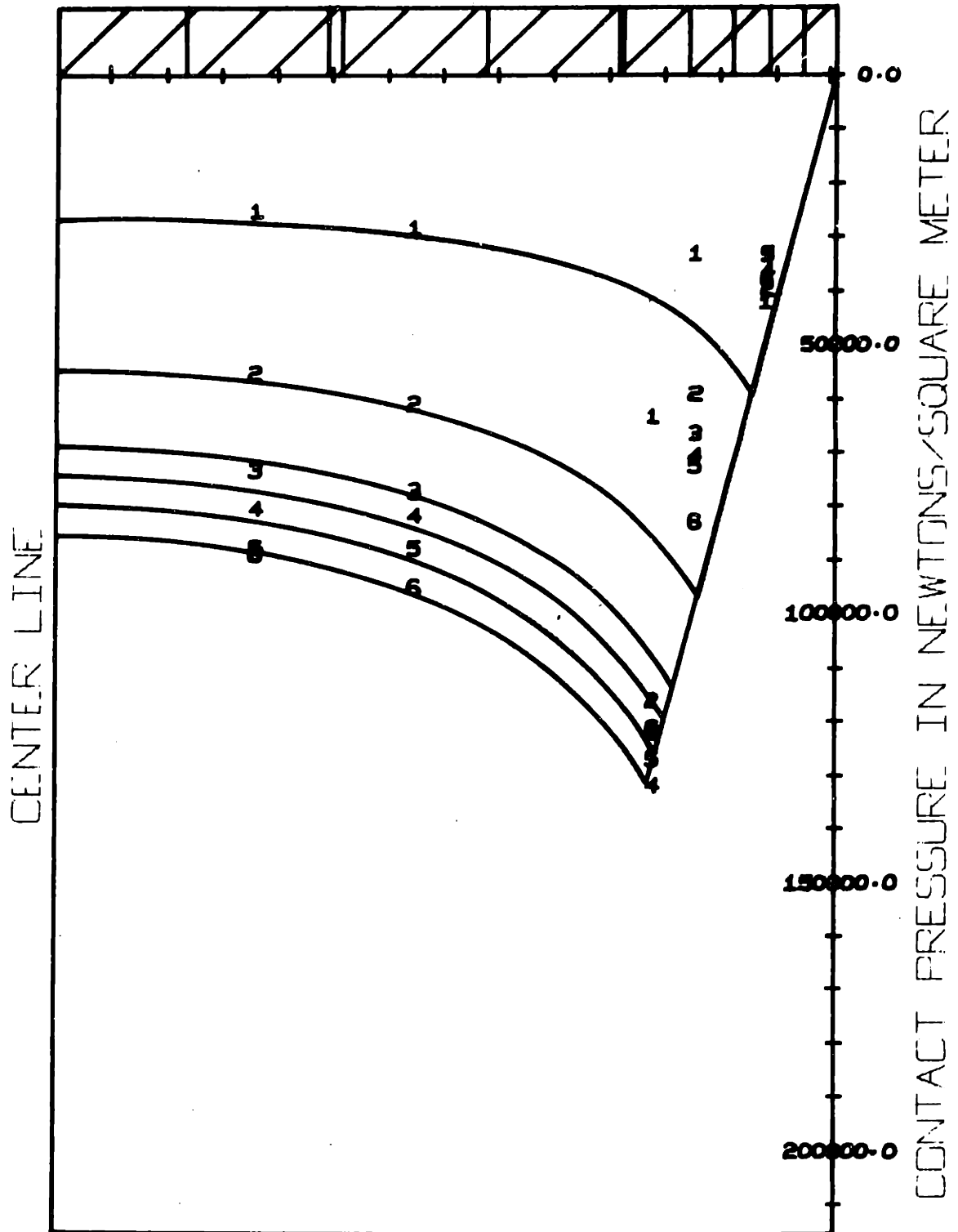
HALFWIDTH = 0.07 METERS



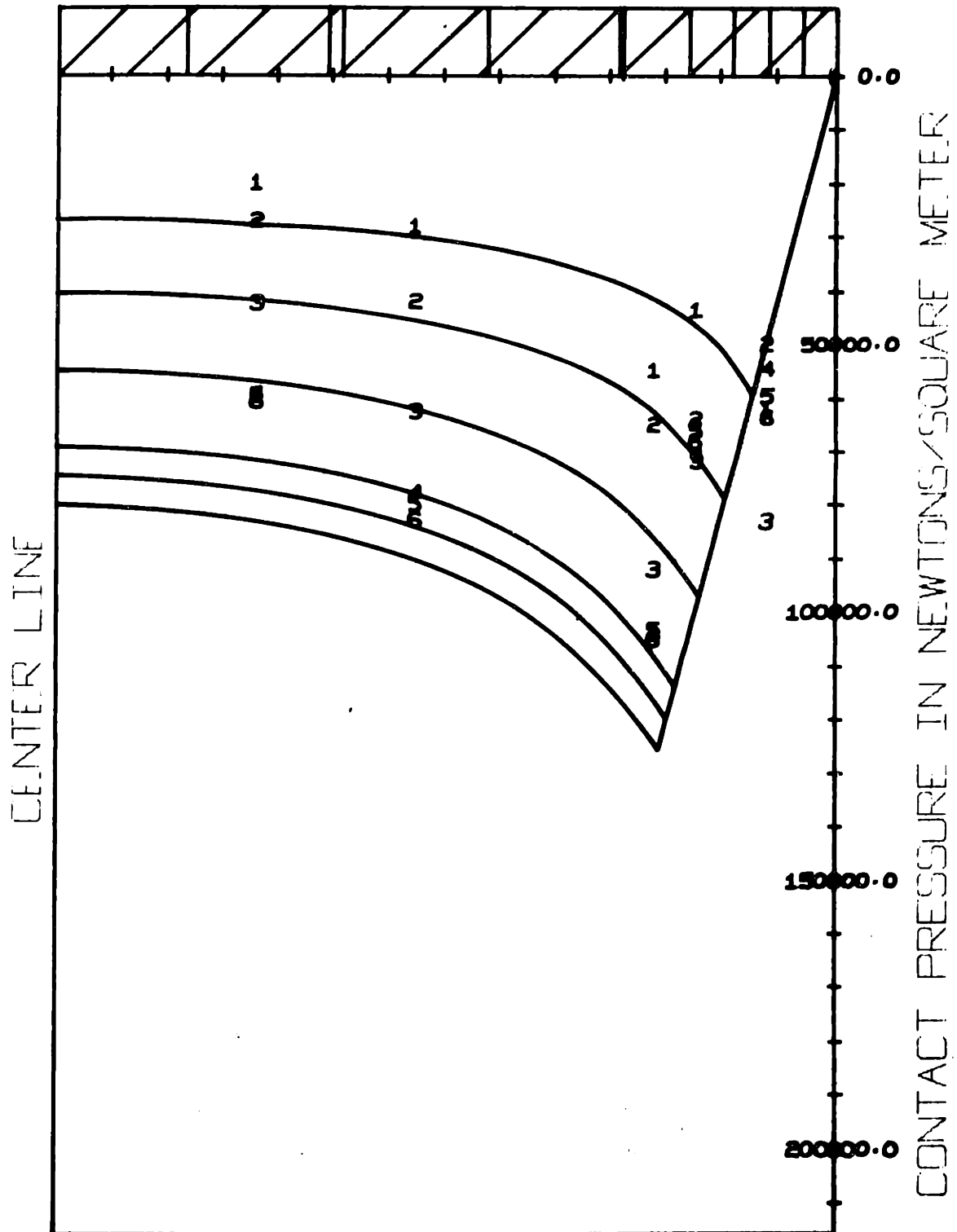
HALFWIDTH = 0.07 METERS



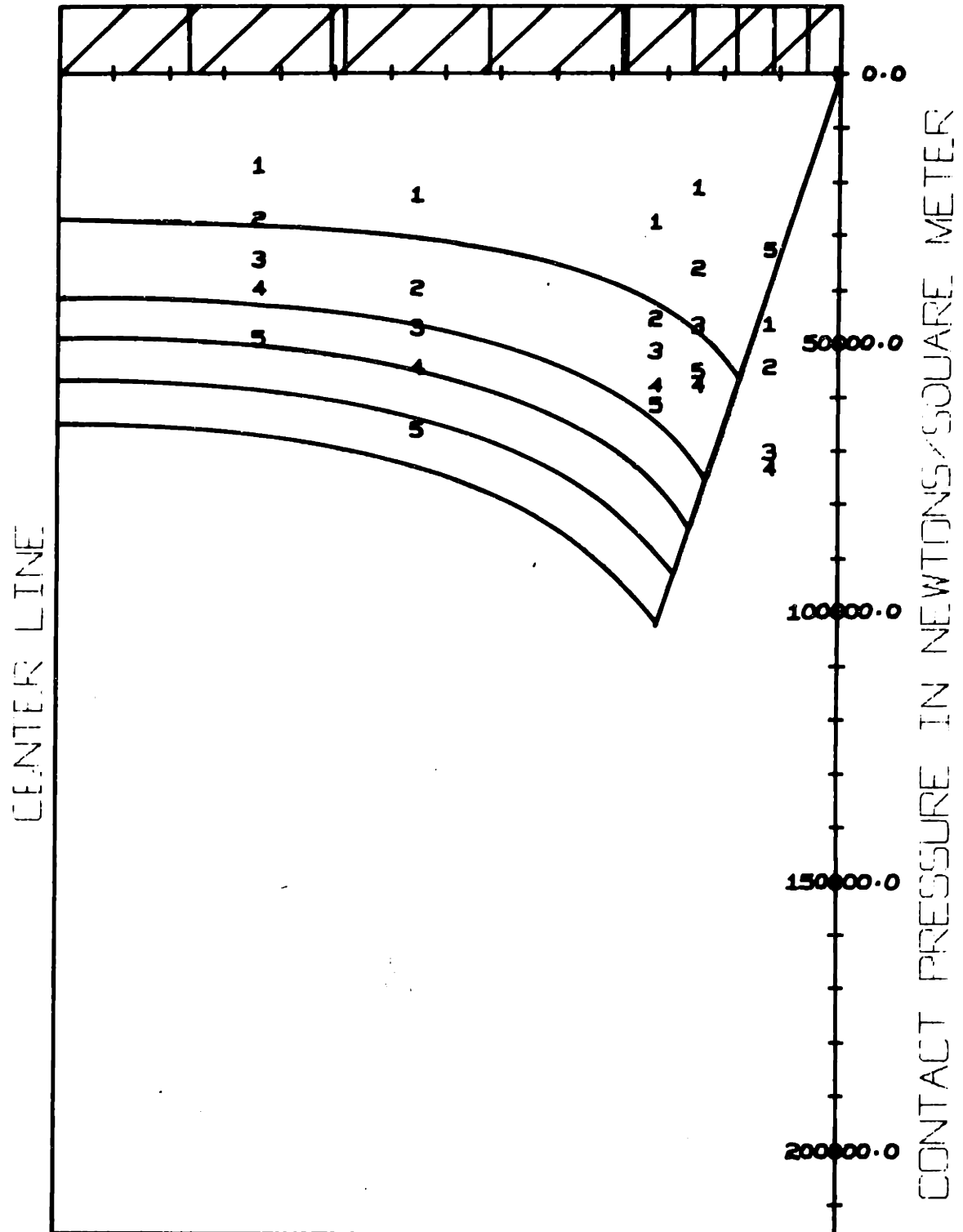
HALFWIDTH = 0.07 METERS



HALFWIDTH = 0.07 METERS



HALFWIDTH = 0.07 METERS



HALFWIDTH = 0.07 METERS

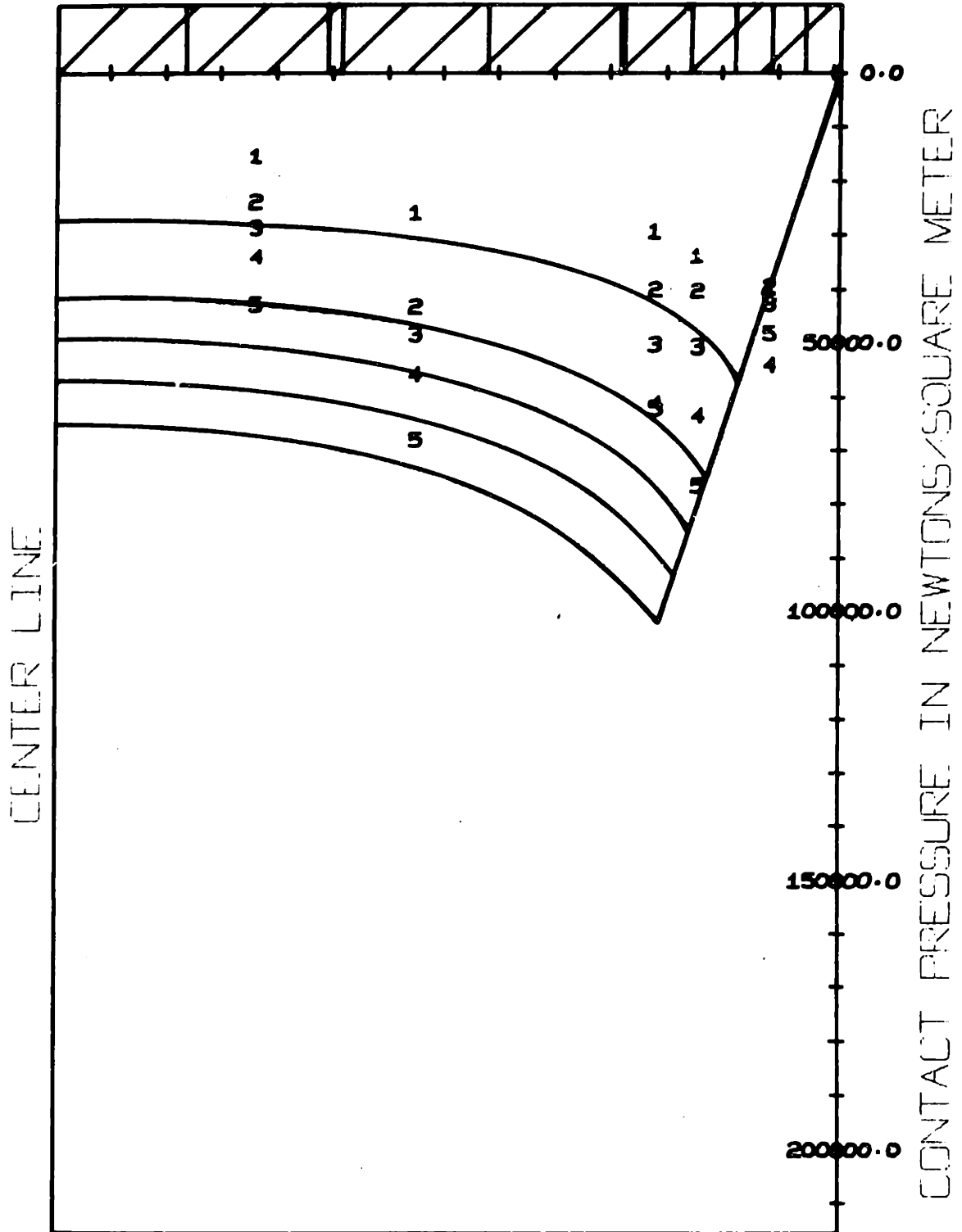


FIG. 4.11

VALUE OF m BACK-CALCULATED  
FOR WHOLE PLATE

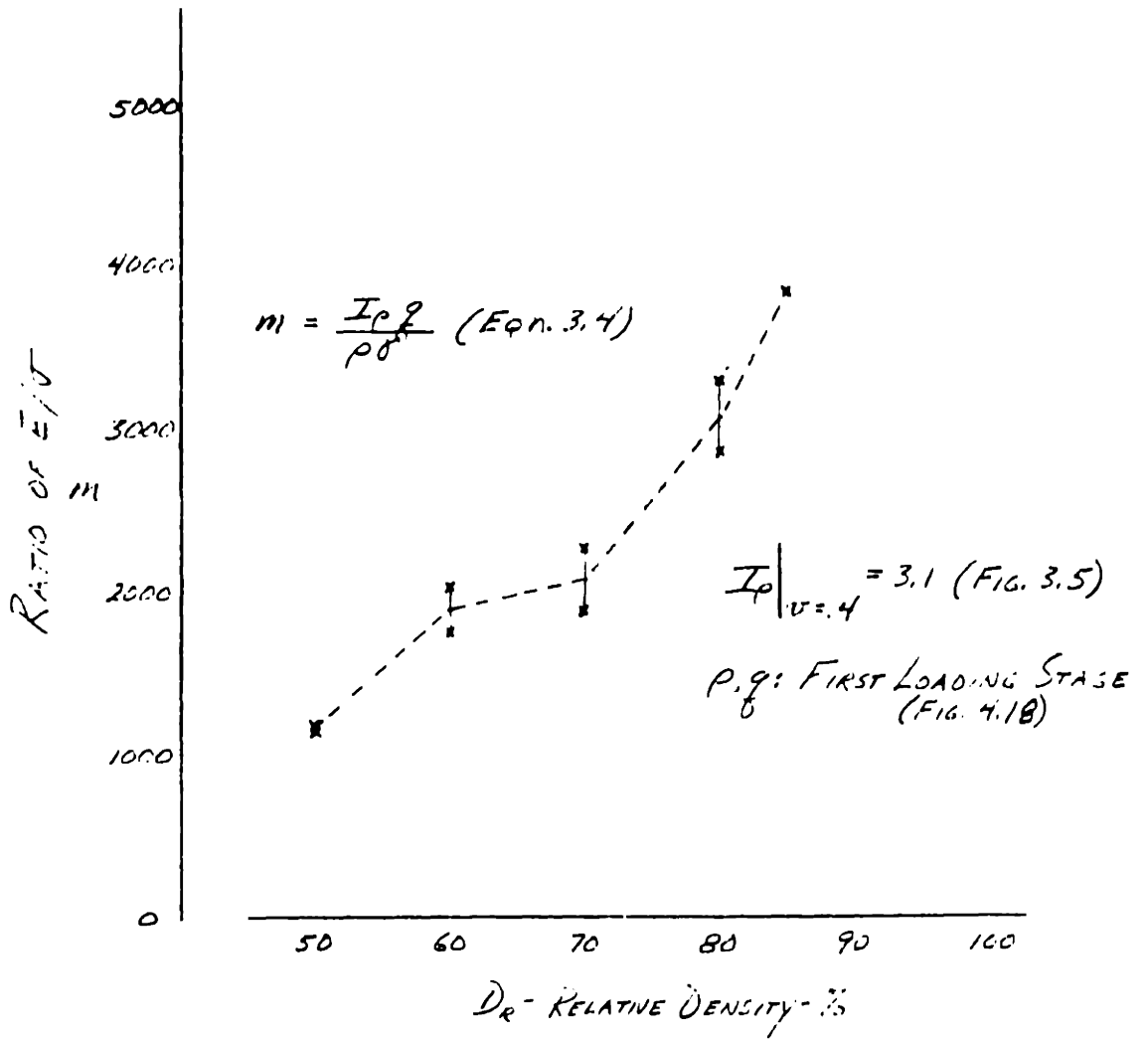
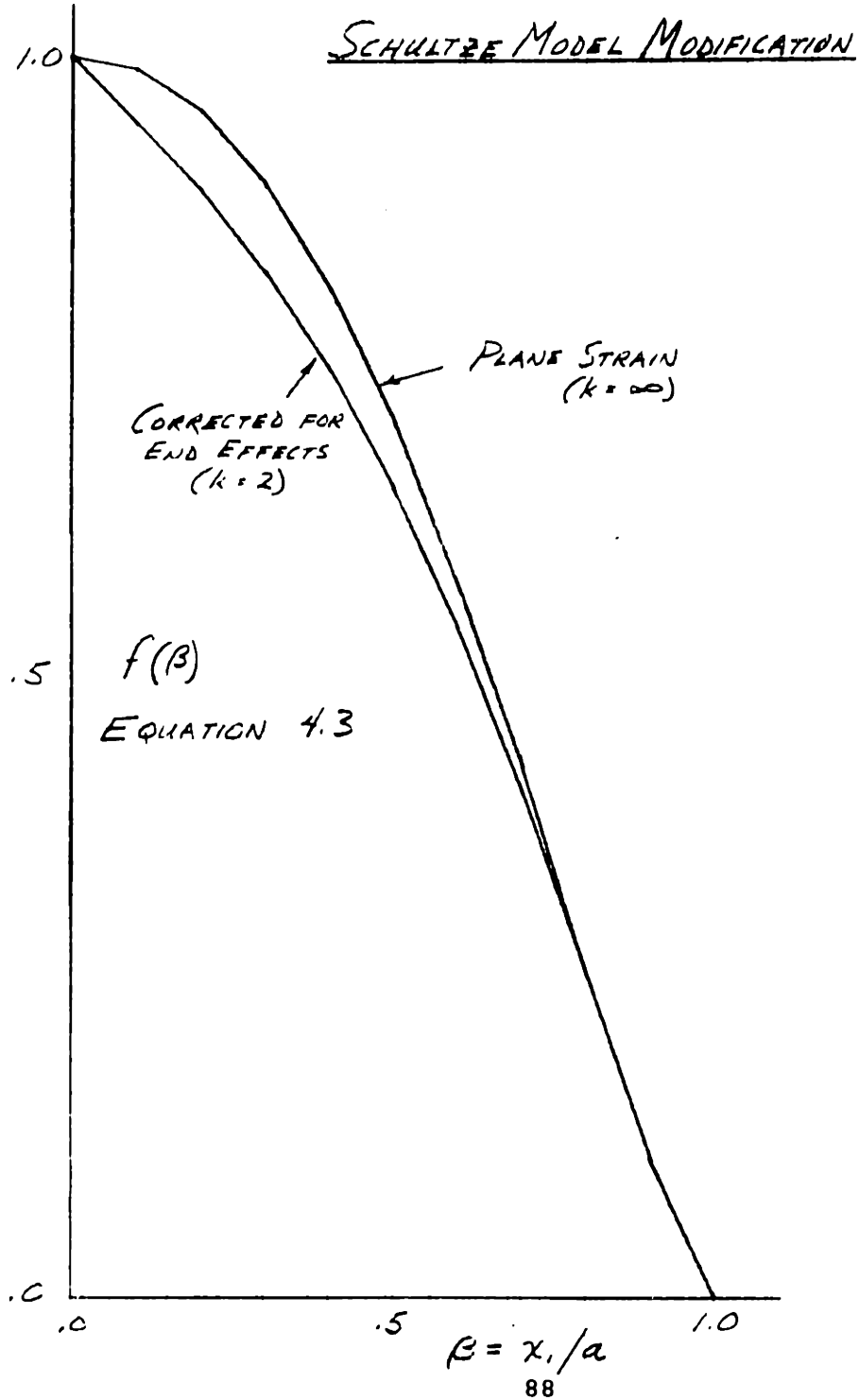




FIG. 4.12



# DAVIS PLASTICITY PARAMETERS

FROM TRIAXIAL CID TESTS

- :  $\sigma_c = 49,000 \text{ NWT/M}^2$
- x :  $\sigma_c = 98,000 \text{ NWT/M}^2$
- + :  $\sigma_c = 245,000 \text{ NWT/M}^2$
- :  $\sigma_c = 196,000 \text{ NWT/M}^2$   
(KR: SATURATED)
- Δ :  $\sigma_c = 93,000 \text{ NWT/M}^2$   
(NIR: PS SATURATED)

$$N_{\phi f} = \frac{\sigma_1 / \sigma_3}{\left(1 - \frac{d\epsilon_{vol}}{d\epsilon_1'}\right)}$$

$$\mu = \frac{\sigma_1}{\sigma_3} \left[ \frac{\left(1 - \frac{d\epsilon_{vol}}{d\epsilon_1'}\right) + 2}{2 \left[ \left(2 - \frac{d\epsilon_{vol}}{d\epsilon_1'}\right) + \frac{\sigma_1}{\sigma_3} \right]} \right]$$

VOID RATIO AFTER CONSOLIDATION

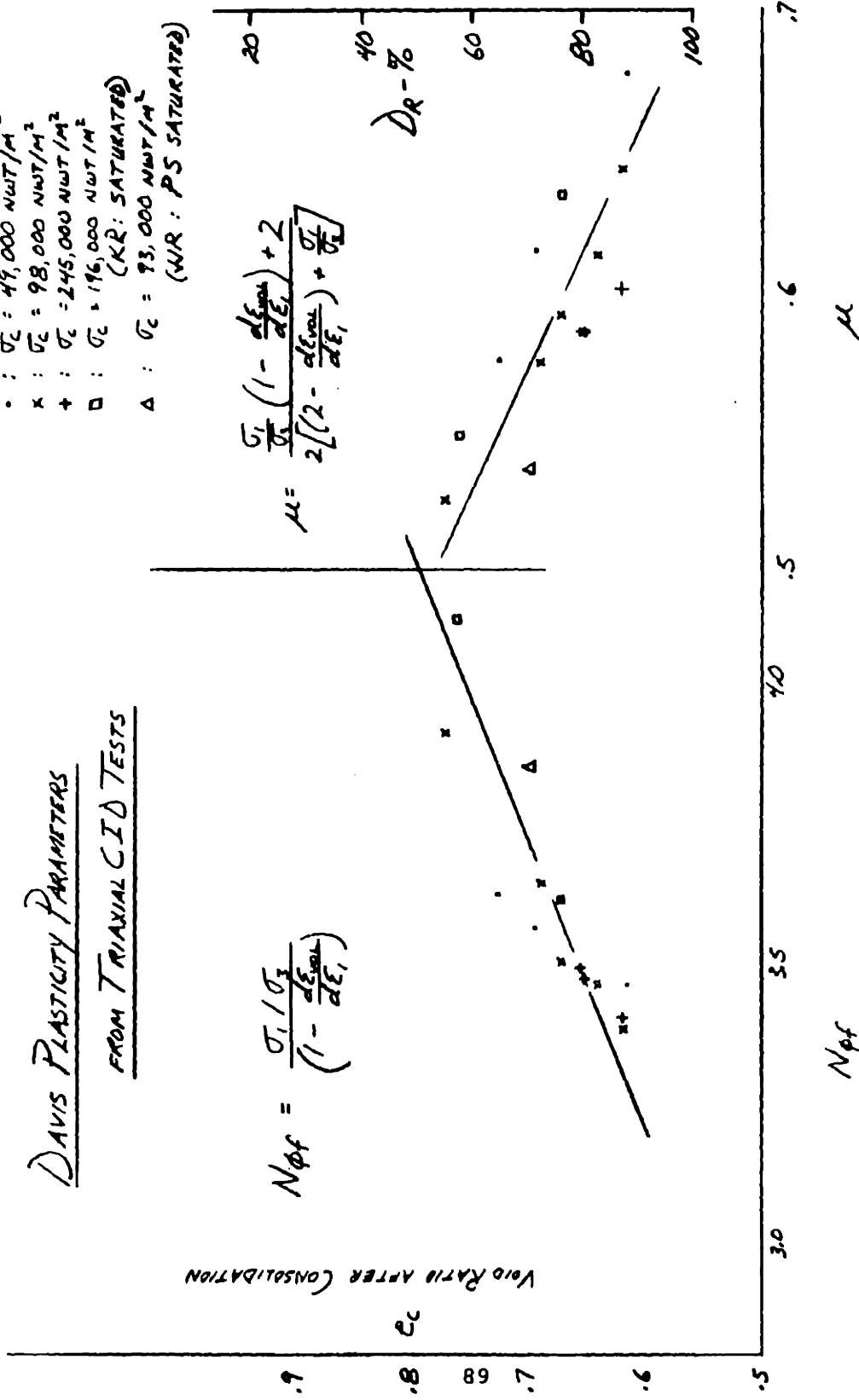


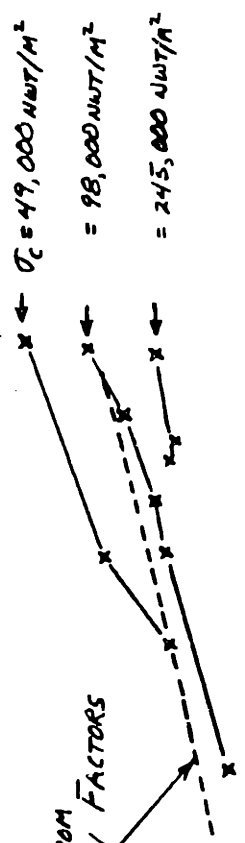
Fig. 4.13

# TRIAXIAL FRICTION ANGLE

$$\tan^2(45^\circ + \frac{\phi_{TRI}}{2}) = \frac{(2\mu + 2\mu N_{AF}) + [(2\mu + 2\mu N_{AF})^2 - 8N_{AF}(1-A)]^{1/2}}{2}$$

FRICTION ANGLE

φ<sub>TRI</sub> CALCULATED FROM  
DAVIS PLASTICITY FACTORS  
(FIG. 4.13)



x - FRICTION ANGLE MEASURED  
IN CID TRIAXIAL TESTS

φ<sub>TRI</sub>

50°

30°

e<sub>c</sub> - VOID RATIO AFTER CONSOLIDATION

D<sub>R</sub> - RELATIVE DENSITY - %

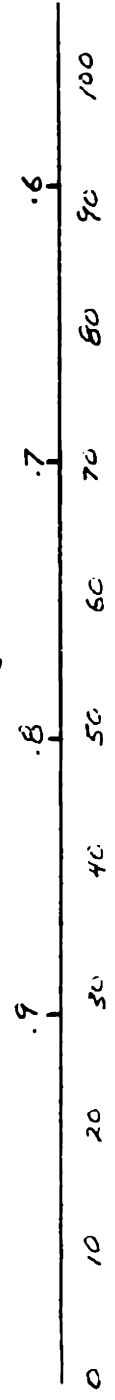
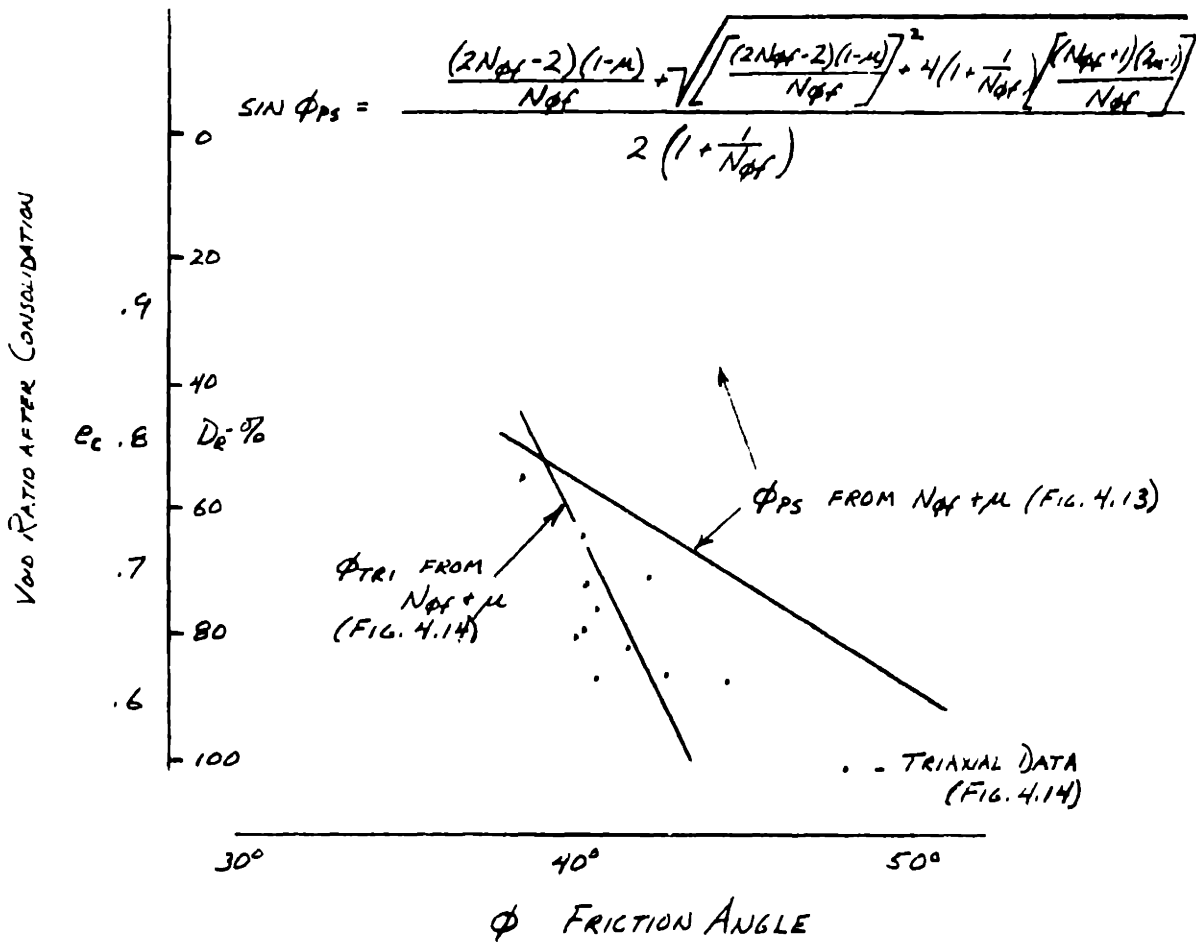


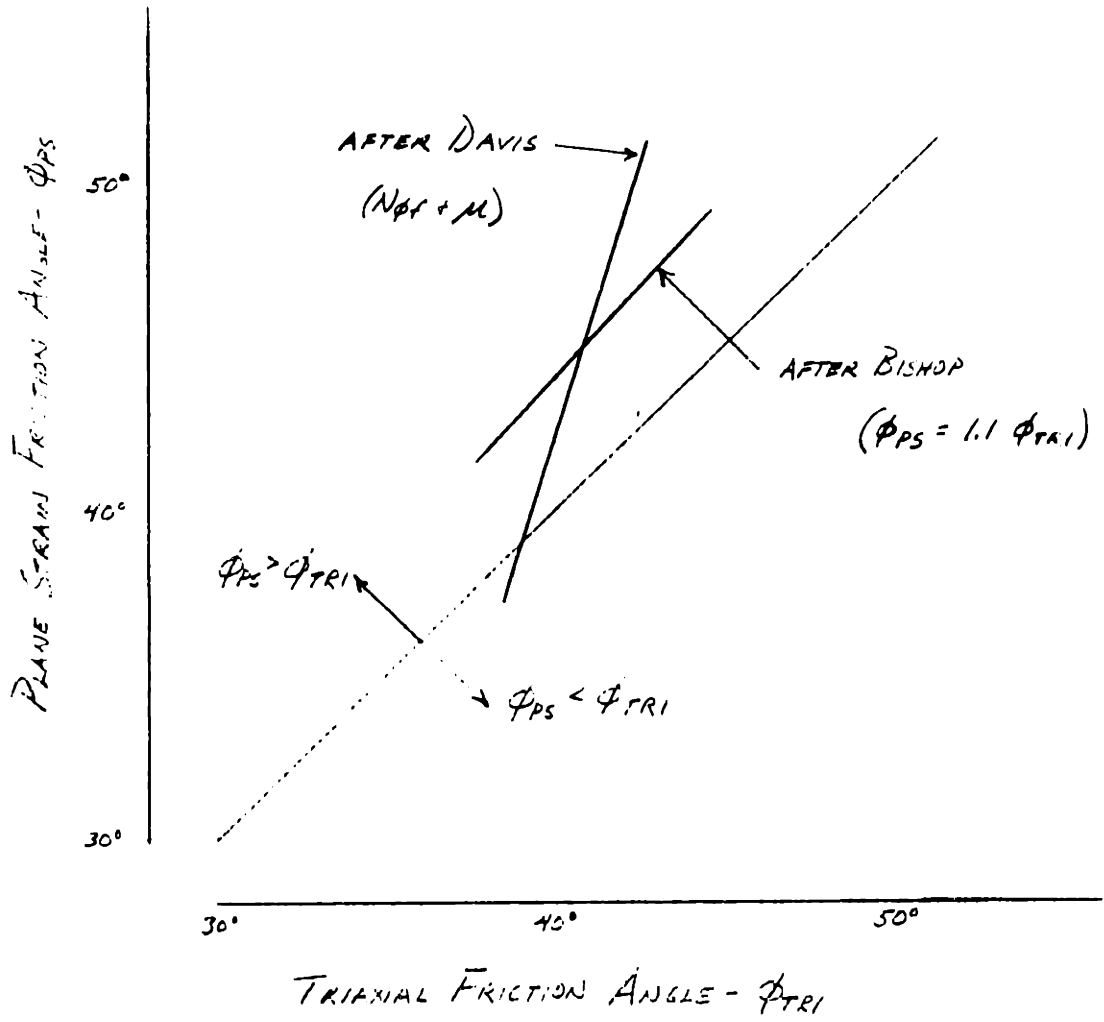
FIG. 4.14

FIG. 4.15

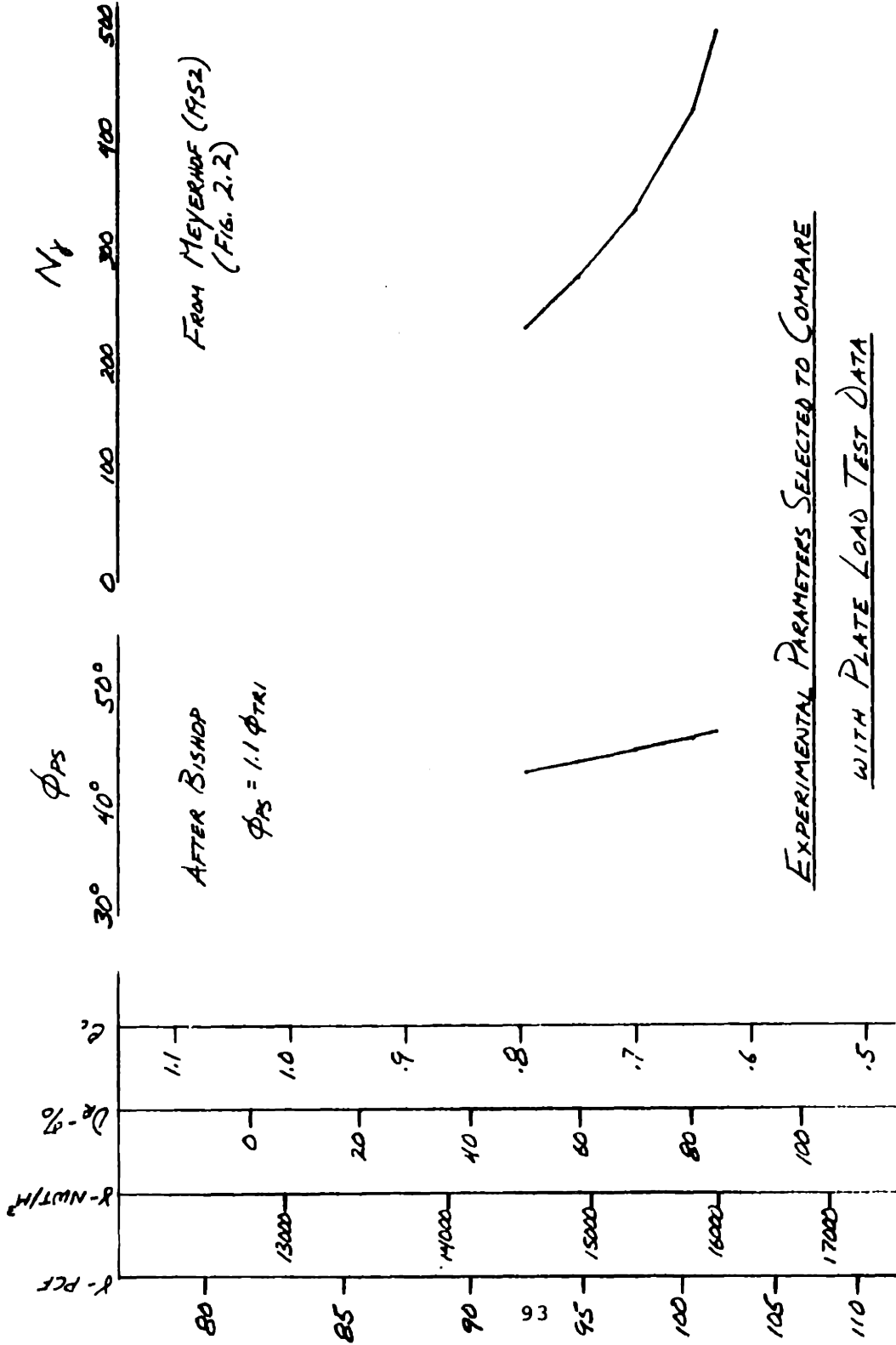


COMPARISON OF  $\phi_{TRI}$  AND  $\phi_{PS}$  FROM  $N_{\phi f}$  AND  $\mu$

FIG. 4.16



FRICTION ANGLE : TRIAXIAL VS. PLANE STRAIN



SEE TABLE 4.2

FIG. 4.17

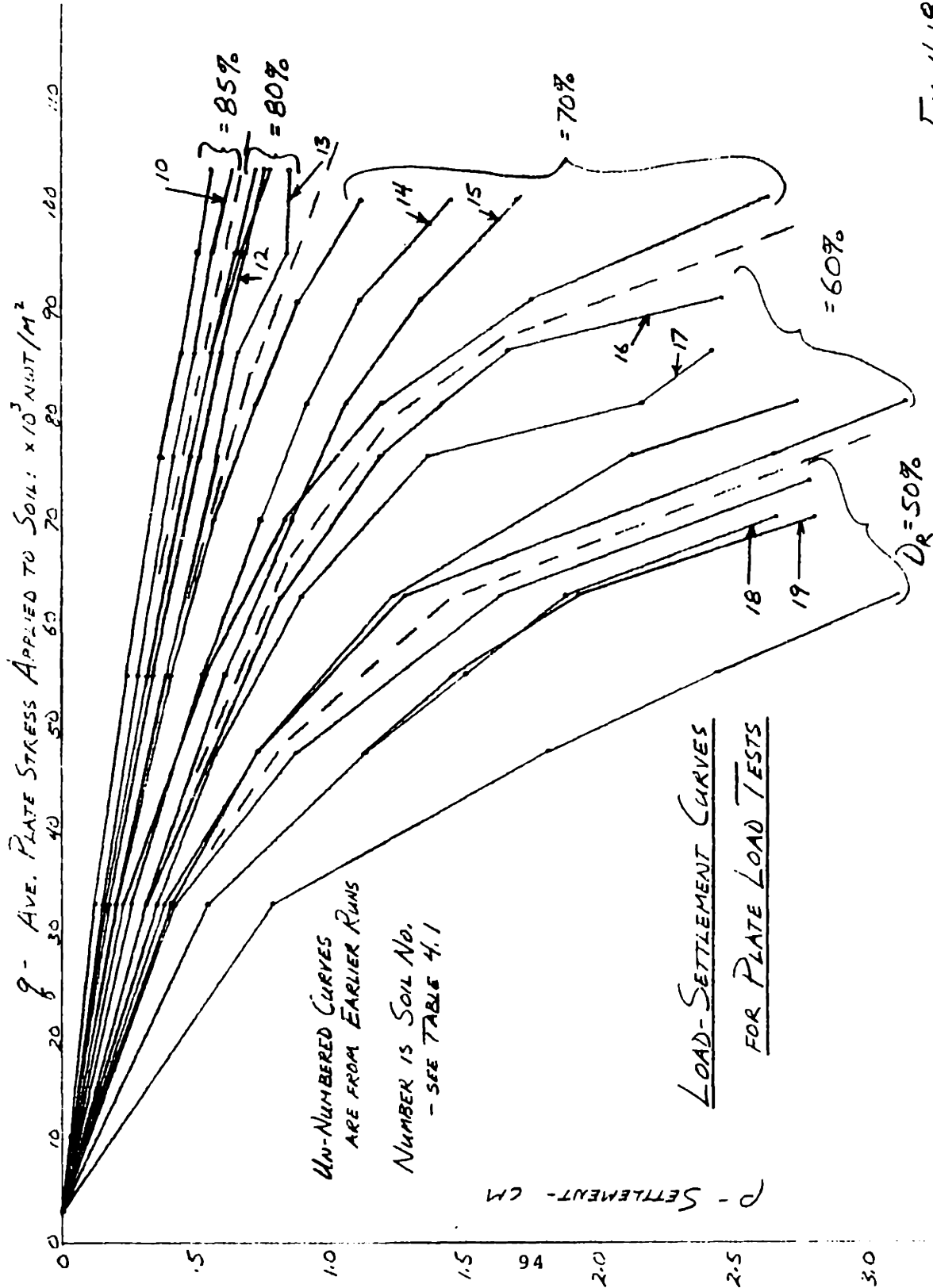


FIG. 4.18

FIG. 4.19

PREDICTED VS. MEASURED FAILURE  
LOAD FOR WHOLE PLATE

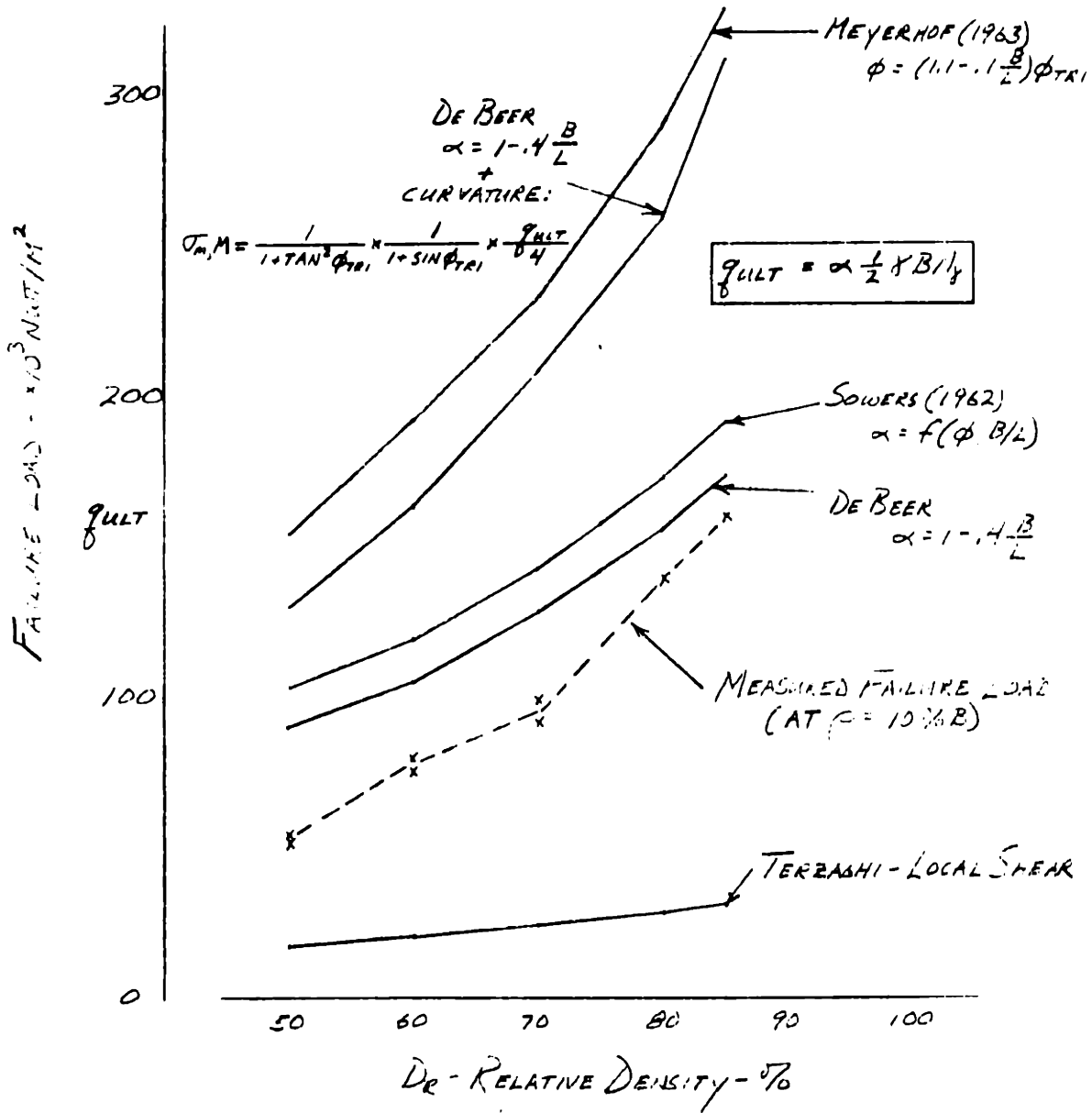
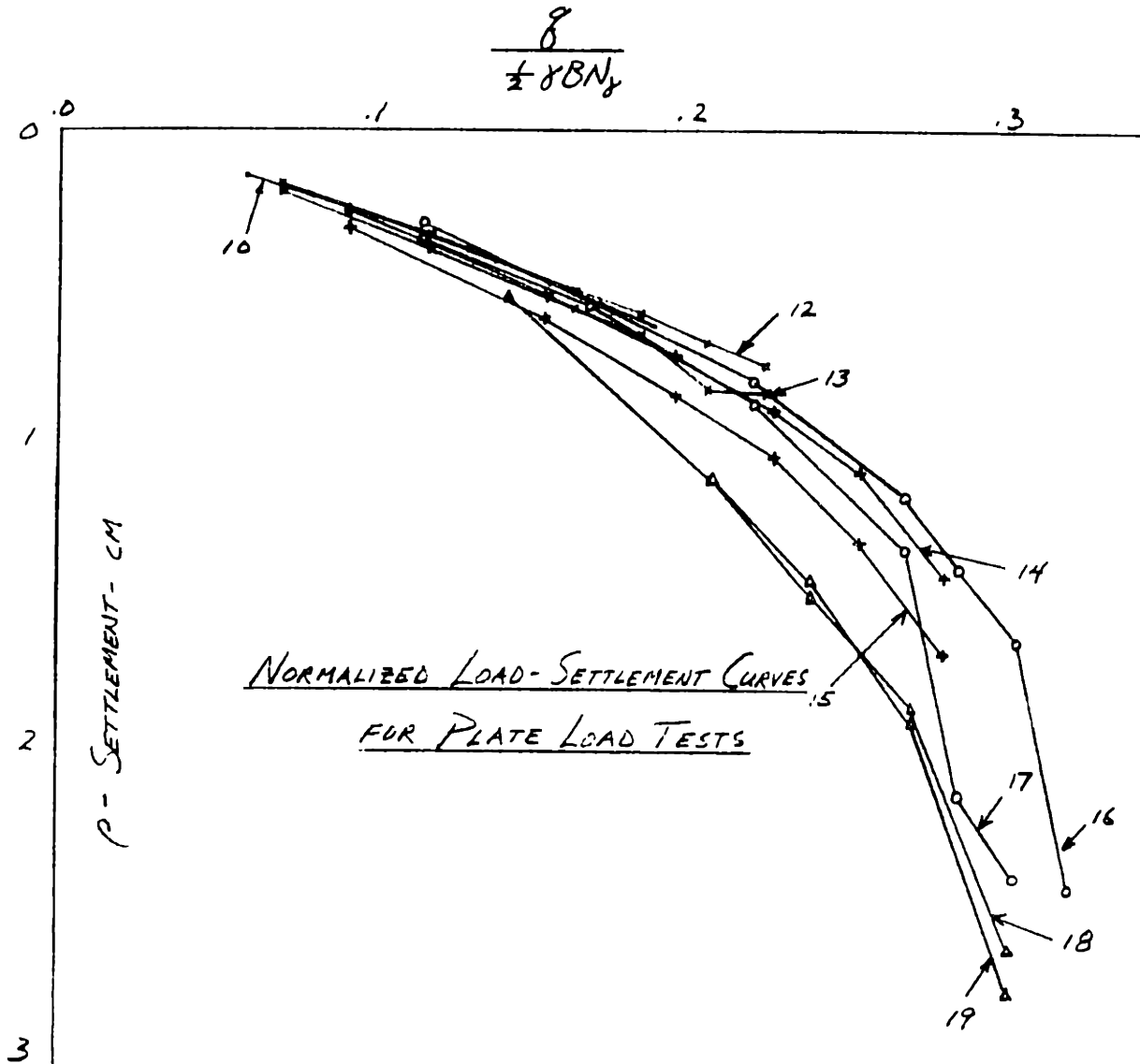


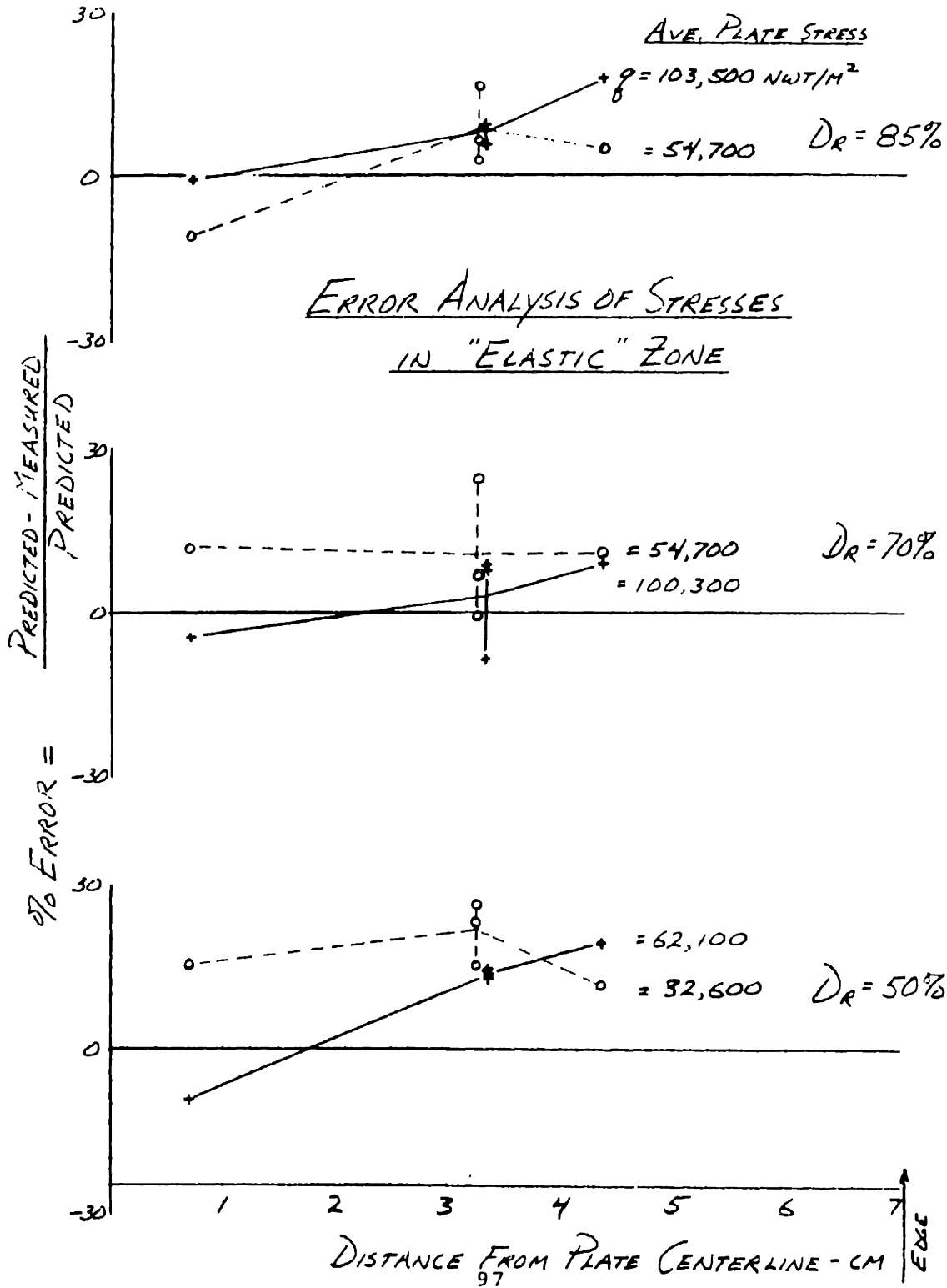


FIG. 4.20



<u>SYMBOL</u>	<u>Dr</u>	<u>SOILS</u>
.	85%	10
x	80%	12; 13
+	70%	14; 15
o	60%	16; 17
Δ	50%	18; 19

FIG. 4.21



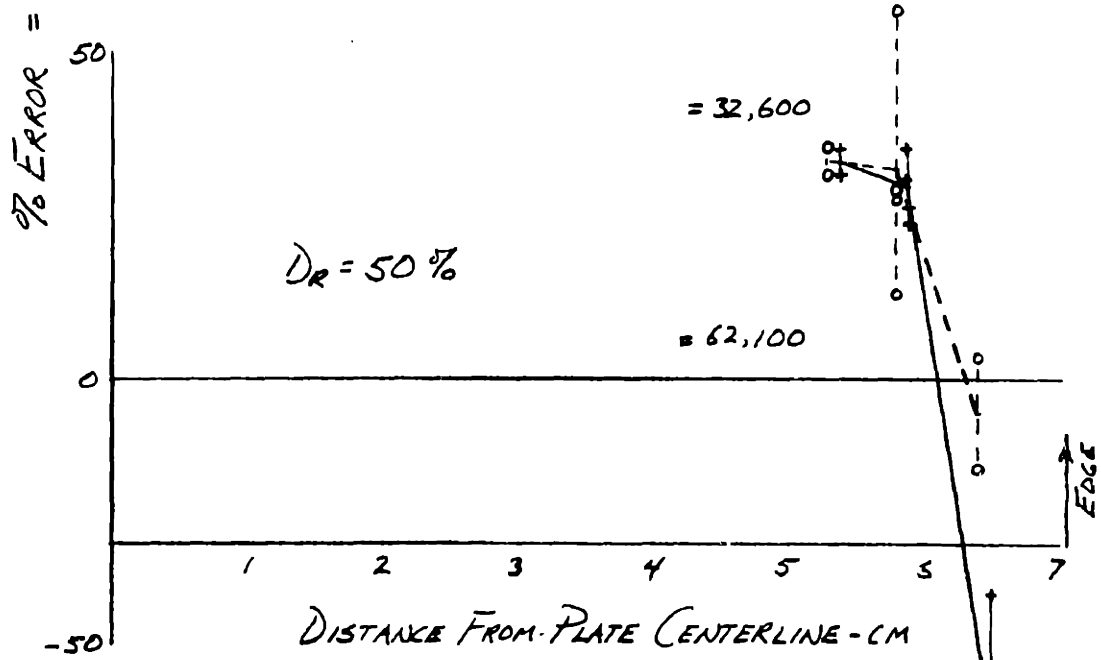
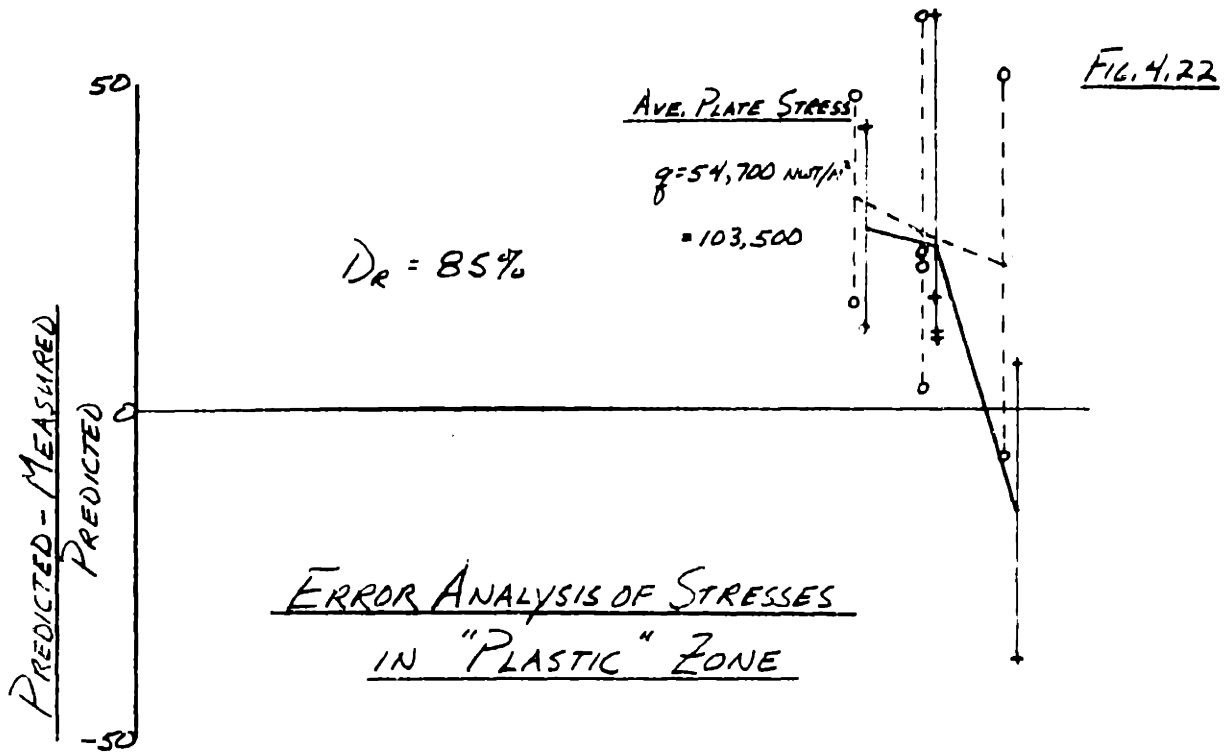


FIG. 4.23

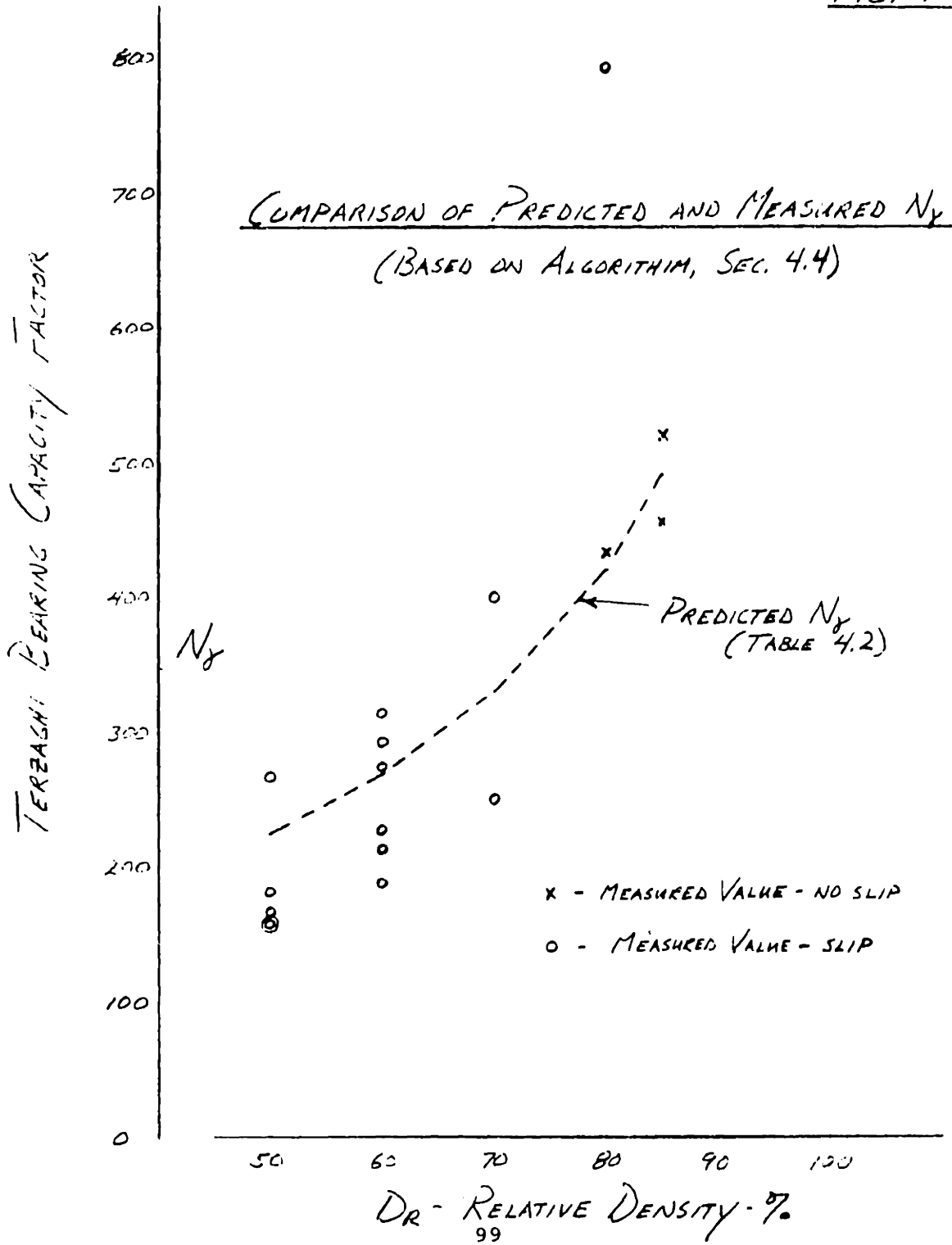


FIG. 4.24

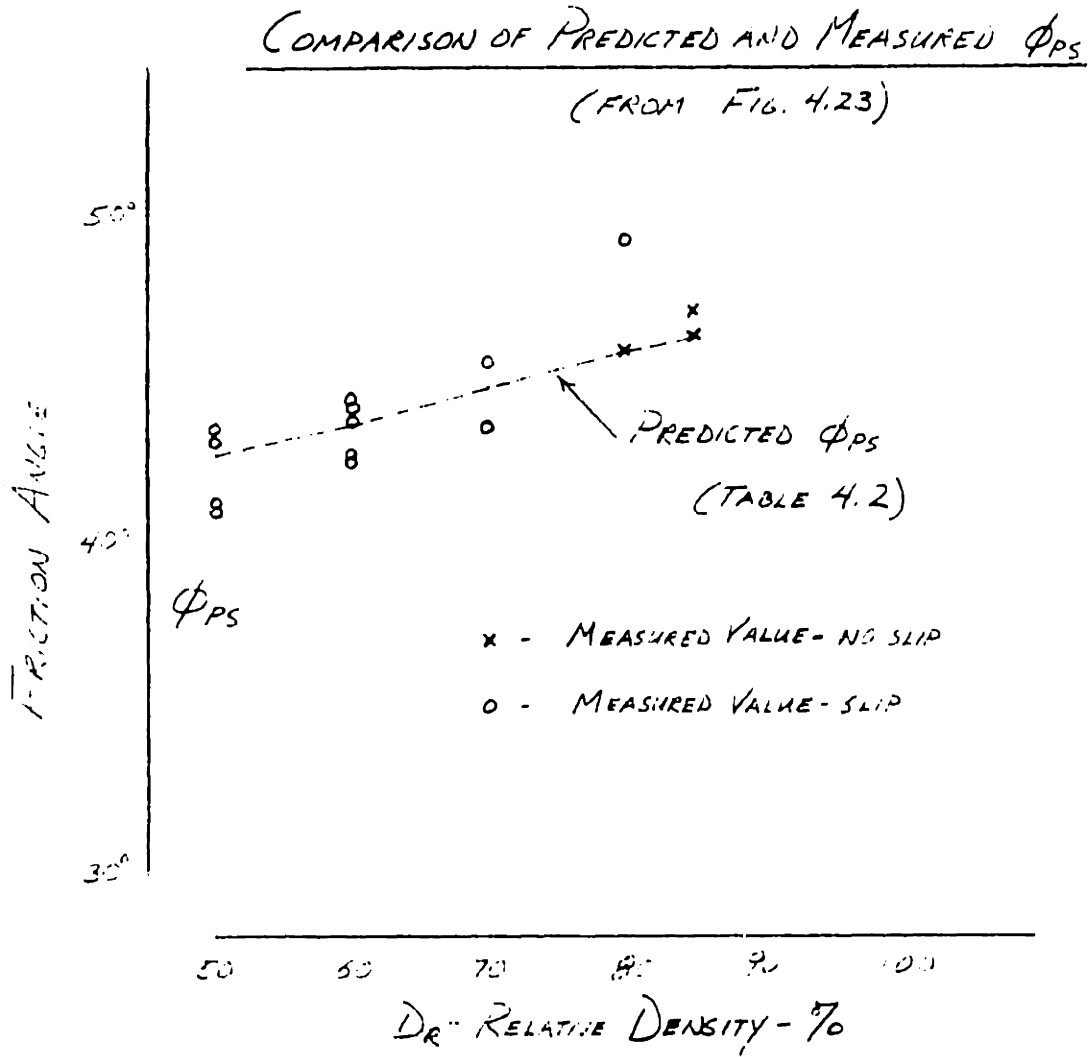
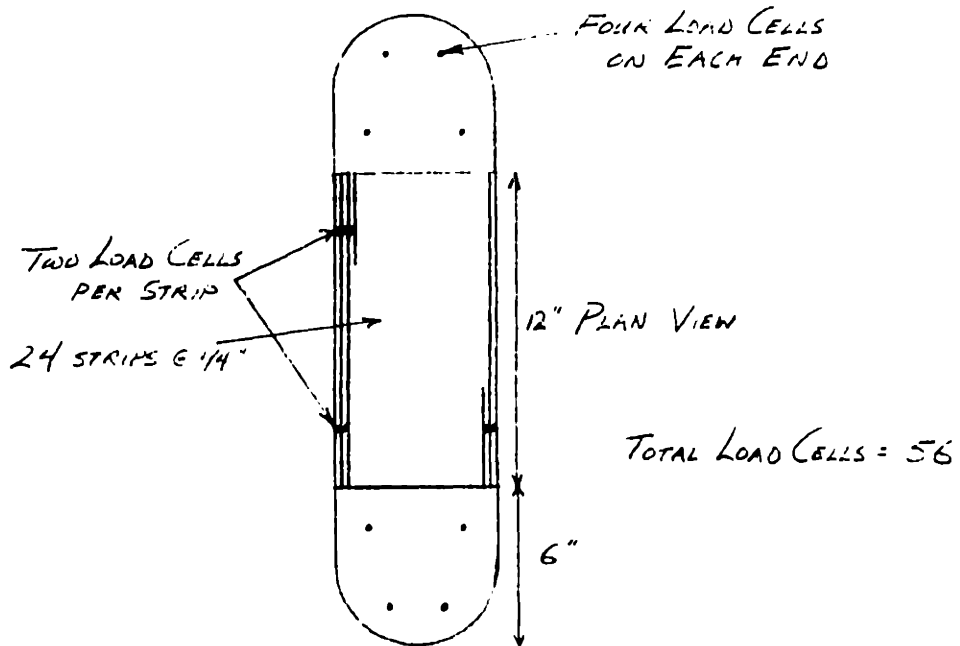
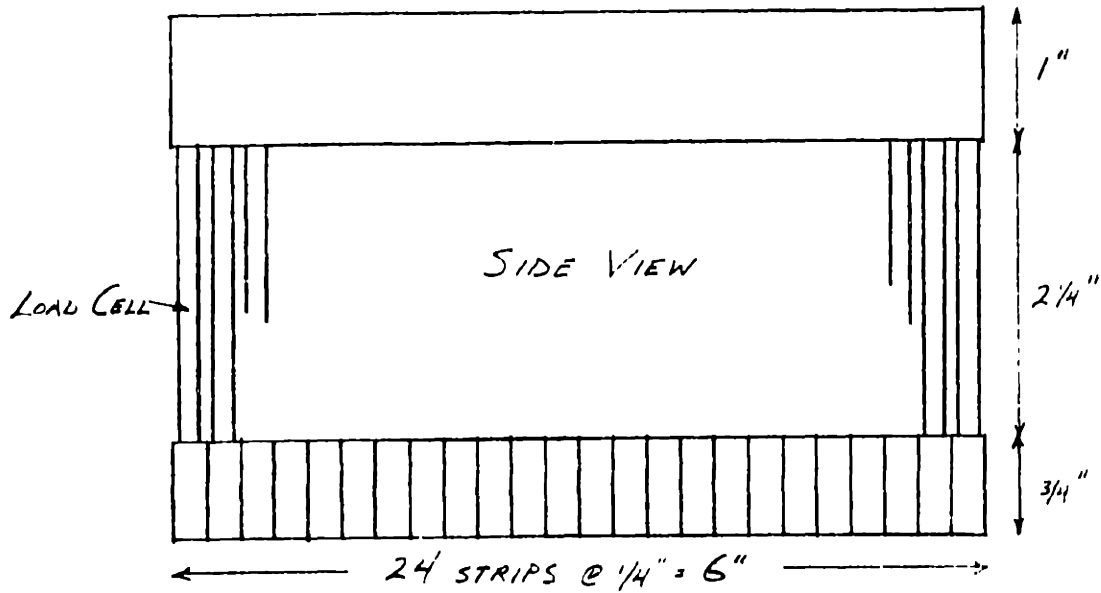
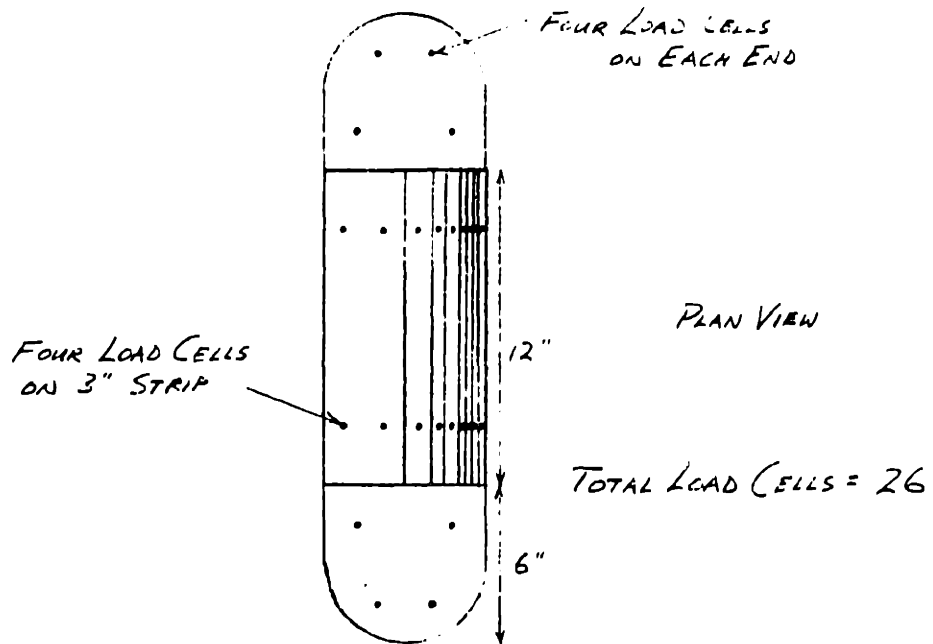
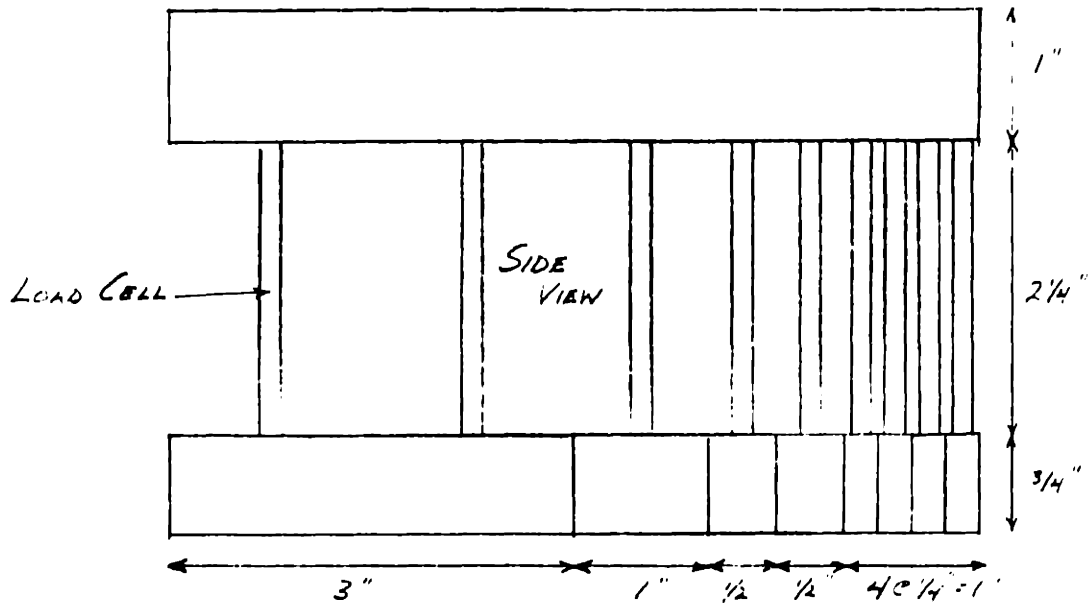


FIG. 5.1



IMPROVED DESIGN FOR INSTRUMENTED PLATE

FIG. 5.2



ALTERNATE DESIGN FOR INSTRUMENTED PLATE

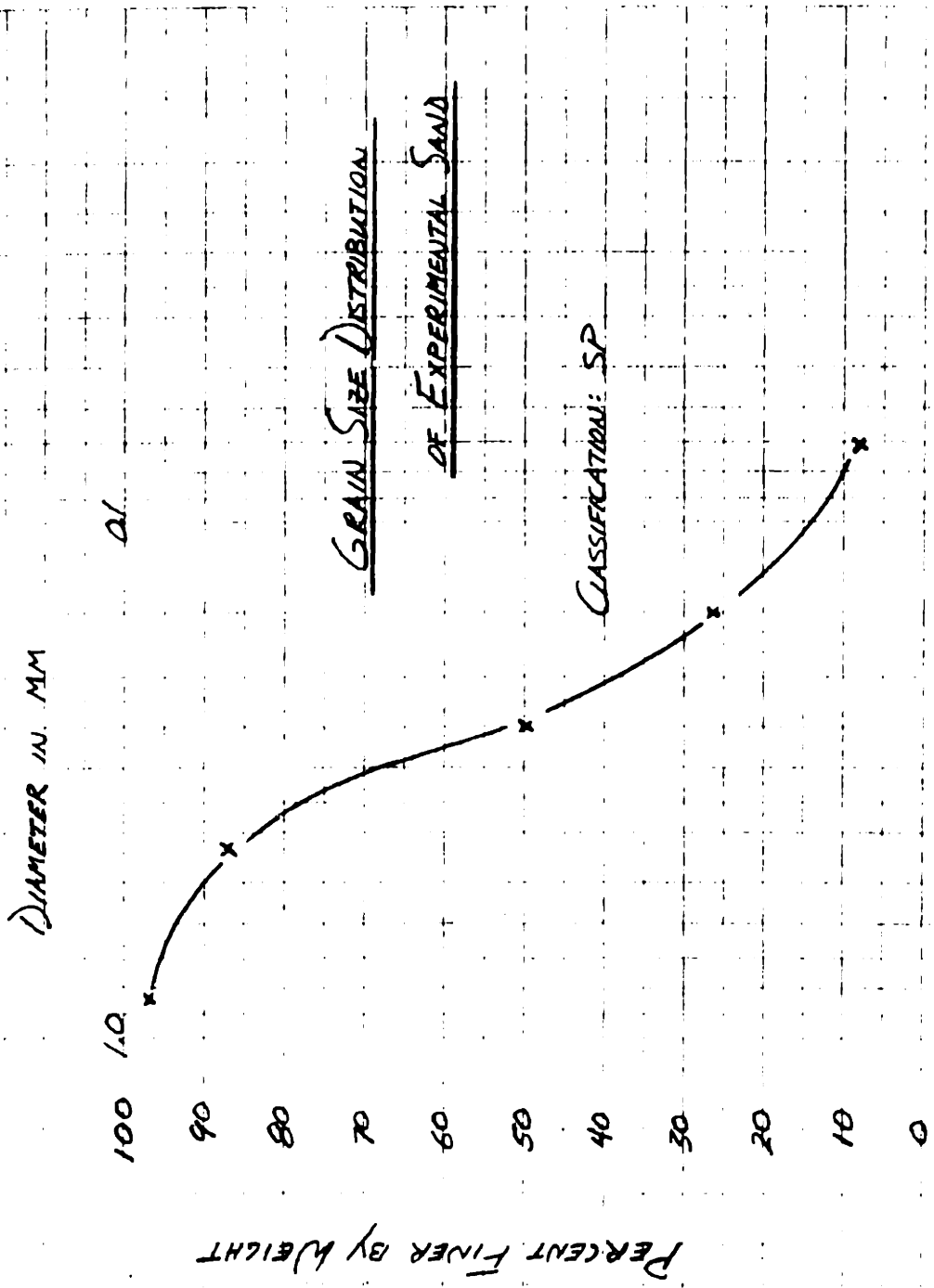


FIG. A1



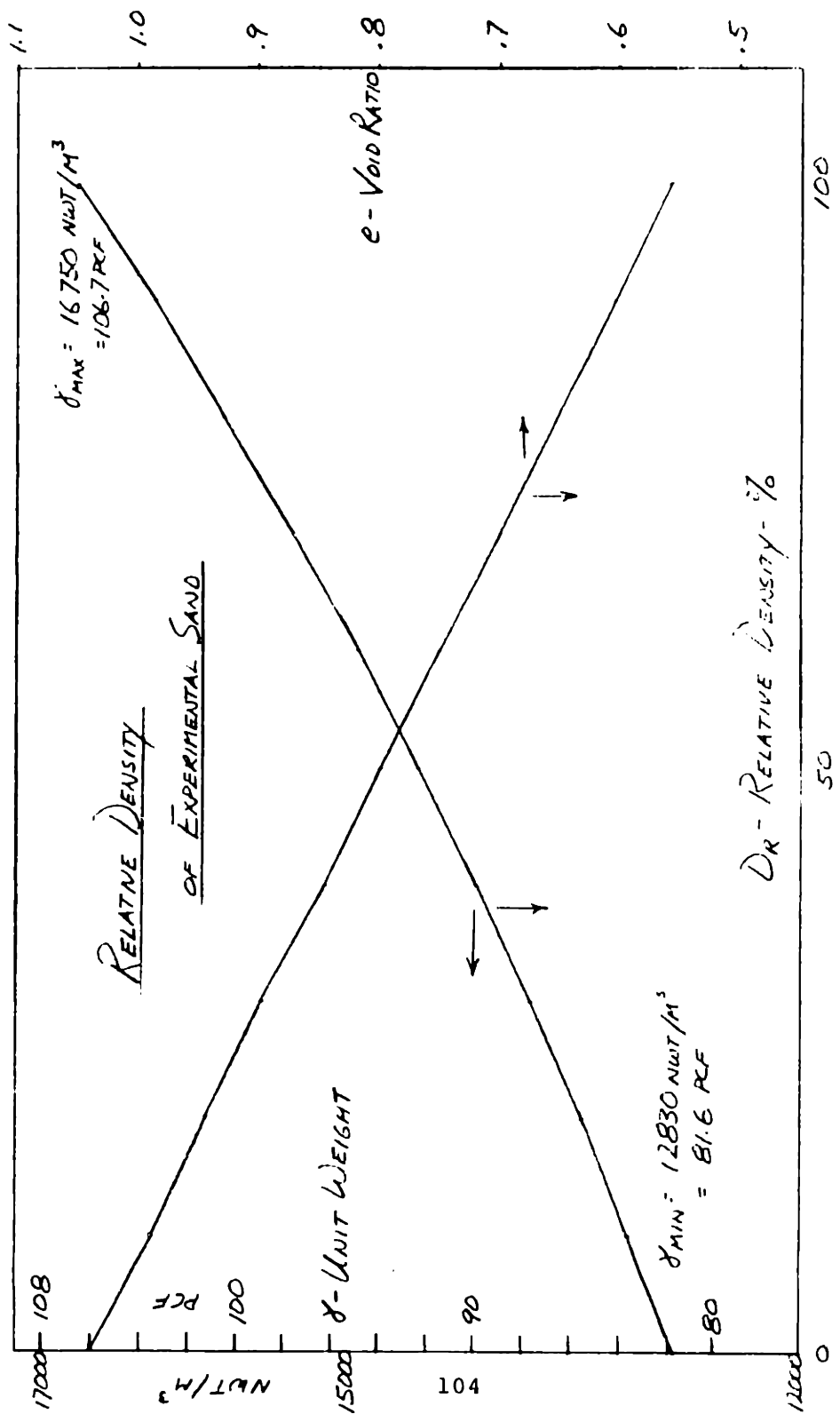


FIG. A.2

FIG. A.3

$D_{ri} = 50\%$   
 $e_c = .796$

DIRECT SHEAR TESTS

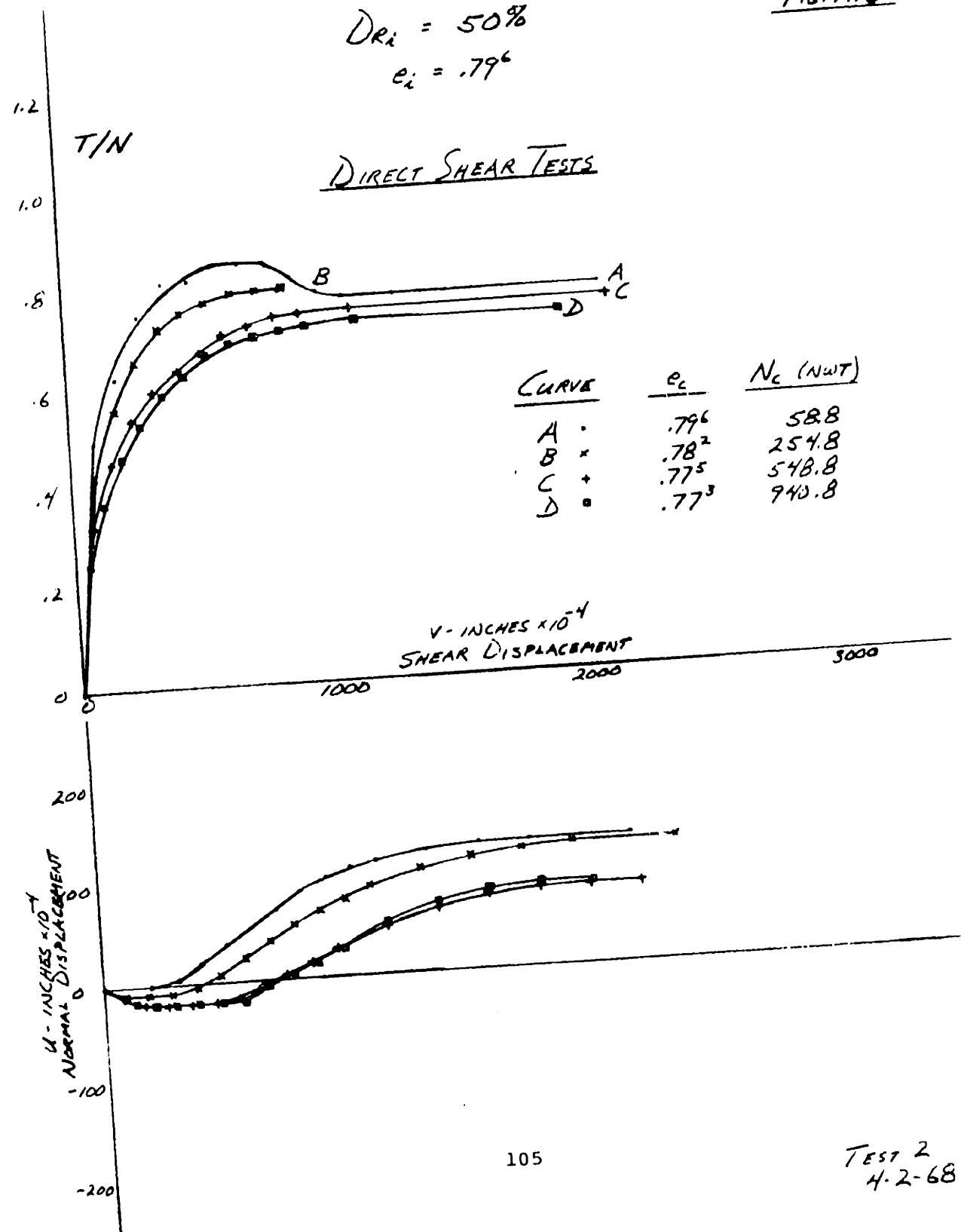


FIG. A.4

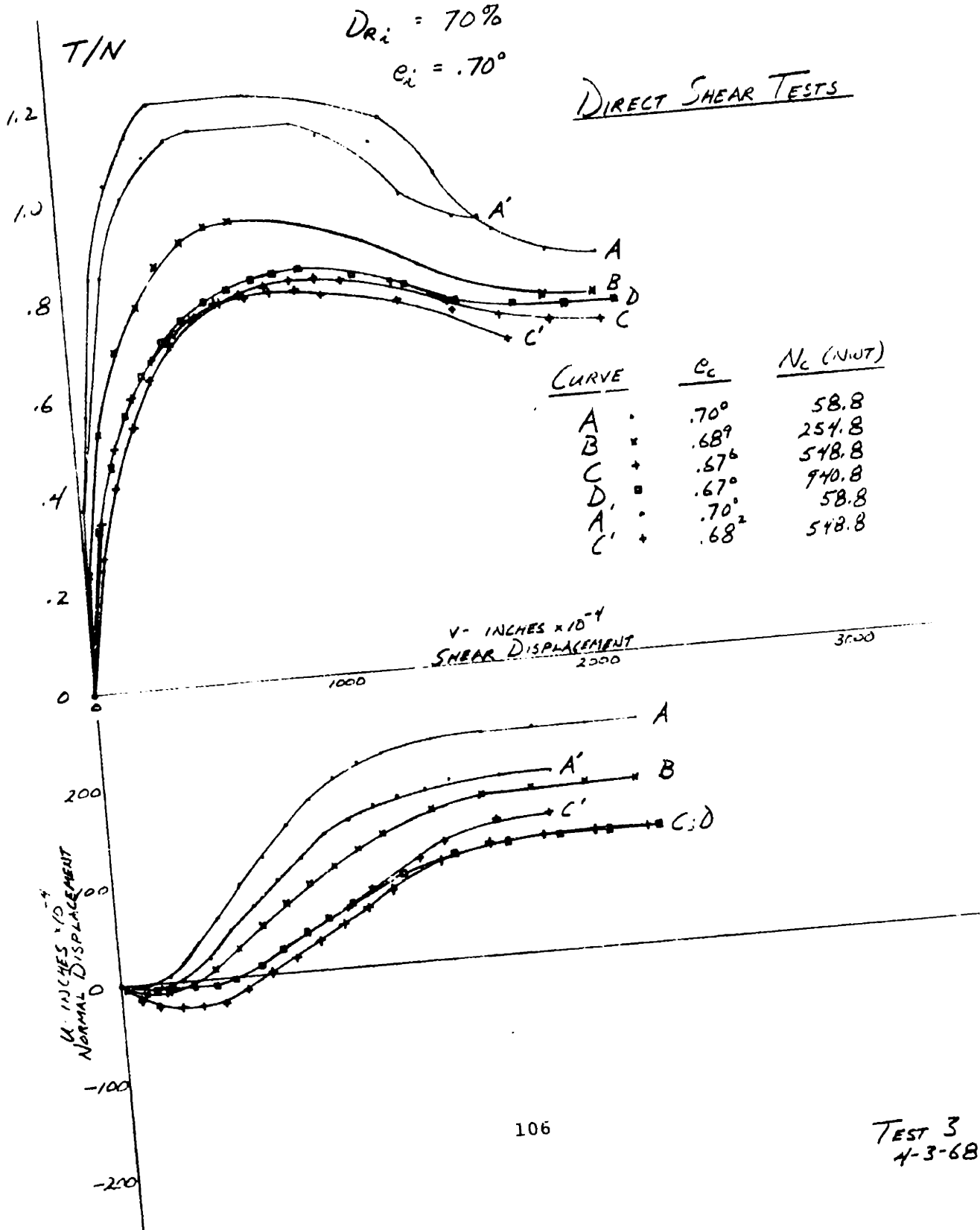


FIG. A.5

$DR_i = 30\%$

$e_i = .89^2$

DIRECT SHEAR TESTS

CURVE	$e_c$	$N_c(NWT)$
A •	.89 <sup>2</sup>	58.8
B ×	.87 <sup>2</sup>	25 <sup>2</sup> .8
C +	.85 <sup>2</sup>	54 <sup>2</sup> .8
D □	.84 <sup>2</sup>	94 <sup>2</sup> .8

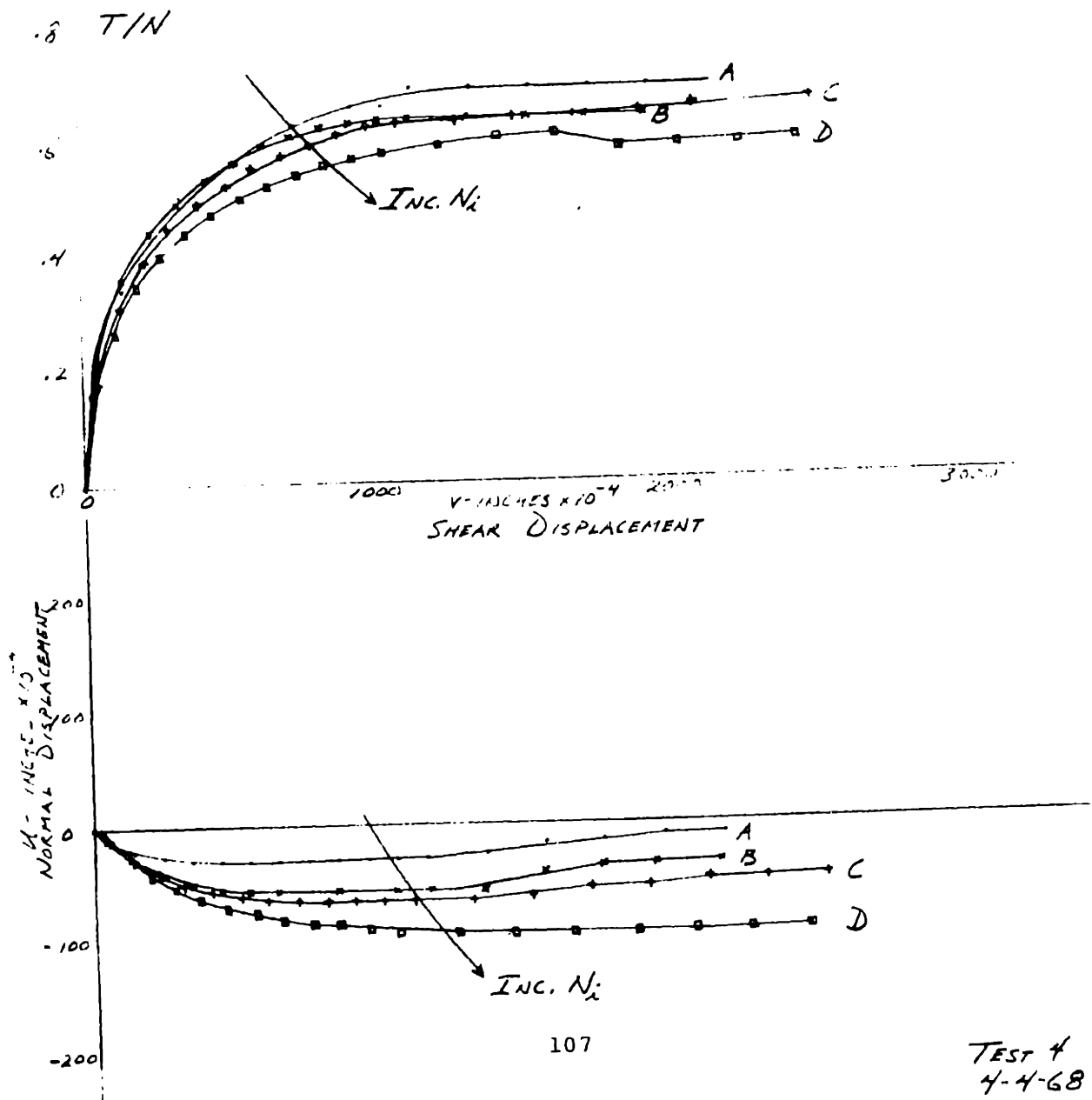
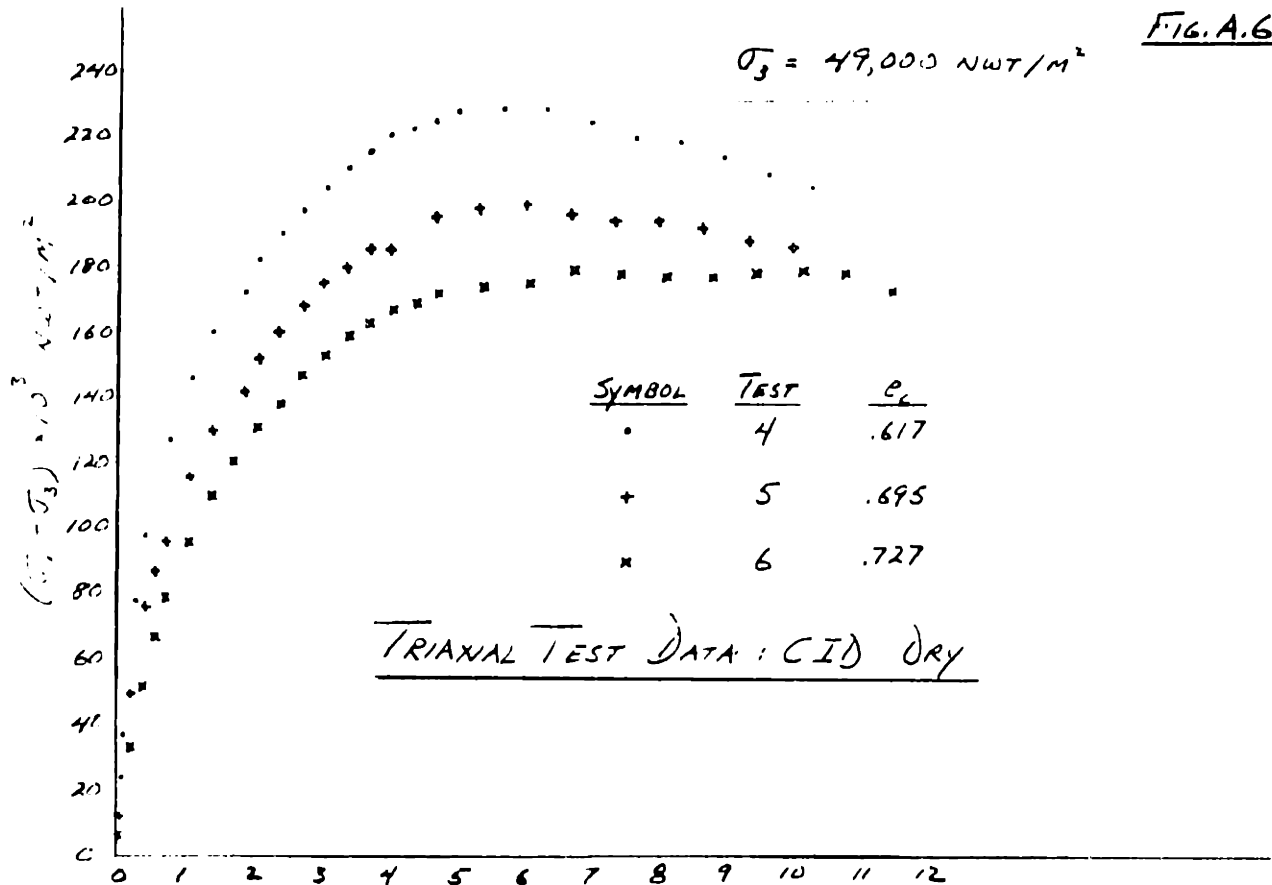
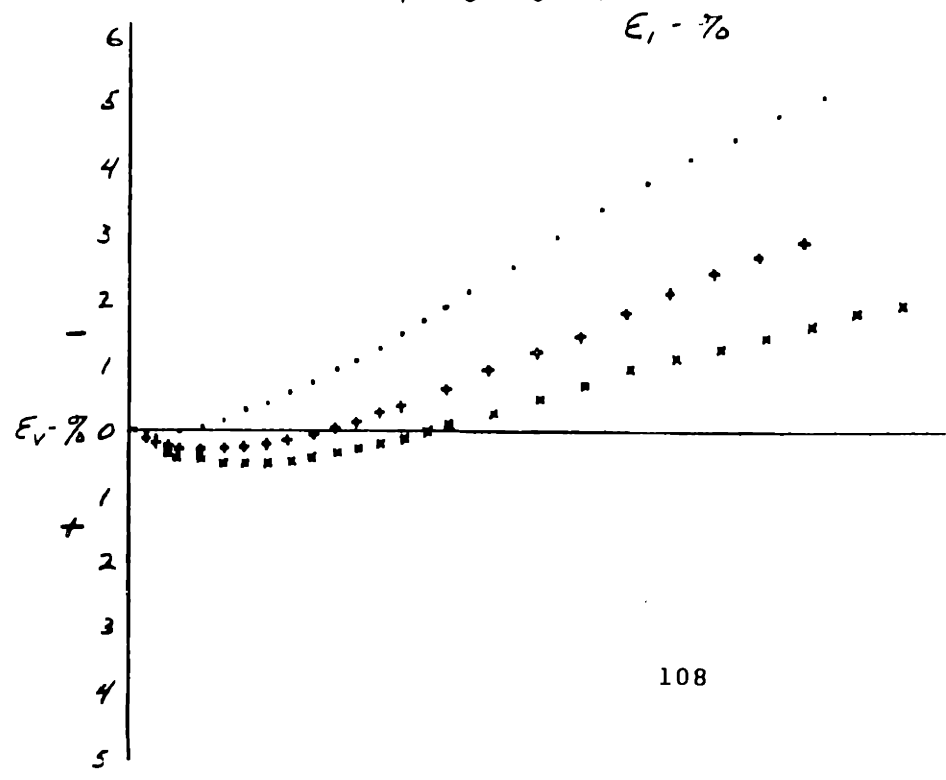


FIG. A.6



TRIAxIAL TEST DATA: CID DRY



$\sigma_3 = 98,000 \text{ NWT/M}^2$  FIG. A.7

TRIAXIAL TEST DATA: CID DRY

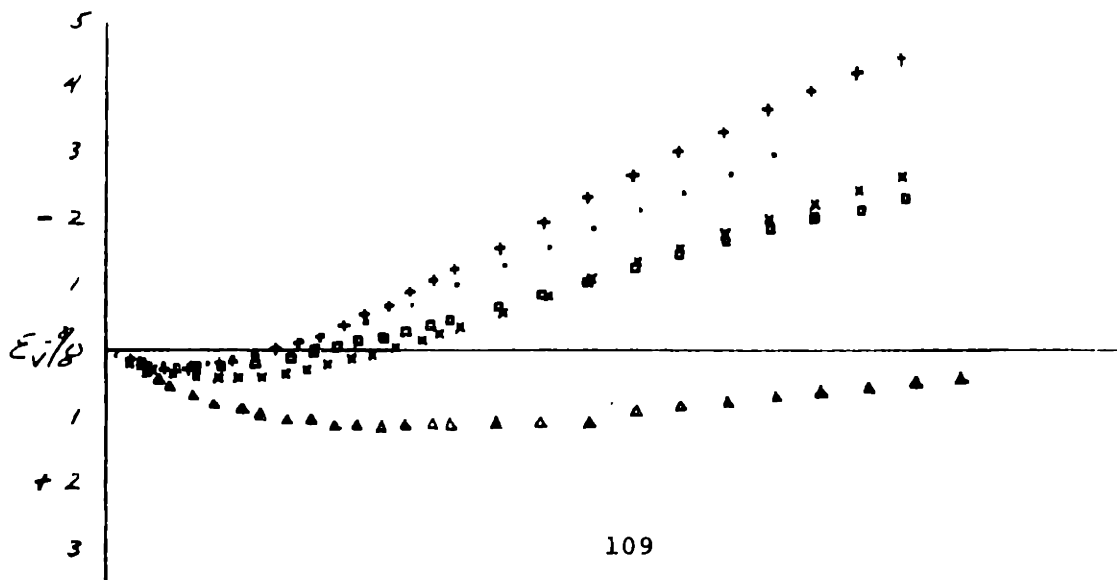
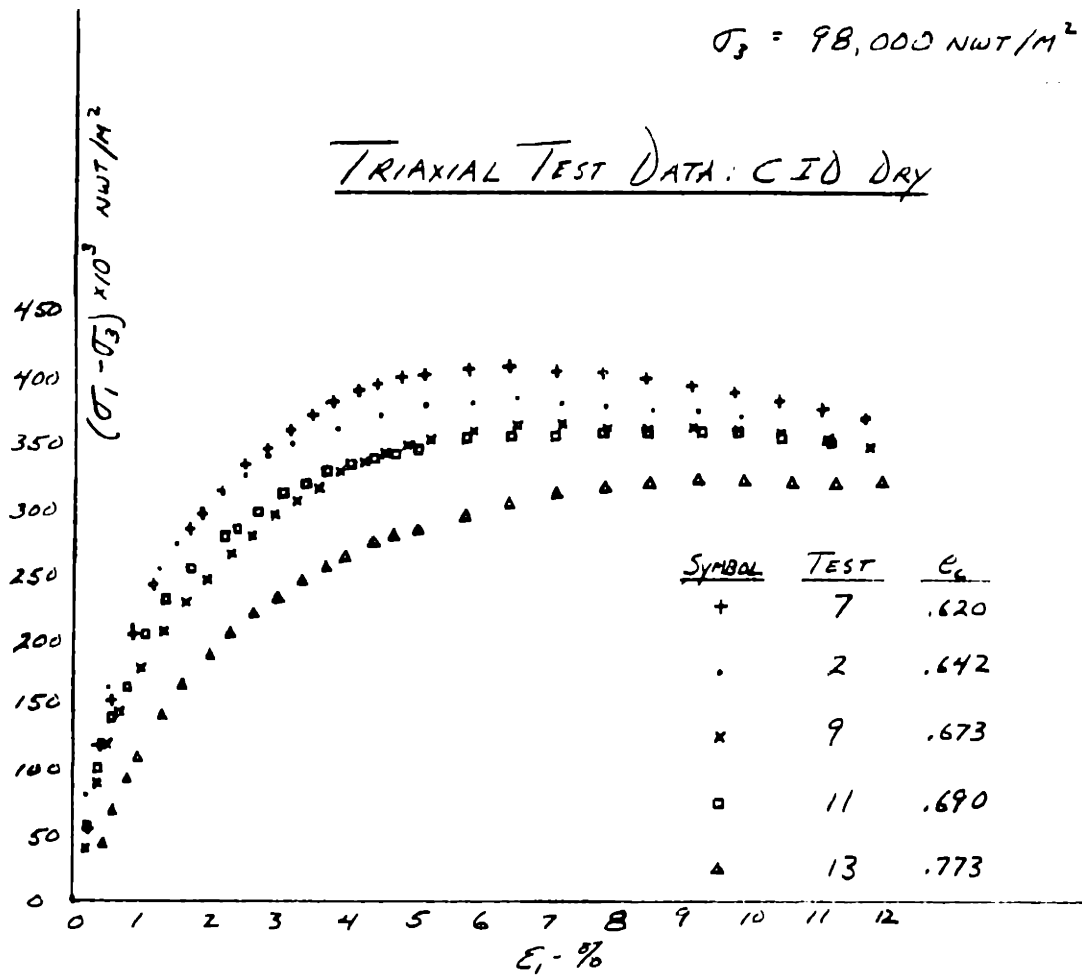
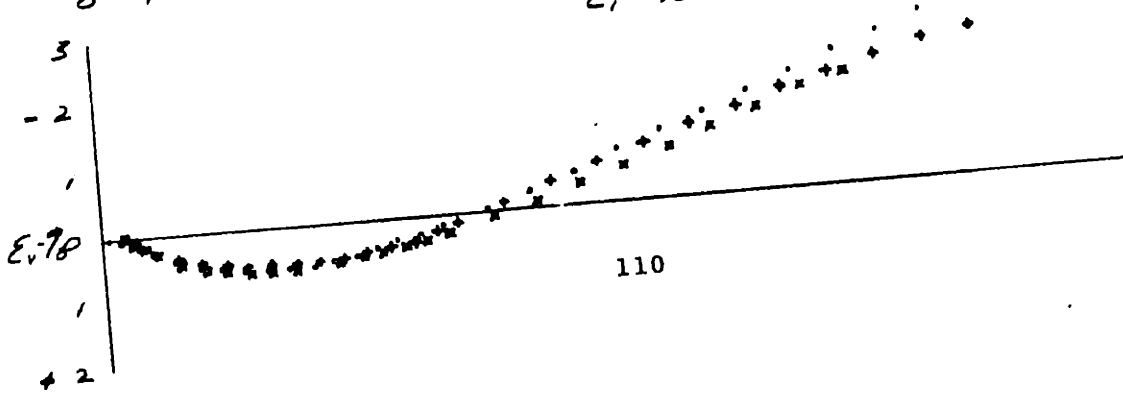
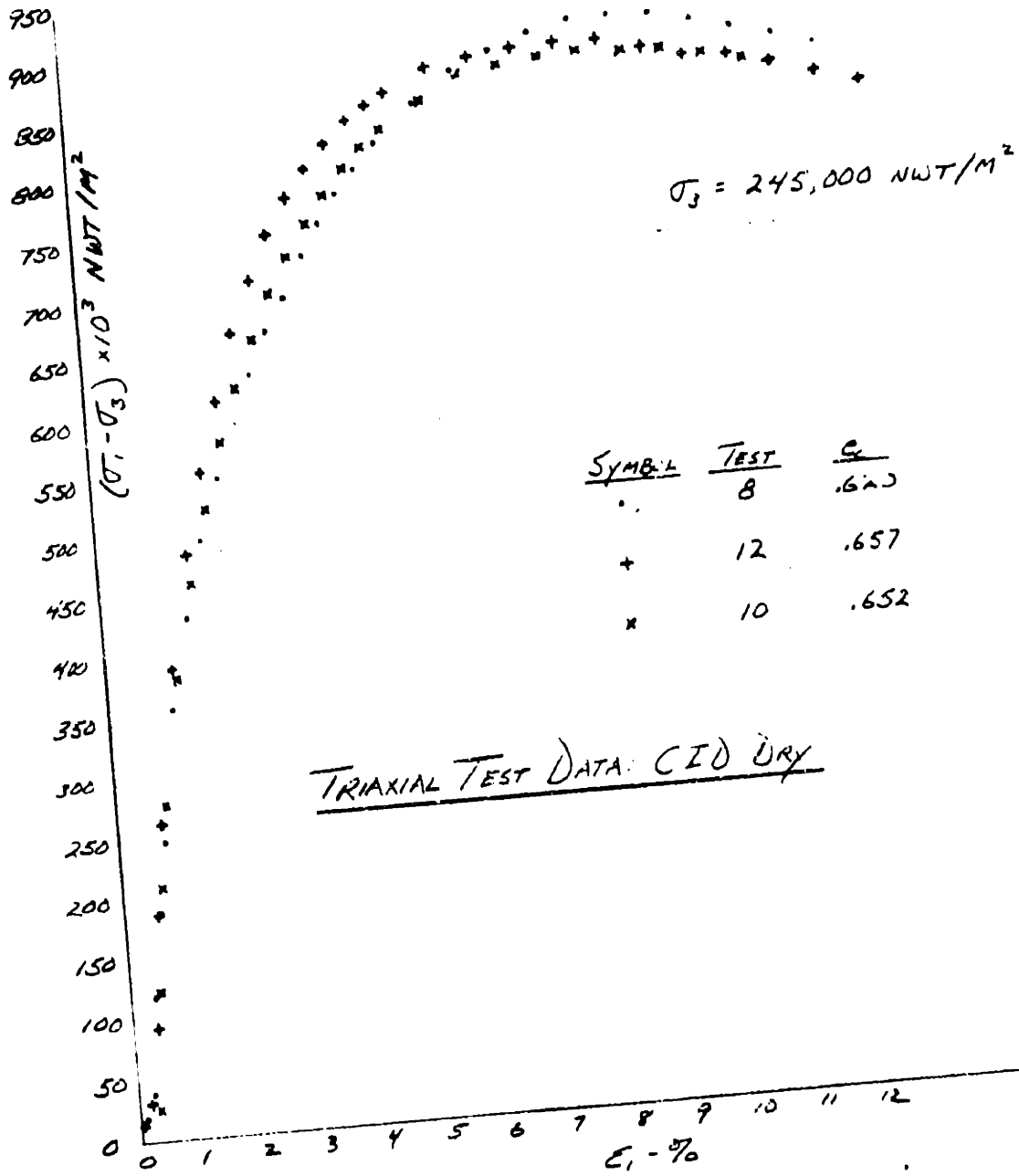


FIG. A.8



INSTRUMENTED LOADING PLATE

FIG. 2.1

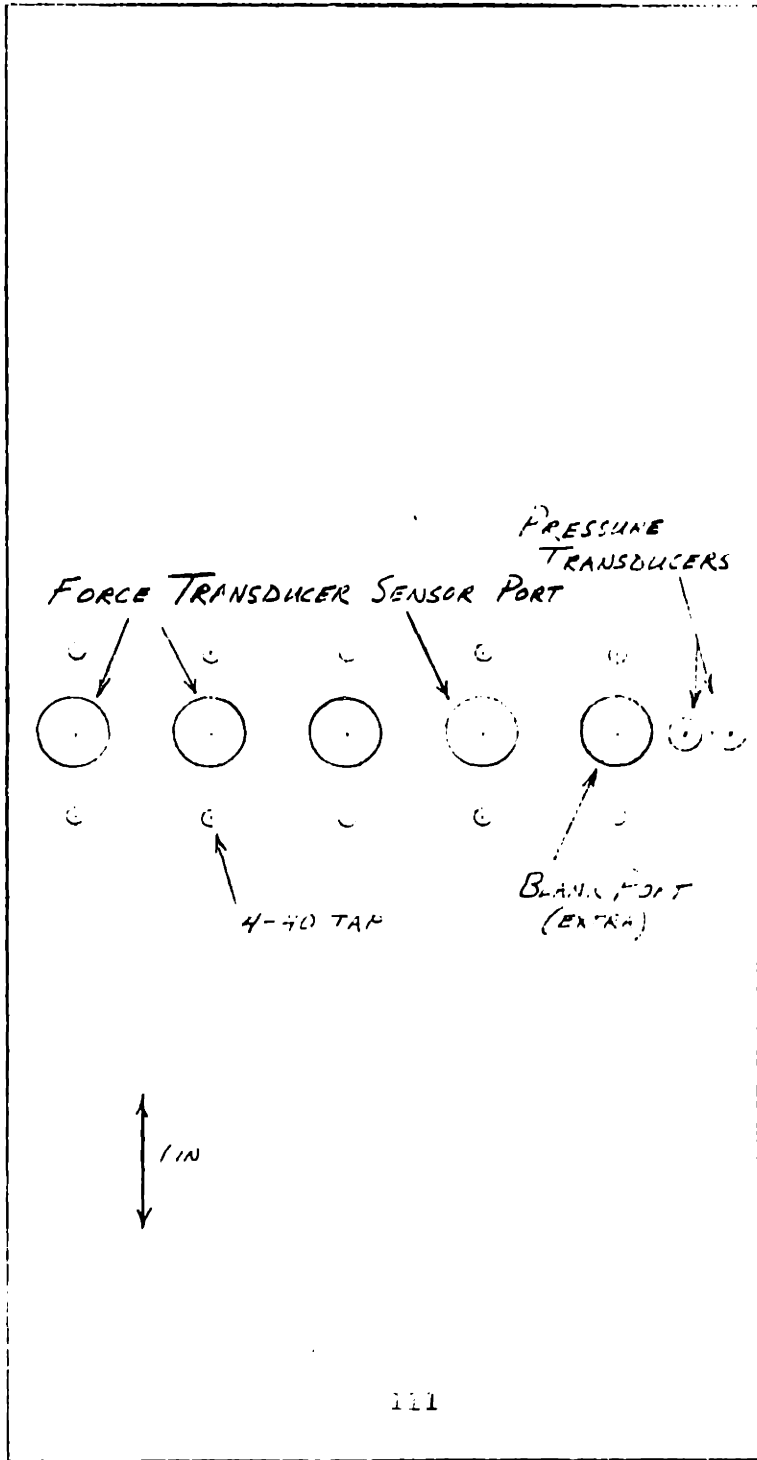
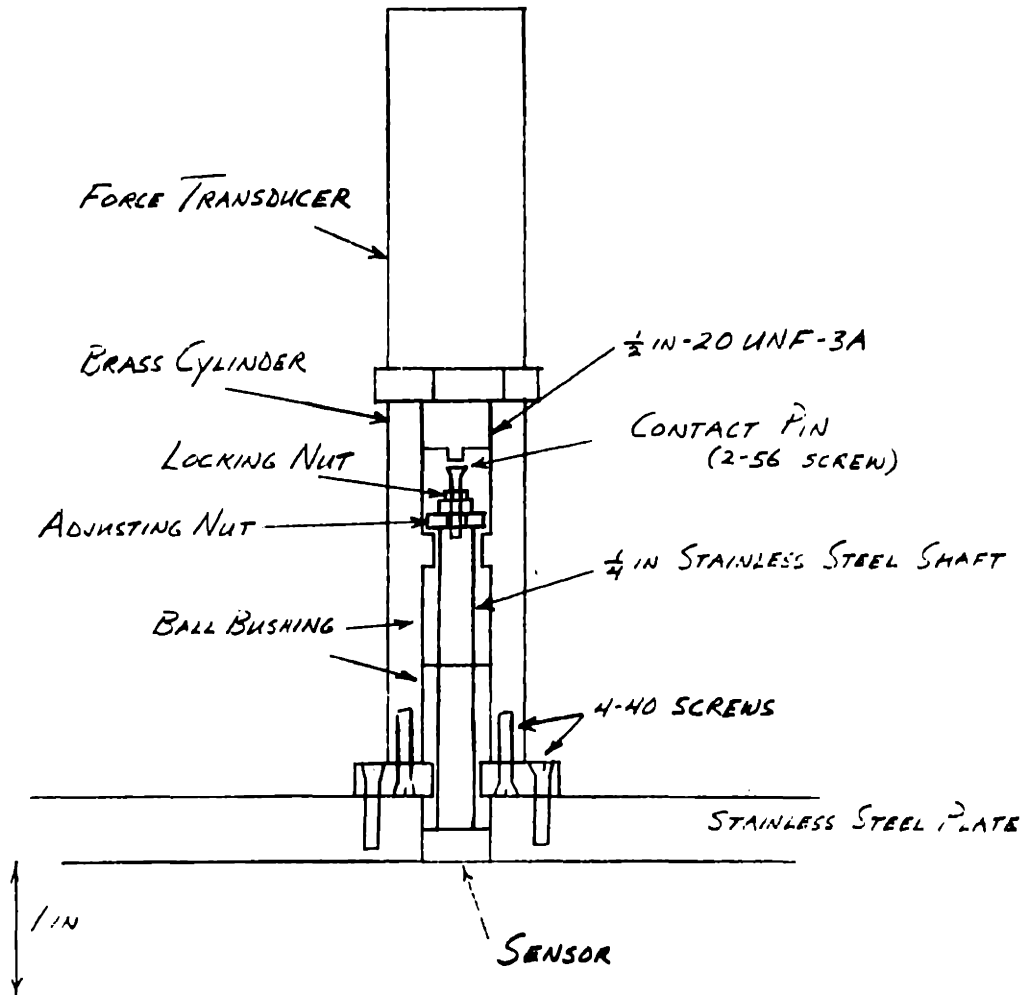




FIG. B. 2



FORCE TRANSDUCER HOUSING

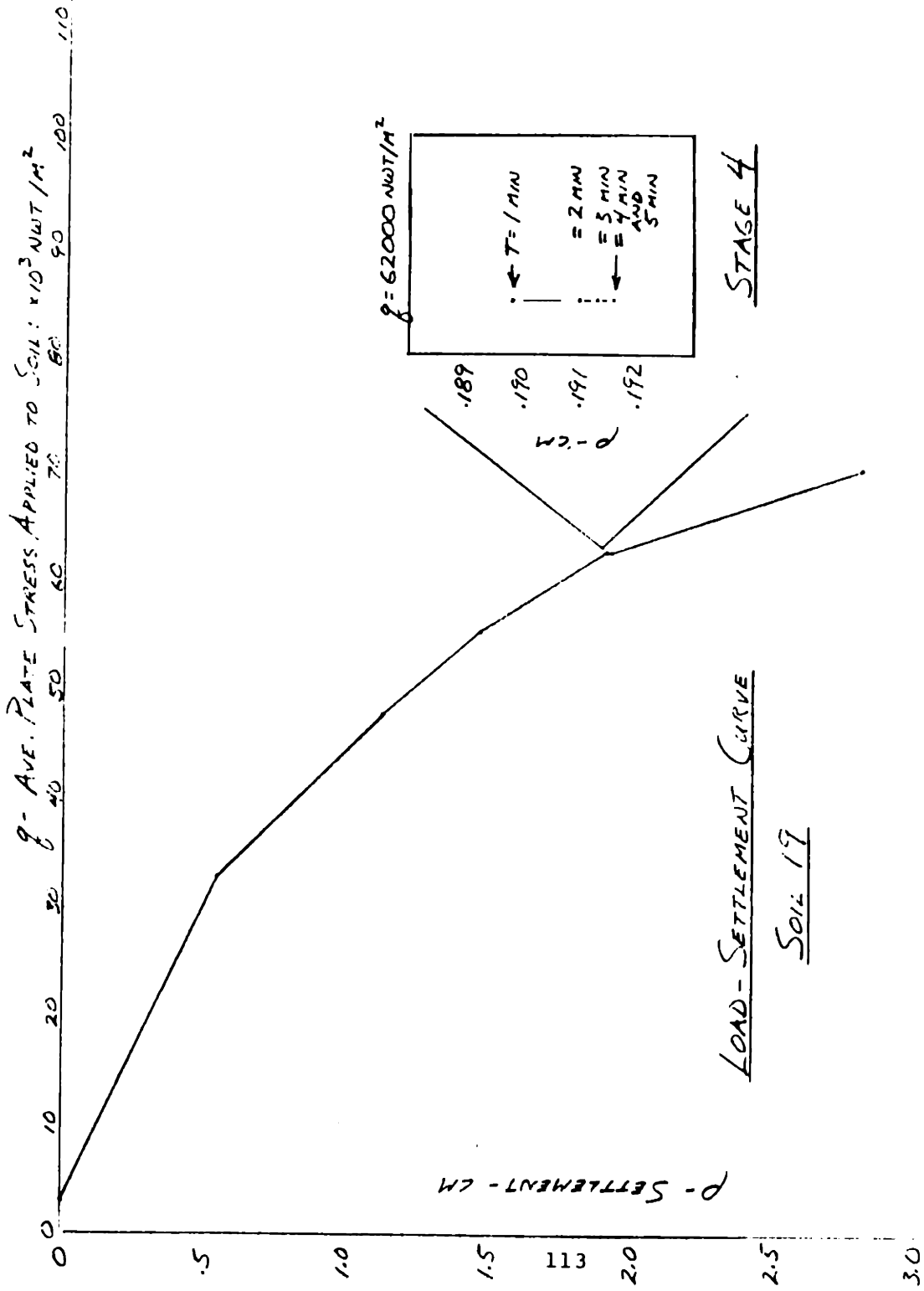
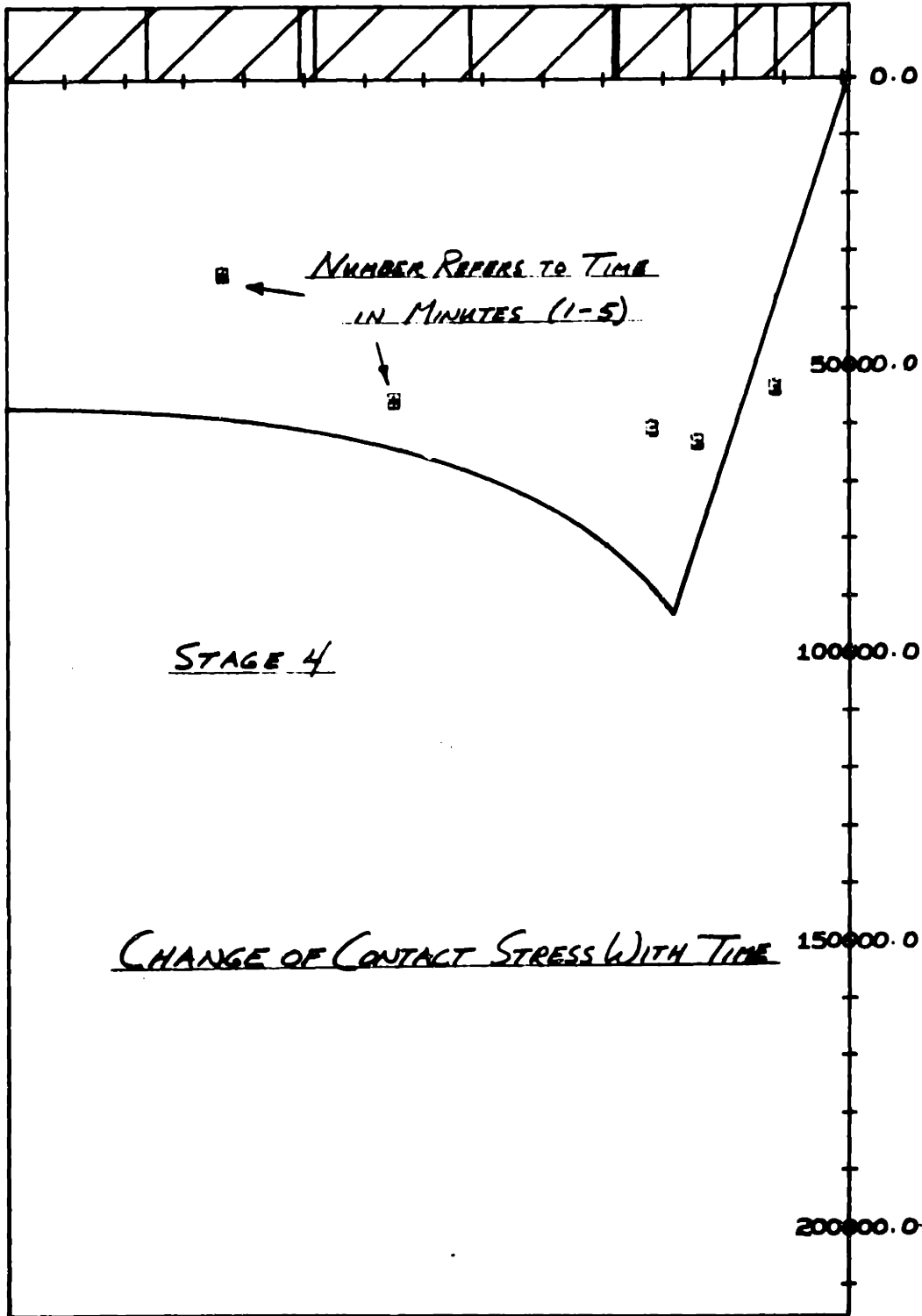


FIG. B.3

FIG. B.4



## APPENDIX A

### STANDARD SOIL MECHANICS TESTS

#### A.1 SIEVE ANALYSIS

A wet sieve analysis was performed on the soil used in the experiments and the result is shown in Fig. A.1.  $D_{50} = .25$  mm;  $D_{60}/D_{10} = 3.5$ ;  $(D_{30})^2/(D_{10} \times D_{60}) = 1.3$ . It was classified as SP according to the Unified Soil Classification System.

#### A.2 SPECIFIC GRAVITY

The Specific gravity of the soil was determined according to the procedures described in Lambe (1951).  $G$  was found to be 2.66.

#### A.3 MAXIMUM AND MINIMUM DENSITY

The Minimum density was found by carefully pouring the sand dry into a Proctor mold through a funnel, the end of which was held just above the apex of the cone formed by the sand. The mold was allowed to overflow and a straight-edge was drawn carefully across the top.  $\gamma_{\min}$  was found to be 12,830 nwt/m<sup>3</sup> (81.6 pcf).

The Maximum density was found by placing the soil in a Proctor mold in five layers. After each layer, the mold was placed on a vibrating table for two minutes with a surcharge of 2460 g applied to the surface of the soil.

$\gamma_{\max}$  was found to be 16,750 nwt/m<sup>3</sup> (106.7 pcf). See Fig. A.2.

#### A.4 DIRECT SHEAR TEST

A series of strain-controlled direct shear tests were run on air-dry soil according to the procedures described

in Lambe (1951). The results of these tests are shown in Table A.1 and Figs. A.3 to A.5. The tests were run in a Wykeham-Farrance Direct Shear Device. The dimensions of the soil samples were 6cm x 6cm x 2.6cm.

The samples were formed by placing a pre-determined weight of soil in the shear box and then tamping the soil with a 3.16 in. rod. The surface was smoothed and compacted with a template to achieve the desired sample height. The shear box was then placed in the load frame; a seating load of 16000 nwt/m<sup>2</sup> due to the hanger was applied before any volume change measurements were made. Weights were then added to the hanger in increments until the desired vertical consolidation pressure was achieved. After each increment, the vertical compression was measured to the nearest 0.0001 in; sufficient time was allowed to ensure that complete compression had occurred.

After the last increment of load was applied, the two halves of the shear box were separated by turning the separation screws 1/2-turn; this corresponds to approximately 1/2mm. With the screws still in place, the volume of the soil would move out slightly into the separation, resulting in a vertical change of less than 0.0020 in. This change was ignored in calculating the void ratio of the sample after consolidation but was considered as a new zero point for measuring the volume changes during shear.

The sample was then sheared at 0.0096 in/min.

#### A.5 TRIAXIAL TEST: CID - C

A series of strain-controlled triaxial tests were run on air-dry soil generally according to the procedures described in Bishop and Henkel (1962). The results of these tests are shown in Table A.2 and Figs. A.6 to A.8. The tests were run in a Wykeham-Farrance Triaxial Cell on

a Wykeham-Farrance Load Frame. The dimensions of the soil samples were approximately  $10\text{cm}^2 \times 8\text{cm}$ .

The samples were formed utilizing a split-ring mold. The mold was first filled half-way and then rodded with a  $3/16$  in. rod a certain number of times,  $N$ , depending on the desired density. The mold was then filled to the top and again rodded  $N$  times. The mold was filled again and rodded  $1/3 N$  times; this process was repeated until the top layer had been rodded  $N$  times. The sample was then levelled with a straight-edge and the loading cap added. A slight vacuum was applied through the cell base so that the split-ring could be removed. The circumference of the soil sample was determined by measuring the total circumference in three places using a paper strip and correcting for the thickness of the membrane (0.007 in.) and paper strip (0.005 in.). An average sample circumference was then used to calculate the area of the sample. The triaxial cell was then assembled and de-aired water placed around the sample. The height was determined by measuring  $z_3$  with respect to the piston and comparing this  $z_3$  with  $z_3$  for a dummy sample of known height. The weight of the sample was determined at the end of the test.

A cell pressure of  $14,700 \text{ nwt/m}^2$  was applied and the vacuum released before any volume change measurements were made. As the tests were on air-dry soil, it was not possible to use the standard burettes in the lab. An air-burette was constructed utilizing a U-tube. By maintaining the water-level in both halves of the tube at the same level, it was possible to measure the volume changes without compressing the air in the sample; with this device, it was possible to estimate the change within 0.01cc.

The cell pressure was then increased in increments to the desired isotropic consolidation stress. After each increment, the vertical compression and the total volume

change was measured. Sufficient time was allowed to ensure that complete compression had occurred.

The sample was then sheared at 0.012 in/min.

## APPENDIX B

### EXPERIMENTAL APPARATUS AND PROCEDURES

A series of plate load tests were run on the soil described in Appendix A, according to the procedures described below. The results of these tests are discussed in Chapter 4.

#### B.1 DESCRIPTION OF PROCEDURE

##### PLACEMENT OF SOIL

The soil was placed in three layers in a plywood bin with these inside dimensions: 16in. deep; 22-1/2in. wide; adjustable length from 0in. to 70-1/2in. The soil was weighed before each test and the length of the bin set for the required density. This length varied from 39in. to 43in. (Relative Density 85% to 50%, respectively). Each layer was compacted with the edge of a shovel and the butt-end of the shovel handle; the amount of compaction was a matter of experience. The top of the soil surface was then smoothed with a straight-edge. For more comments, see Sec. B.6 below.

##### LOADING OF PLATE

(See Photographs of Experimental Apparatus)

The instrumented plate was then rolled into place, with the load frame straddling the soil bin. The level of the soil was checked with a carpenter's bubble level and the level of the plate adjusted to match the soil surface; this adjustment was accomplished by means of a screw-foot at each leg of the load frame. This method was generally satisfactory, but occasionally resulted in slight tilting of the plate; the bubble level was capable of detecting angular rotations as small as 0.001 radians.



The Remote Data Acquisition System was activated and readings taken every minute; the plate was then gently lowered onto the surface of the sand and an Ames dial was set for measuring displacement. The initial settlement of the plate due to its own weight is thus not measured, although the load imposed is less than .5psi.

The plate was then loaded in a series of steps by adding lead weights. At the end of each stage, the displacement of the plate is measured to the nearest 0.0001in. and the force on the transducers to the nearest .1 psi. Sufficient time (3 to 5 minutes) was allowed for each stage to ensure that full displacement had occurred.

It is recommended that in future tests, the loading should be strain-controlled rather than stress-controlled. This would permit far less manual labor as well as more detail in the load-displacement curve for the plate tests. It is also suggested that a force transducer be used to impose the load; this would permit utilizing the Data Acquisition System, as well as accurately determining exactly when the plate contacts the surface of the soil. A displacement transducer would also be helpful, provided it has sufficient travel.

After the maximum load was imposed, the test was terminated and the data recorded permanently. The data were then punched on computer cards and a specially-written computer program plotted the results of the test, as shown in Figs. 4.1 to 4.10. This program is described in Appendix C.

#### REMOVAL OF SOIL

The soil was removed simply by shovelling it into boxes mounted on wheels to facilitate moving and weighing.

It is recommended that in future tests, an aerial bin be used, as this would permit emptying the bin more easily and with less effort by bottom dumping.

PLATE

(See Fig. B.1)

The instrumented plate consists of a 1/2-in. thick stainless steel plate, 5.56in. wide by 11.11in. long. Along the short axis, a series of 1/2-in. diameter holes were drilled; the first with its center 1/2-in. from the plate edge and the rest 1-in. from center-to-center. These are the sensor ports. Associated with each port are two tapped holes (4-40) in which the transducer housings are mounted to the plate.

Aligning all three holes requires excellent machining and although no problems with binding occurred, a clamping arrangement for the transducer housings would be simpler and easier to operate. It should also be emphasized that machining stainless steel is about twice as difficult as standard steel; two 4-40 taps were left permanently in the plate.

In addition, two 1/4-in. holes were added later near the edge of the plate in line with the other ports. This was to mount the two small pressure transducers.

TRANSDUCER HOUSINGS

The transducer housing is diagrammed in Fig. B.2. This design, employing a piston and cylinder, was adopted to eliminate the effect of lateral soil stresses on the force transducer readings. The design requires excellent machining to insure alignment of all the pieces. The ball bushings ensure against lateral movement and are virtually frictionless.

Assembly of the housing on the plate is a trial-and-error process. The contact pin and locking nut must be moved up and down until the piston is just flush with the

face of the plate when the pin contacts the force transducer probe. The adjusting nut must also be set to provide just a little slack; this will aid in the detection of any binding.

#### FORCE TRANSDUCERS

The force transducers were purchased from Dynisco, at a cost of \$525 each and a wait of 45 days. They are rated at 5 lb. in compression and can be safely overloaded to 10. They require 6v DC excitation and yield a signal measured in millivolts, which are recorded by the Remote Data Acquisition System. A local digital voltmeter was also used to monitor the testing.

The transducers are calibrated in place by inverting the plate and placing known weights on the piston and measuring the response. It is necessary to correct this calibration for the weight of the piston by adding twice this weight to the calibration curve.

These transducers are extremely accurate and very stable. Over a period of 24 days, the calibration changed by less than 0.5%. Because of the great sensitivity of the transducers, it would have been possible to use smaller pistons (although this would have presented machining problems). However, it is recommended that in future tests, alternative methods of sensing the stress be investigated and evaluated.

#### PRESSURE TRANSDUCERS

After running a series of tests with three force transducers in different positions on the plate, it was decided to install two small pressure transducers near the edge of the plate. These were supplied by Scientific Advances and are as expensive as the force transducers. They are rated from 0 to 30 psia and can be safely overloaded to 45 psia; they require 3v DC excitation. In calibrating the transducers, they were found to have a small amount of hysteresis

but were accurate within 0.3 psi, or 1% full scale. Epoxy was found to be the best for mounting the pressure transducers but it is difficult to remove them once they are in place. Methylene chloride is the only known solvent for epoxy, but it is poor at best.

### B.3 FLEXURAL RIGIDITY OF THE INSTRUMENTED PLATE

A perfectly rigid plate, of course, requires infinite stiffness. It was necessary to determine how rigid the instrumented plate actually was. Terzaghi (1943) presents an equation (p.389) which may be used to estimate the relative rigidity of a uniformly loaded plate:

$$K_r = \frac{1}{6} \frac{1 - \nu_s^2}{1 - \nu_p^2} \frac{E_p}{E_s} \left(\frac{H}{a}\right)^3 \quad (B.1)$$

where:  $\nu_s$  = Poisson's Ratio of Soil  
 $\nu_p$  = Poisson's Ratio of Plate  
 $E_s$  = Young's Modulus of Soil  
 $E_p$  = Young's Modulus of Plate  
 $H$  = Thickness of Plate  
 $a$  = Halfwidth of Plate

Fig. 125 in Terzaghi shows that for  $K_r \geq 10$ , a plate is considered rigid. A simple calculation shows that for the instrumented plate,  $K_r > 1500$  for the densest soil, and so even though the plate is not loaded uniformly, it is rigid.

### B.4 ECCENTRICITY OF PLATE

Already mentioned in Sec. B.1 above was the very slight eccentricity involved in leveling the plate before pushing it into the soil. It was also necessary to determine how much eccentricity occurred due to sloppiness in the ball bushing block. In one test, it was found that the differential settlement was less than 0.2% of the footing width and

less than 1% of the total settlement. This test was on a soil with relative density = 50% and thus large total settlement occurred; with denser soils, the total settlement would be less and so would the differential settlement.

#### B.5 TIME EFFECT BENEATH THE PLATE (CREEP)

In Sec. B.1, it was mentioned that 3 to 5 minutes were required between stages. For completeness, the fourth stage of Soil 19 was computed in detail and is presented in Figs. B.3 and B.4. It can be seen that there is virtually no change in the stresses with time. The creep of the plate is assumed due to re-arrangement of soil grains; the major portion of this re-adjustment occurs in just a few minutes, but much longer time-dependent phenomena also occur. For a number of tests, the last stage was left on over a longer period (45 minutes). It was found that the additional settlement was on the order of 2% of the total settlement for the high densities and 0.5% for the low densities. Also, the stresses measured by the transducers changed .1% for the high densities and 0.5% for the low densities.

#### B.6 SOIL UNIFORMITY

There is no question that the placement of the soil in the bin is crude at best. In particular, the surface compaction due to the smoothing-off is critical. In future tests, it is recommended that the soil be poured through a screen at a constant height, and that the bin be overfilled and the excess scraped off very carefully.

Nonetheless, the results in Fig. 4.17 are encouraging: the numbered runs for each relative density were made at different positions in the bin without changing the soil; in the unnumbered runs, the soil was removed and placed between each run. It can be seen that the soil is quite

uniform, even at low densities but that it is difficult to repeat the compaction. This is another reason for the above recommendations.

#### B.7 PLATE ROUGHNESS

A perfectly rough plate requires that there be no relative movement between the soil particles and the plate. Since some finite displacement is required to mobilize frictional resistance, this condition can never be met exactly; by the same token, a perfectly smooth plate is also impossible to achieve.

The friction angle between the plate and the soil at  $D_R = 50\%$  was determined to be  $26^\circ$ , or about  $2/3\phi$ , which is a typical value; and thus the plate would be considered rough. The results of the non-homogeneous elastic analysis of the shear stresses beneath a rough plate also indicate that the plate is sufficiently rough.

#### B.8 EFFECT OF SIDES AND BOTTOM OF BIN

Theoretical work by Livneh (1965) for a weightless soil on a rigid base has shown that the base affects the bearing capacity if the depth to the base is less than 20 times the footing width. This would require a bin of tremendous dimensions to accommodate the present footing.

However, this problem does not seem to have bothered other experimenters. A review of work by Eggstad (1963), Feda (1961), Feda and Pruska (1965), and Hansen (1961) has shown that the relative dimensions of the present tests are more than reasonable. Clearly, though, this problem should be investigated in more detail.

#### B.9 ARCHING

The phenomenon of arching has troubled all of the investigators who have attempted to measure stresses in

soil; the deflection of the sensing diaphragm is critical. Barden (1963) reported that arching may be avoided if the ratio of the diaphragm diameter to the deflection is greater than 1000. The transducers used in this investigation satisfy this criterion.

In addition, the results of Soil 16 (Fig. 4.7) show that if everything works properly, the integral of the measured stresses equals the average stress applied to the soil through the plate. On these bases, it was concluded that arching was not a problem in this investigation.

#### B.10 PLANE STRAIN ZONE BENEATH PLATE

In discussing the bearing capacity of purely cohesive soils, Meyerhof (1952) found:

Assuming the plastic zones and composite failure surface of strip and circular foundations are identical in cross section, for the case of a rectangular foundation of length  $L$  and width  $B$  with semi-circular ends of radius  $R = B/2$ , the plastic zones are continuous, with the result that the stresses in the central portion of length  $(L-B)$  are the same as those of a strip foundation (with the addition of longitudinal stresses which do not affect plastic equilibrium).

Although the soil in this investigation is not cohesive and further the plate has square corners, it still seems reasonable to assume that plane strain conditions exist in the central portion of the plate where the transducers are located.

APPENDIX C  
MASSACHUSETTS INSTITUTE OF TECHNOLOGY  
DEPARTMENT OF CIVIL ENGINEERING  
DEVISION OF SOIL MECHANICS

PROGRAM PLOTTER  
USER'S MANUAL

Date: 1968

Language: FORTRAN IV

Programmer: W. David Carrier, III

Description: The program is a specialized one, written for the programmer's ScD Thesis. It is designed to take data from the Remote Data Acquisition (RDA) Console in millivolts and volts and plot the corresponding normal stresses beneath a rigid plate in newtons/meter .

Input Data Format:

- (1) Symbol Width Card (F10.3)  
Defines the width of characters in the x- and y- axes (in inches).
- (2) Symbol Height Card (F10.3)  
Defines the height of characters in the x- and y- axes (in inches).
- (3) Figure Plate Halfwidth Card (F10.3)  
Defines the plate halfwidth plotted on paper (in inches).
- (4) Scale Factor Card (F10.3)  
Defines increment of y-axis.
- (5) Plate Halfwidth Card (F10.3)  
Defines actual halfwidth of loading plate (in meters).
- (6) Plate Length Card (F10.3)  
Defines actual length of loading plate (in meters).
- (7) Secondary Symbol Width Card (F10.3)  
Defines width of smaller characters (in inches).



- (8) Secondary Symbol Height Card (F10.3)  
 Defines height of smaller characters (in inches).
- (9) Number of Transducers (I5)
- (10) Transducer Position and Calibration Cards  
 (a) Transducer Position Card (2 I5, 2F10.5)

<u>cc</u>	<u>Item</u>
1-5	Transducer Number
6-10	Number of calibration cards (no more than six)
11-20	Horizontal distance of transducer from centerline of plate (in meters).
21-30	Diameter of transducer (in meters).

(b) Calibration Cards (2F10.5)

<u>cc</u>	<u>Item</u>
1-10	Pressure in PSI
11-20	Corresponding voltage output in mv/v (Each set of calibration cards follows the respec- tive Transducer Position Card).

When it is desired to plot a series of tests which have the above information in common, it is necessary only to stack the following information for each test:

(11) Test Card (3I5)

<u>cc</u>	<u>Item</u>
1-5	Number of Stages in Test
6-10	Soil Type (Reference Number)
11-15	0 If theoretical plot is not desired 1 If theoretical plot is desired.

(12) Output Data Cards (I5, 2F10.5)

Output is presented in numerical sequence for each transducer, for each stage.

<u>cc</u>	<u>Item</u>
1-5	Stage number
6-10	Transducer number
11-20	Output of transducer (in millivolts)

(13) Displacement and Weight Cards (I10, 3F10.5)

Data are presented in numerical sequence for each stage.

<u>cc</u>	<u>Item</u>
1-10	Stage Number
11-20	Excitation (in volts)
21-30	Displacement of loading plate (in inches)
31-40	Mass applied to soil (in kilograms)

(14) Unit Weight and Terzaghi Bearing Capacity Factor (2F10.1)

<u>cc</u>	<u>Item</u>
1-10	Unit Weight (nwt/m <sup>3</sup> )
11-20	$N_{\gamma}$

PROGRAM USE: The program must be run on the IBM 1130 at the Civil Engineering Systems Laboratory (CESL) at MIT.

## APPENDIX D

MASSACHUSETTS INSTITUTE OF TECHNOLOGY  
DEPARTMENT OF CIVIL ENGINEERING  
SOIL MECHANICS DIVISION

### PROGRAM USERS MANUAL

FEAST - DJD (INCREMENTAL ELASTIC APPROACH)

Date: May, 1968  
Language: FORTRAN IV G LEVEL  
Programmer: E. L. Wilson (Univ. of Calif., 1966)  
Modified: J. T. Christian, MIT  
D. J. D'Appolonia, MIT  
Reference: D. J. D'Appolonia (1968)

**DESCRIPTION:** This program uses the finite element method to determine stresses and deformations within soil bodies for axisymmetric and plane strain problems. The program is written for soil mechanics applications where the stress and deformation patterns are required over the full range of loading. Bi-linear elastic material properties are considered using a piecewise linear analysis for incremental loads. Both frictional and non-frictional anisotropic materials can be specified. The effects of displacement or stress boundary conditions and gravity stresses are included. The program performs a total stress analysis in all cases and pore pressures may be computed on the basis of computed changes in total stress. Incompressible materials cannot be specified; however, in most cases numerical inaccuracies are small provided that the bulk modulus of the soil does not exceed about one million psi.

**PROGRAM CAPABILITIES:** The following restrictions are placed on the size of problems that can be handled by the program:

Nodal Points	450
Elements	450
Materials	25
Load Increments	100

The program incorporates a data generating facility whereby only a minimum amount of information need be input to specify problem geometry. Material properties can be input element by element or as layered systems. The use of triangular and quadrilateral elements as well as skew boundaries are permitted.

Printed output includes:

1. Reprint of input data
2. Nodal Point displacements
3. Stresses, strains and pore pressures at the center of each element

Punch output of element geometry, nodal point displacements and element stresses can be obtained for plotting program use.

Computer running time depends primarily upon the band width of the global stiffness matrix rather than the number of elements. For typical problems the running time varies between about 20 seconds and one minute per load increment.

PROGRAM USE: The program must be run on the IBM 360/65 with OS control cards. Two scratch tapes must be mounted on logical units 8 and 9. The source deck has been punched on the 029 key punch (EBCDIC).

Any number of problems can be submitted on the same job. If errors are found in processing the input data for a particular problem, that problem will be flushed but the following problems will be taken. Problems should be separated by a card having \*\*\*\* (A4) in the first four columns.

## APPENDIX E

### EARLIER EXPERIMENTAL RUNS

A series of experimental runs with the instrumented plate which were not included in the back-calculation of  $N_{\gamma}$  and  $\phi$  are presented here for completeness. These results confirmed the general behavior predicted by the Schultze Model, but it was decided to add two small pressure transducers near the edge of the plate to better define the slope of the contact stress distribution. Another series of tests were then run and are presented in detail in Chapter 4.

The data are presented in two groups; the transducers were mounted in different positions on the plate in each set of data.

In the first set of data, the stresses from Transducers 1 and 2 were used in the elastic error analysis of Fig. 4.21. (Transducer 1 had not yet been damaged.)

In the second set of data, the stresses from only Transducer 2 were used in the elastic error analysis, because Transducer 1 had been accidentally damaged.

The stresses from Transducer 3 from both sets of data were not used in the algorithm to calculate  $N_{\gamma}$  because it was felt that the small transducers provided much more accurate data.

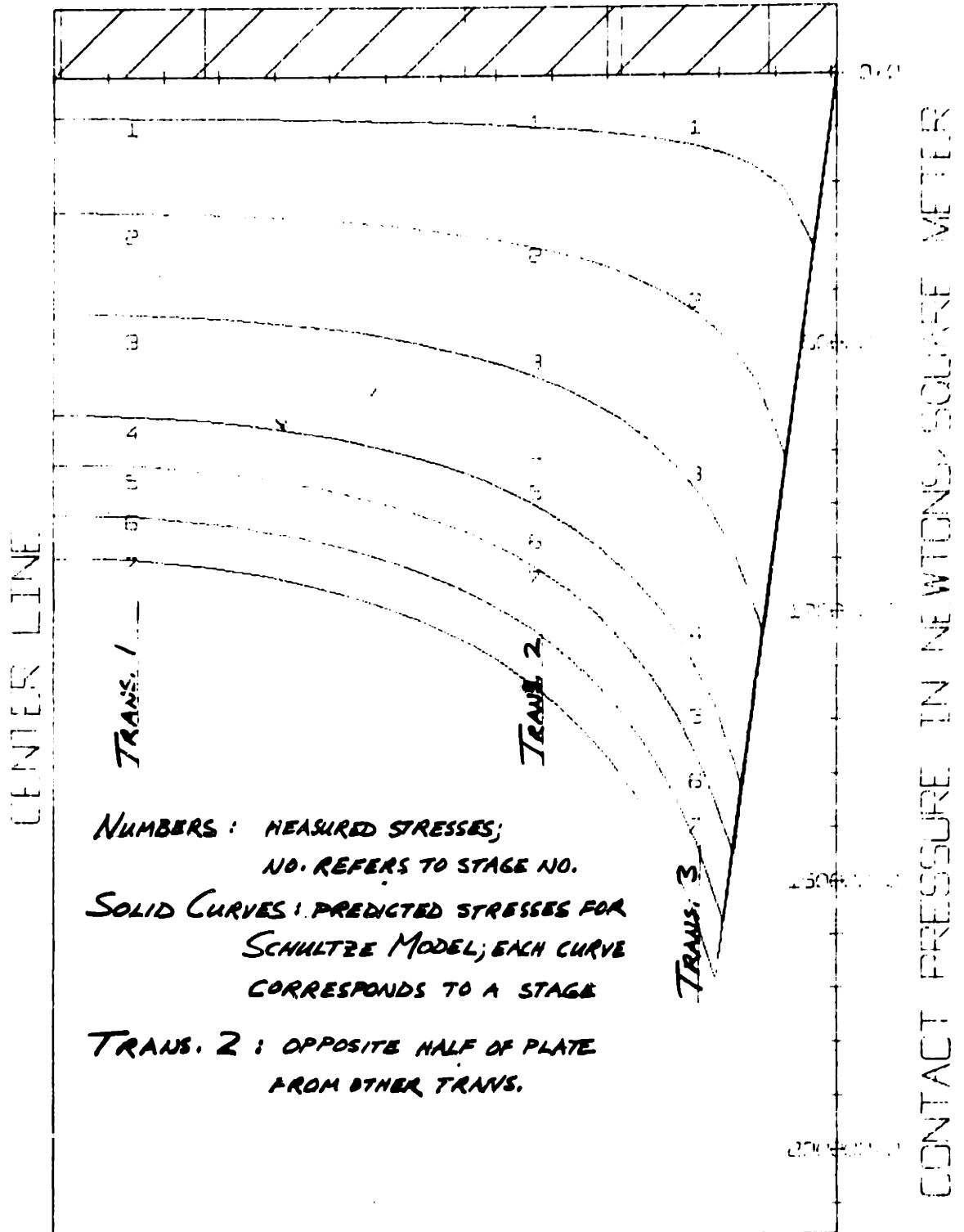
The load-settlement curves for these tests are included in Fig. 4.18.

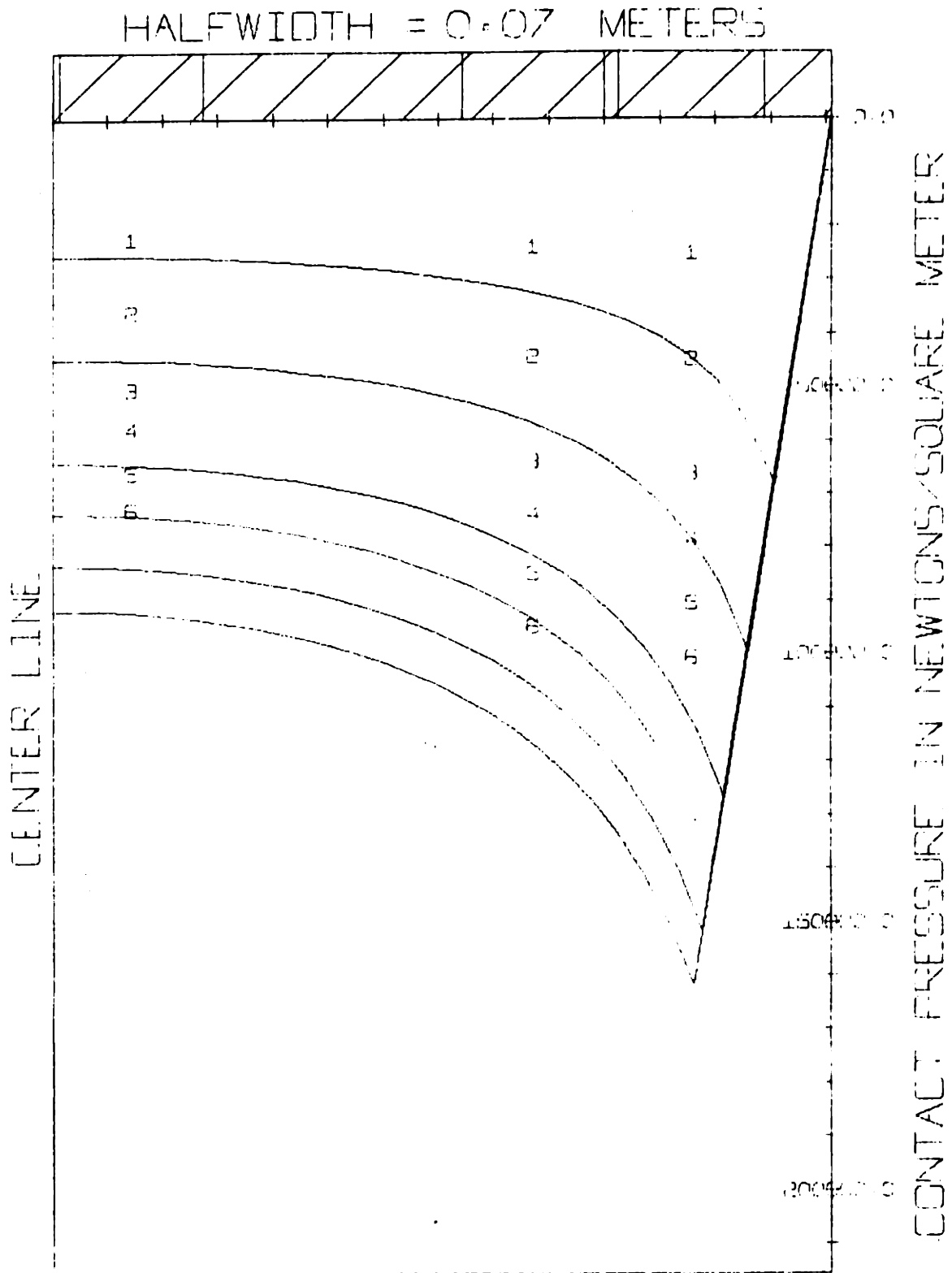
<u>SOIL No.</u>	<u>RUN No.</u>	<u>REL. DENSITY</u>	<u>UNIT WT.</u> (NWT/M <sup>3</sup> )	<u>NO. OF STAGES</u>
5	5	85%	16000	7
6	6	80%	15780	6
3	8	70%	15340	6
8	9	60%	14920	6
4	11	50%	14520	5

q: AVE. PLATE STRESS - X 10<sup>3</sup> NWT/M<sup>2</sup>

<u>SOIL No.</u>	<u>STAGE No.</u>						
	1	2	3	4	5	6	7
5	10.5	32.6	54.7	75.6	85.4	95.3	103.5
6	32.6	54.7	75.6	85.4	95.3	103.5	—
3	"	"	69.5	80.5	90.3	100.3	—
8	10.5	32.6	47.3	62.1	75.6	80.5	—
4	"	"	"	"	73.2	—	—

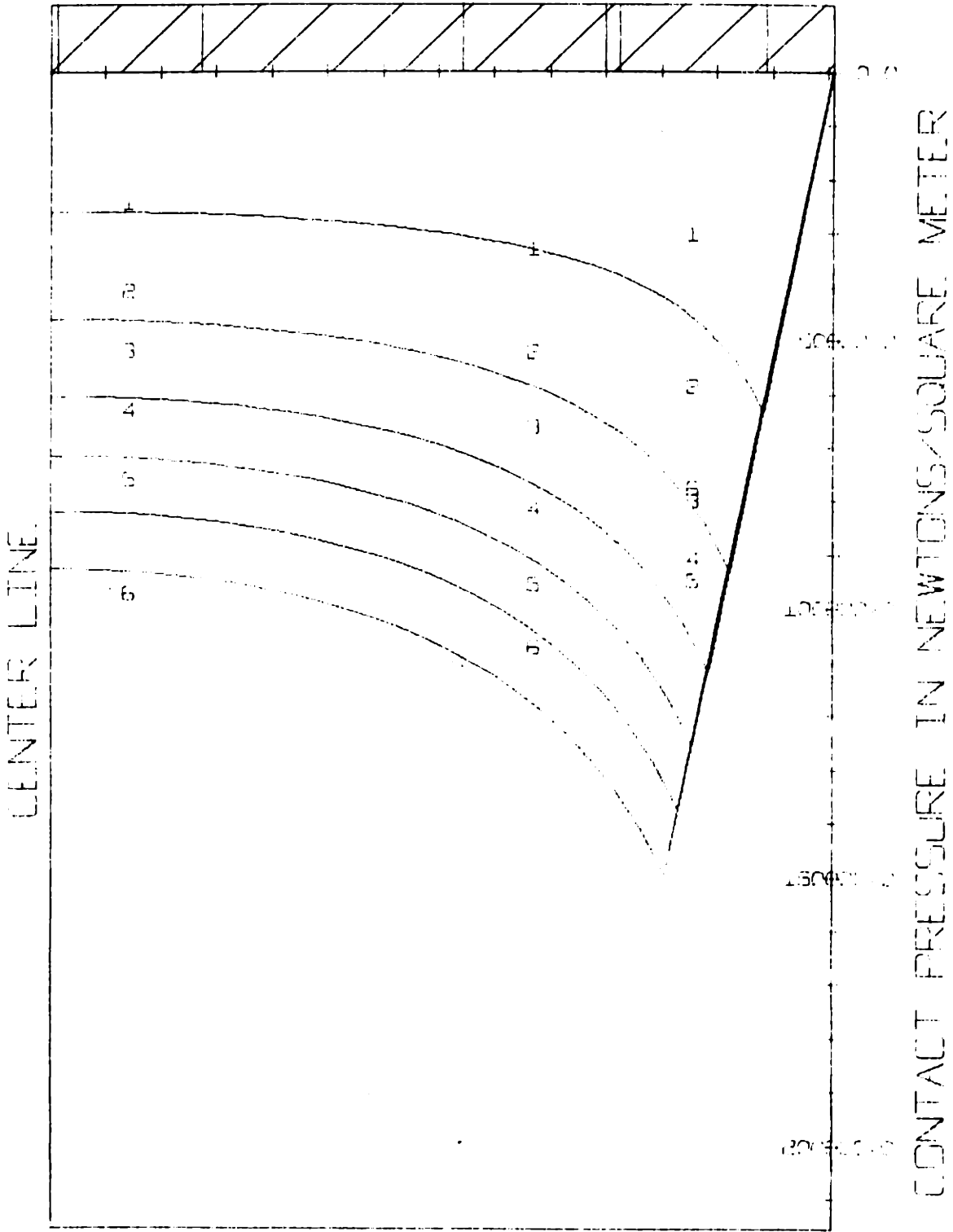
HALFWIDTH = 0.07 METERS

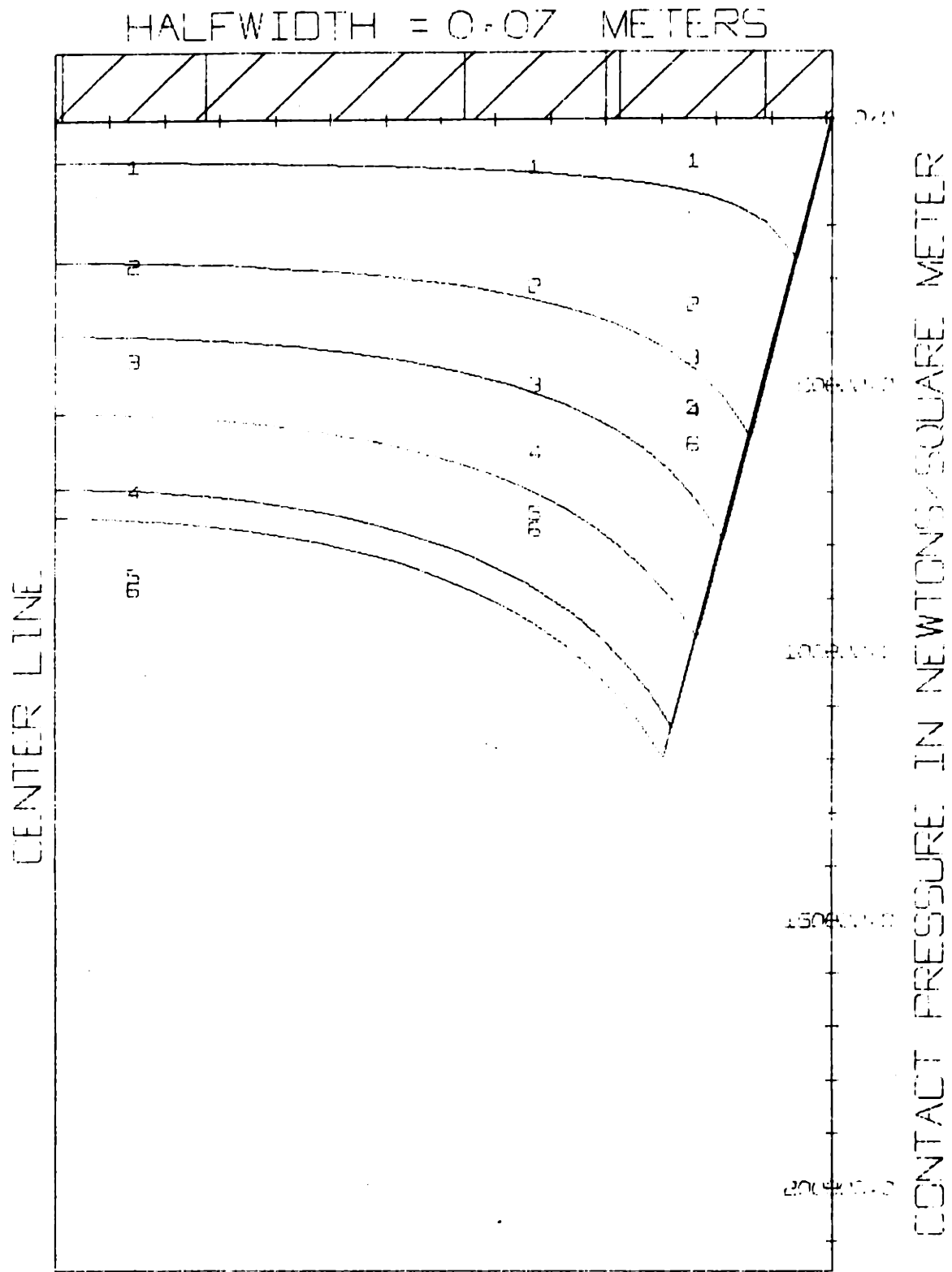




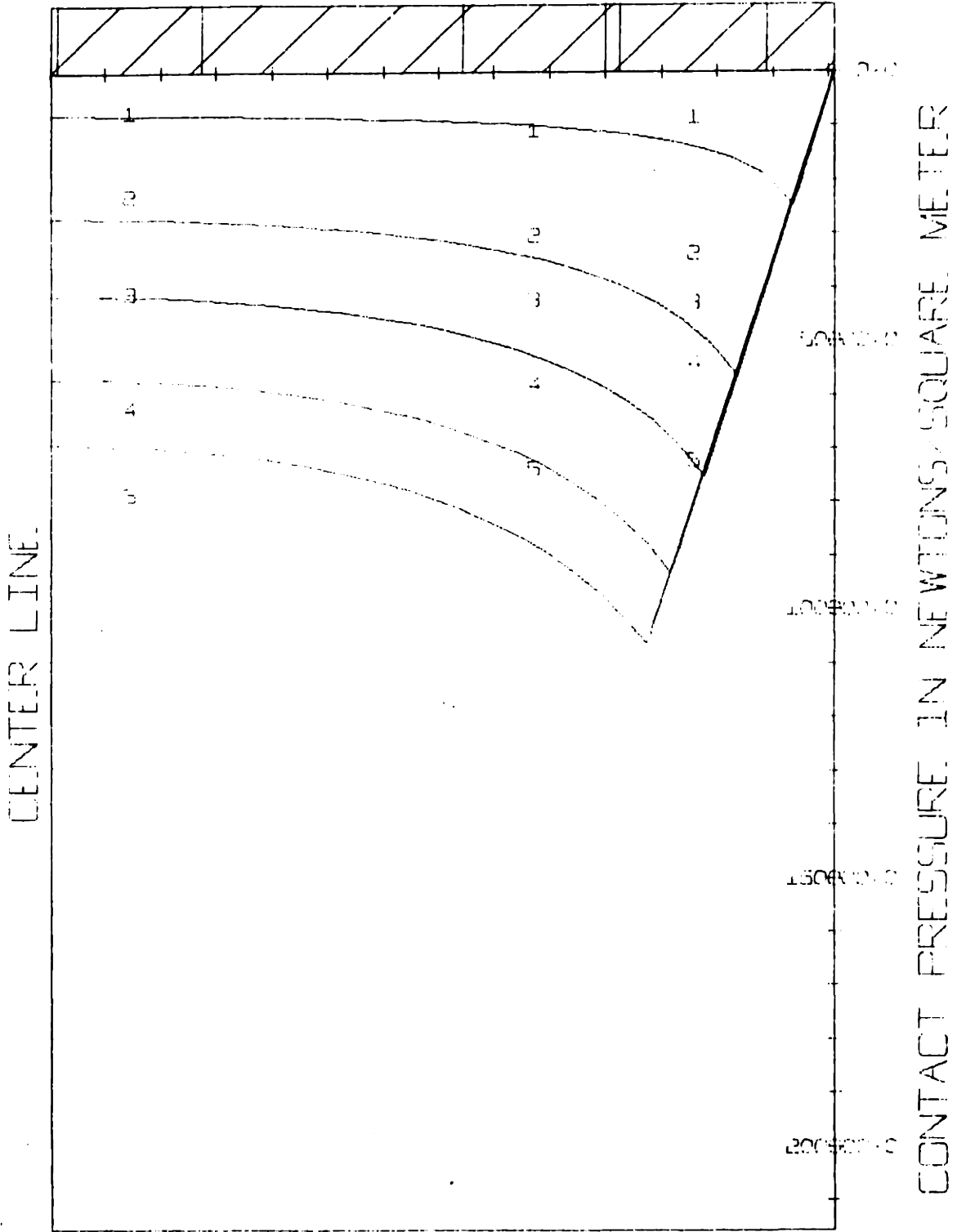


HALFWIDTH = 0.07 METERS





HALFWIDTH = 0.07 METERS

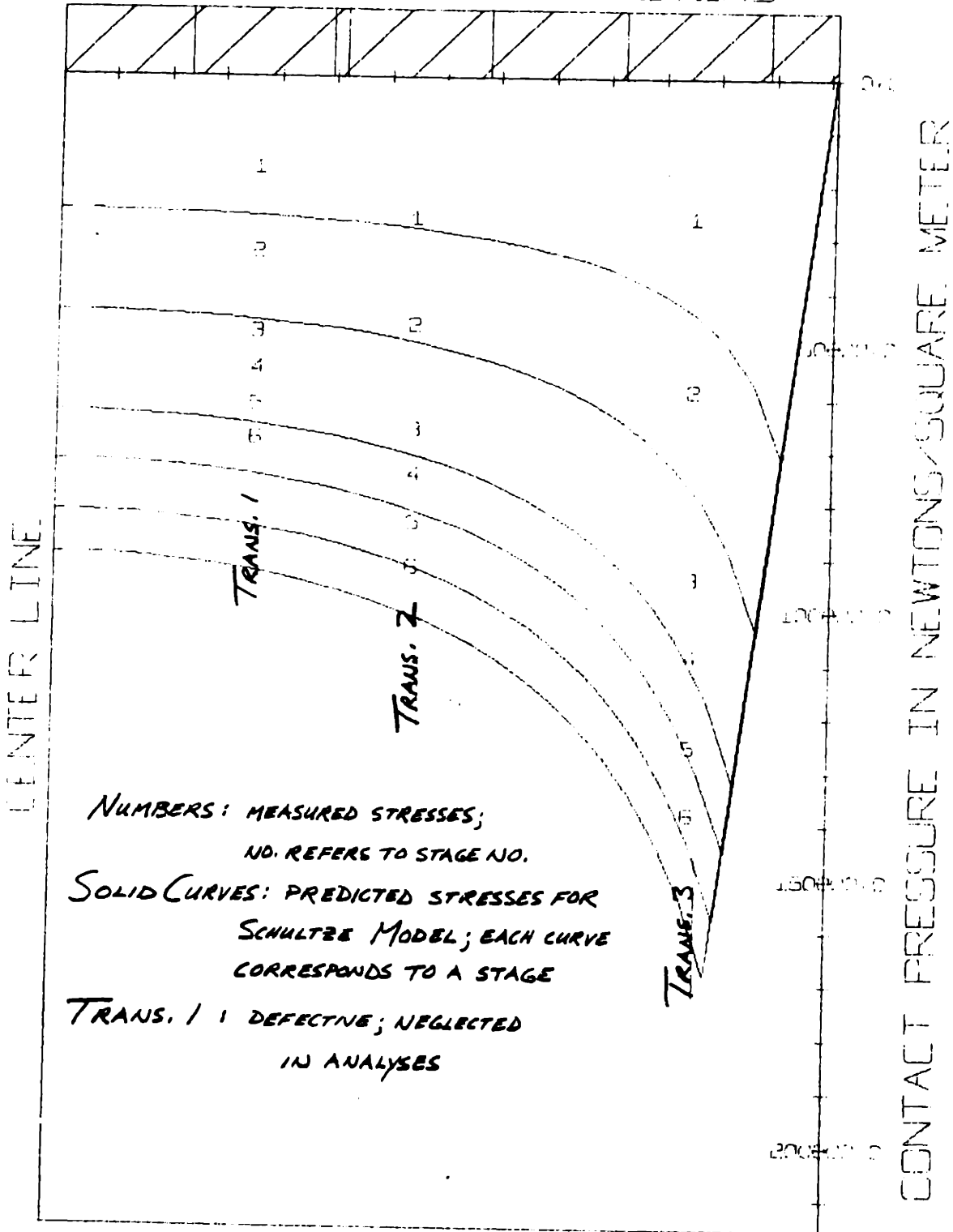


<u>SOIL No.</u>	<u>RUN No.</u>	<u>REL. DENSITY</u>	<u>UNIT WT.</u> (NWT/M <sup>3</sup> )	<u>No. OF STAGES</u>
5	12	85%	16000	6
6	13	80%	15780	6
3	14	70%	15340	6
8	15	60%	14920	5
4	16	50%	14520	4

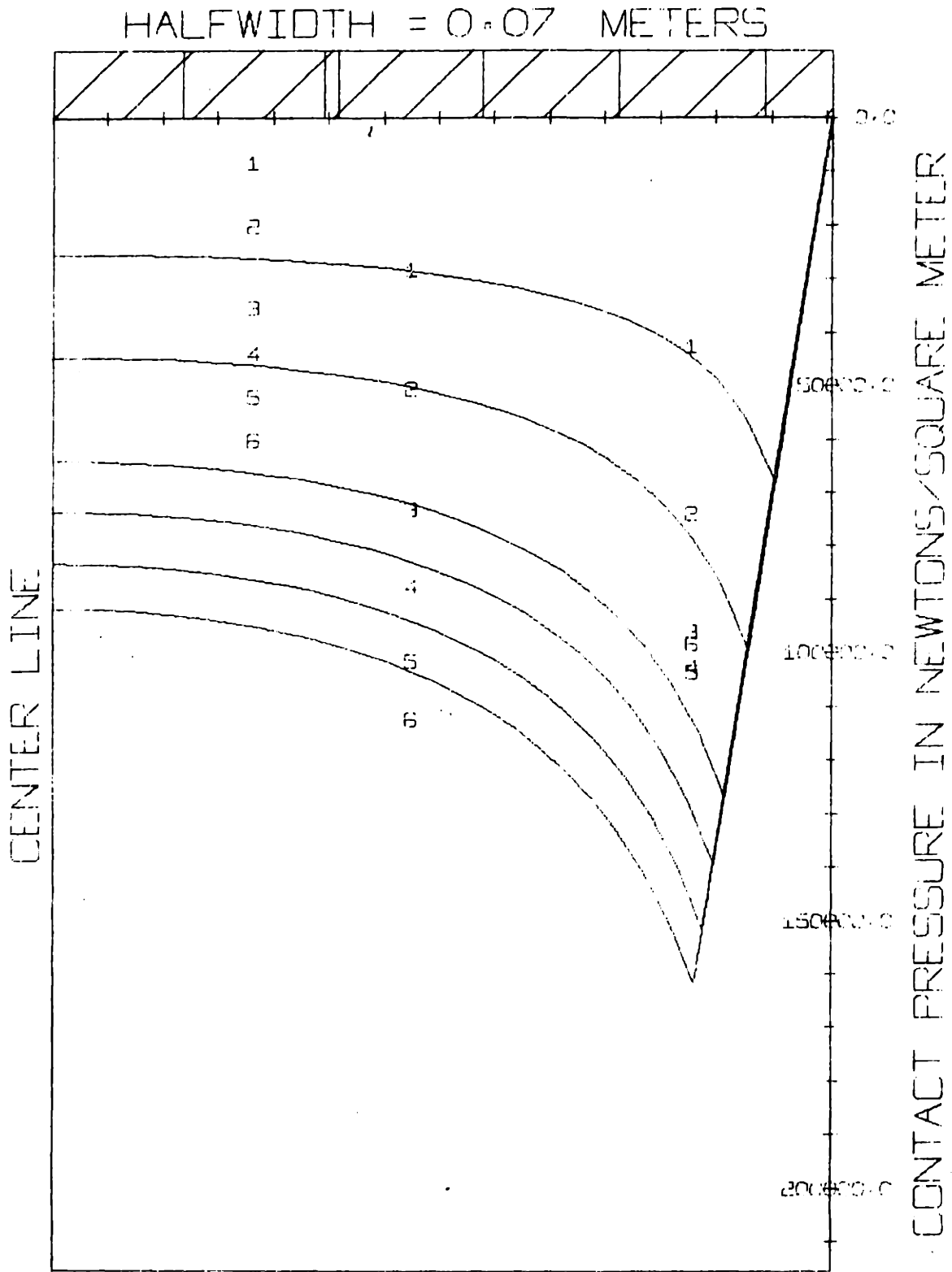
q: AVE. PLATE STRESS -  $\times 10^3$  NWT/M<sup>2</sup>

<u>SOIL No.</u>	<u>STAGE No.</u>					
	1	2	3	4	5	6
5	32.6	54.7	75.6	85.4	95.3	103.5
6	"	"	"	"	"	"
3	"	"	69.5	80.5	90.4	100.3
8	"	47.3	62.1	75.6	80.5	—
4	"	47.3	54.7	62.1	—	—

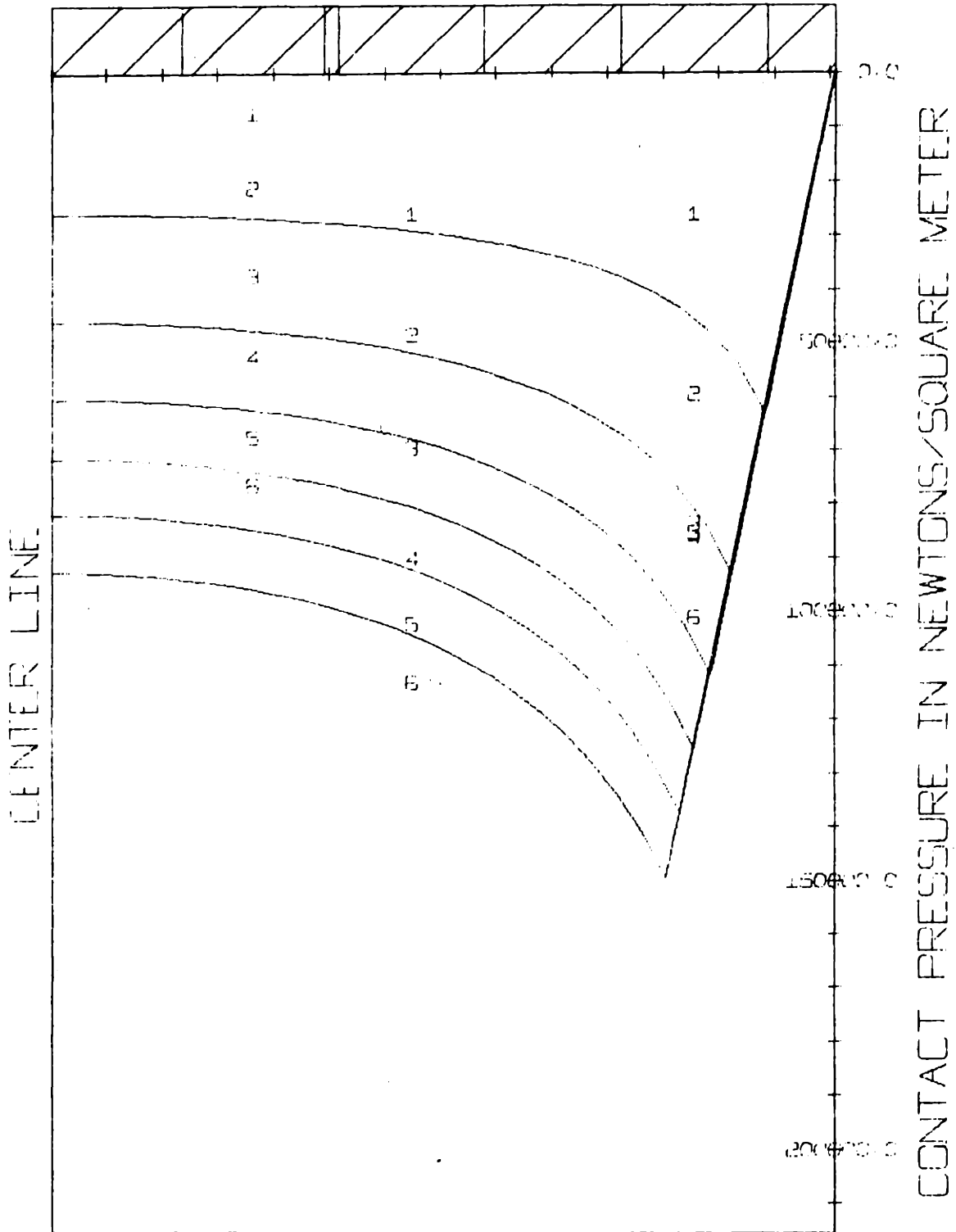
HALFWIDTH = 0.07 METERS



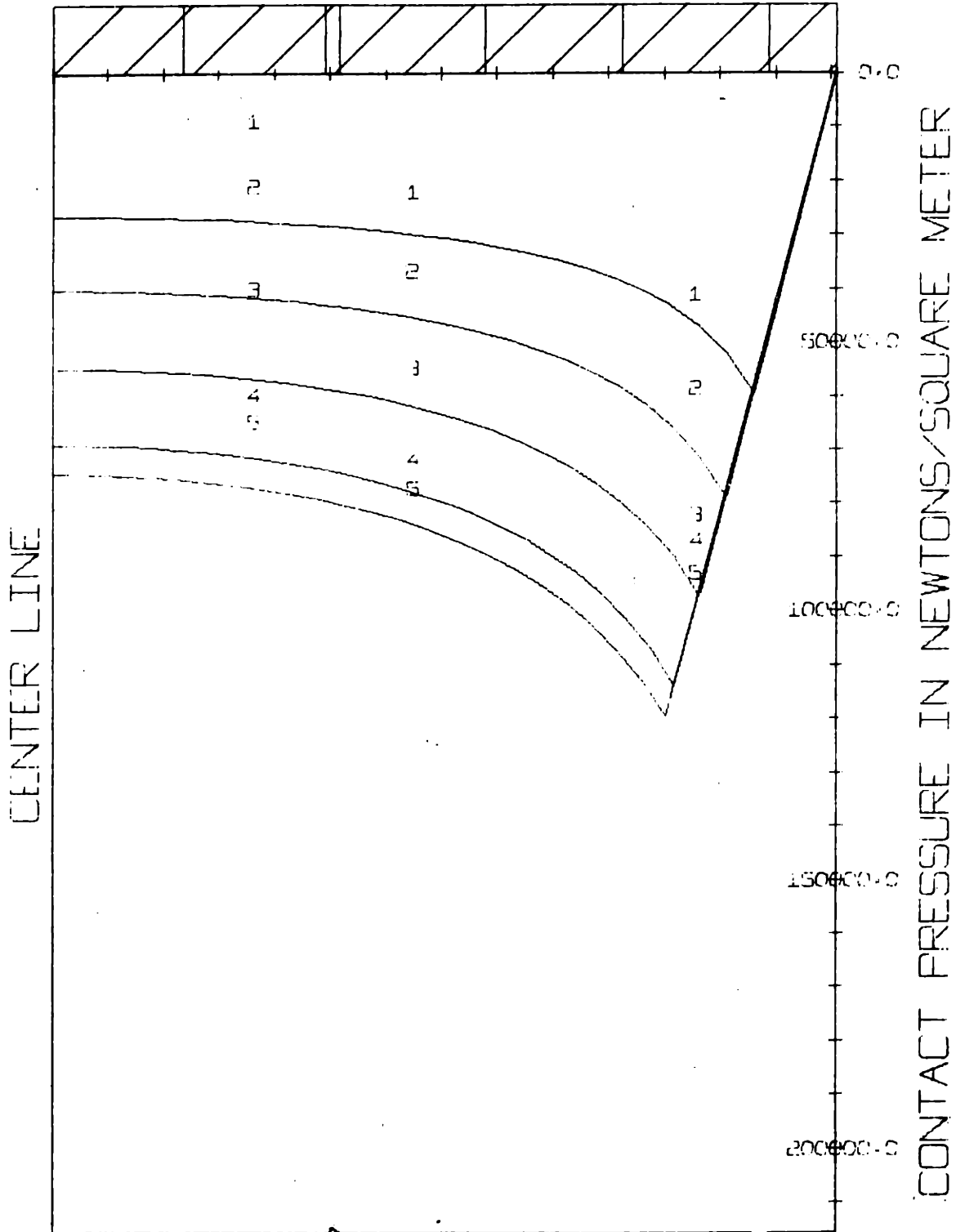
NUMBERS: MEASURED STRESSES;  
NO. REFERS TO STAGE NO.  
SOLID CURVES: PREDICTED STRESSES FOR  
SCHULTZE MODEL; EACH CURVE  
CORRESPONDS TO A STAGE  
TRANS. 1 1 DEFECTIVE; NEGLECTED  
IN ANALYSES



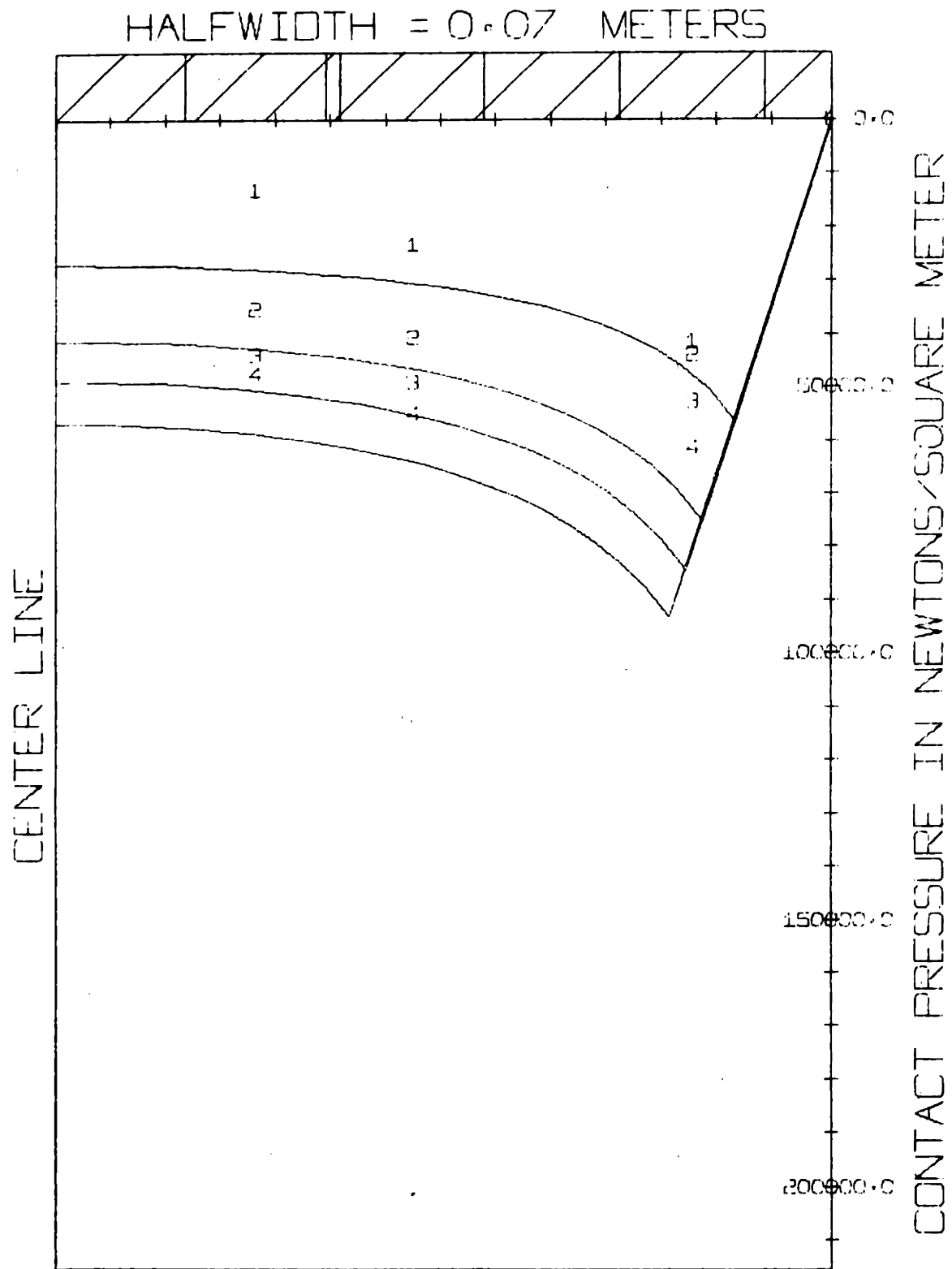
HALFWIDTH = 0.07 METERS



HALFWIDTH = 0.07 METERS



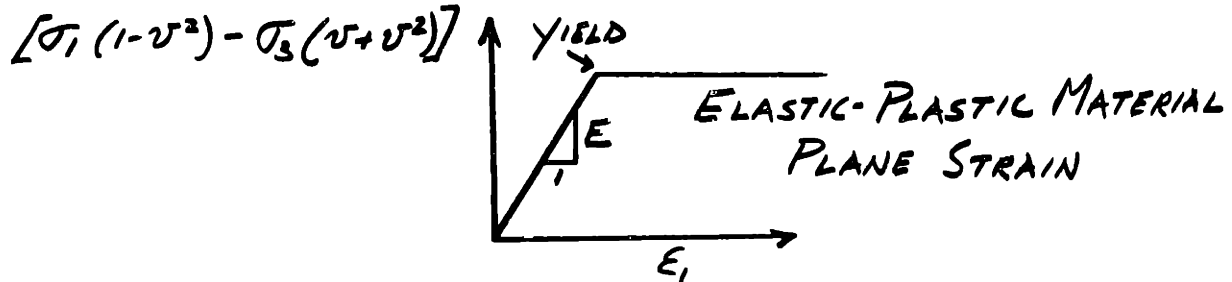




## APPENDIX F

### DAVIS PLASTICITY PARAMETERS

To analyze an elastic, perfectly plastic material, it is necessary to define the state of stress which corresponds to failure and the magnitude and direction of the plastic



strain rates.

For the first part of the problem, the Mohr-Coulomb yield criterion is usually adopted for a frictional-cohesive material:

$$|\sigma_1 - \sigma_3| = (\sigma_1 + \sigma_3) \sin \phi + 2c \cos \phi \quad \text{Eqn. F.1}$$

The strain rate is usually determined either by assuming the soil is incompressible (as in the method of characteristics: Cox, 1963 and Sokolovskii, 1965) or that the soil has an associated flow rule, i.e., the volumetric plastic strain rate is normal to the yield envelope. The upper and lower bound theorems have only been proven for a material with normality and so this latter assumption is usually made (as Terzaghi, 1943 and Meyerhof, 1952). However, this is not to say that these theorems do not exist for materials without normality, only that it has not been proven.

It has been found for sands that normality does not exist if we assume the validity of the Mohr-Coulomb failure criterion. Sand does dilate during shear, but not nearly enough to satisfy normality. One school of thought has attempted to modify the yield criterions such that normality does exist (Drucker, et al., 1957 and Roscoe, et al., 1963). Davis (1968), on the other hand,

has suggested the concept of a linear plastic material whose volumetric strain rate may be specified. His basic equations are:

$$\frac{\partial \epsilon_i}{\partial \sigma_i} = \lambda = \text{const.}$$

Eqn. F.2

$$\frac{\partial \epsilon_j}{\partial \sigma_i} = -\mu\lambda = \text{const.}$$

which are analogous to the perfectly elastic equations:

$$\frac{\partial \epsilon_i}{\partial \sigma_i} = \frac{1}{E}$$

Eqn. F.3

$$\frac{\partial \epsilon_j}{\partial \sigma_i} = \frac{-\nu}{E}$$

It may be then shown for plane strain that:

$$\mu = 1/2(1 + \sin\psi \sin\phi)$$

Eqn. F.4

where  $\mu$  is a parameter which expresses the "degree" of normality. For  $\psi = \phi$ ,  $\mu = 1$  and the soil has normality; for  $\psi = 0$ ,  $\mu = 1/2$  and the soil is incompressible.

At one time during the course of this investigation, it was hoped that Davis' concept of an ideal plastic material could be incorporated into the finite element analysis of an elastic-plastic soil.

The value of  $\mu$  was to be determined from triaxial test data and input into the computer program as another variable. In personal conversations with Davis, the equations for direct shear and triaxial and plane strain compression tests were derived for  $c = 0$ :

DIRECT SHEAR

$$\tan \phi_k = \frac{\cos \psi \sin \phi}{1 - \sin \psi \sin \phi}$$

Eqn. F.5

where  $\phi_k$  is the friction angle from the direct shear test and

$$\tan \psi = (\Delta v / \Delta u)_{\max}$$

$\Delta v$  = normal displacement of soil during shear

$\Delta u$  = transverse displacement of soil during shear

TRIAxIAL

$$N_{\phi_f} = \frac{\sigma_1 / \sigma_3}{\left(1 - \frac{d\epsilon_v}{d\epsilon_1}\right)}$$

Eqn. F.6

$$\mu = \frac{\frac{\sigma_1}{\sigma_3} \left(1 - \frac{d\epsilon_v}{d\epsilon_1}\right) + 2}{2 \left[ \left(2 - \frac{d\epsilon_v}{d\epsilon_1}\right) + \frac{\sigma_1}{\sigma_3} \right]}$$

PLANE STRAIN

$$N_{\phi_f} = \frac{\sigma_1 / \sigma_3}{\left(1 - \frac{d\epsilon_v}{d\epsilon_1}\right)}$$

Eqn. F.7

$$\mu = \frac{\frac{\sigma_1}{\sigma_3} \left(1 - \frac{d\epsilon_v}{d\epsilon_1}\right) + 1}{\left(2 - \frac{d\epsilon_v}{d\epsilon_1}\right) \left(1 + \frac{\sigma_1}{\sigma_3}\right)}$$

$N_{\phi_f}$  is another Davis parameter which expresses the effect of dilatancy on the strength of the soil.

$N_{\phi_f}$  and  $\mu$ , the Davis Plasticity Parameters, are supposed to be independent of stress state, whereas  $\phi$  is not. Thus, it should be possible to find  $N_{\phi_f}$  and  $\mu$  from any type of test and then calculate  $\phi$  for the particular stress system under consideration.

Thus, Eqn. F.5 and F.4 may be used with direct shear tests to calculate  $N_{\phi_f}$  and  $\mu$ ; similarly, Eqn. F.6 may be used with

triaxial tests to calculate  $N_{\phi f}$  and  $\mu$ . The author has derived an equation from Eqn. F.7 which may be then used to calculate the plane strain friction angle from  $N_{\phi f}$  and  $\mu$ :

$$\sin \phi_{ps} =$$

$$\frac{\frac{(2N_{\phi f} - 2)(1 - \mu)}{N_{\phi f}} + \sqrt{\left[\frac{(2N_{\phi f} - 2)(1 - \mu)}{N_{\phi f}}\right]^2 + 4\left(1 + \frac{1}{N_{\phi f}}\right)\left[\frac{(N_{\phi f} + 1)(2\mu - 1)}{N_{\phi f}}\right]}}{2\left(1 + \frac{1}{N_{\phi f}}\right)}$$

Eqn. F.8

Also, an equation was derived from Eqn. F.6 for calculating the triaxial friction angle:

$$\tan^2\left(45^\circ + \frac{\phi_{tri}}{2}\right) = \frac{(2\mu + 2\mu N_{\phi f}) + \left[(2\mu + 2\mu N_{\phi f})^2 - 8N_{\phi f}(1 - \mu)\right]^{1/2}}{2}$$

Eqn. F.9

As mentioned in Sec. 4.5, it was found that the direct shear tests were uninterpretable. That is, the values of  $N_{\phi f}$  followed no consistent pattern. The triaxial tests, on the other hand, were far more internally consistent. But when Eqn. F.8 was used to calculate  $\phi_{ps}$ , the values were greatly overestimated and it was necessary to use an empirical correction.

The author has concluded that the concept of a linear plastic material is excellent for explaining the meaning of normality, but is not of practical use.